

University of Nevada, Reno

**Modeling Mercury Transport and Bioaccumulation in the Carson River and
Lahontan Reservoir System, Nevada**

A dissertation submitted in partial fulfillment of the
requirements for the degree of Doctor of Philosophy in
Hydrology

by

Rosemary W.H. Carroll

Dr. John J. Warwick/ Dissertation Advisor

May, 2010



University of Nevada, Reno
Statewide • Worldwide

THE GRADUATE SCHOOL

We recommend that the dissertation
prepared under our supervision by

ROSEMARY W.H. CARROLL

entitled

**Modeling Mercury Transport and Bioaccumulation in the Carson River and
Lahontan Reservoir System, Nevada**

be accepted in partial fulfillment of the
requirements for the degree of

DOCTOR OF PHILOSOPHY

John J. Warwick, Ph.D., PE, Advisor

Greg M. Pohl, Ph.D., Committee Member

Kumud Acharya, Ph.D., Committee Member

Mark Stone, Ph.D., Committee Member

Sudeep Chandra, Ph.D., Graduate School Representative

Marsha H. Read, Ph. D., Associate Dean, Graduate School

May, 2010

Abstract

A fully dynamic transport model is developed to capture loading mechanisms for total and dissolved mercury (Hg) species for all flow regimes in the Carson River Lahontan Reservoir (CRLR) system. The conversion of inorganic Hg into the toxic, and highly bioavailable, methylmercury (MeHg), is defined with methylation and demethylation (M/D) ratios. M/D occurs in the channel and reservoir bed sediments as well as in channel bank sediments, with bank M/D adjusted for moisture history. Monte Carlo, generalized likelihood uncertainty estimates and first-order second-moment analysis help define what components in the model are well understood and what components remain highly uncertain. Uncertainty in dissolved species in the downstream reservoir is dominated by uncertainty in higher flow loading mechanisms upstream and not from uncertainty related to reservoir benthic fluxes. The CRLR system affords the opportunity to test sensitivity of predicted body burdens in the planktivorous Sacramento blackfish (*Orthodon microlepidotus*) to a variable water quality signal in the context of uncertainty in that signal. A bioenergetic and mercury mass balance model (BMMBM) is developed and shows that dynamic and constant loading scenarios produce statistically similar results in predicted MeHg body burden at any given location in the reservoir. However, results suggest that coupling of peak dissolved MeHg loads with periods of maximum plankton growth and maximum fish consumption rates can account for large burdens in the planktivore. Lags in downstream transport can decouple processes and body burden estimates decrease. Sensitivity to the timing of fluvial inputs to the reservoir is greatest in the upstream receiving basin where there is little attenuation in fluvial loads.

Dedication

This work is dedicated to my husband Torrey Carroll and our two children; Ethan Carroll and Maxwell Carroll. Their daily patience, support and love helped keep things in perspective and made this work possible. I also want to recognize my mother Stephanie W. Hart, who taught me anything is possible and to never to give up; and my sister Emily Hart who is the ultimate cheerleader.

Acknowledgments

Funding for this project came from the Nevada Institute of Water Resources Research (NIWRR) contract number 06HQGR0098. The U.S. Geological Survey (USGS) contributed federal money while the Desert Research Institute provided matching support. Partial funding for geomorphic analysis came from the National Science Foundation (EAR-9712857). I would like to thank my advisor John Warwick for his invaluable assistance and confidence, and my entire committee; Greg Pohl, Kumud Acharya, Sudeep Chandra and Mark Stone, for their time given to me and the project. Additional acknowledgement is given to Karen Thomas with the USGS in Carson City, Nevada and to Joseph J. Cech at the University of California, Davis, for sharing data and ideas. Paul Neeley is recognized for his invaluable IT assistance during Monte Carlo.

TABLE OF CONTENTS

Abstract	i
Dedication	ii
Acknowledgments	iii
List of Figures	vi
List of Tables	viii
Introduction	1
References Cited	3
CHAPTER 1	
Evaluating the Impacts of Uncertainty in Geomorphic Channel Changes on Predicting Mercury Transport and Fate in the Carson River system, Nevada.....	5
Abstract	5
1.1 Introduction	6
1.2 Site Description	7
1.3 Modeling Procedures.....	8
1.3.1 Model Description	8
1.3.2 Previous Modifications to RIVMOD.....	11
1.3.3 Modeling Bank Erosion and Overbank Deposition	12
1.3.4 Modeling Lahontan Reservoir	14
1.3.5 Modeling Mercury Transport.....	15
1.3.6 Methylation in the Bank Sediments.....	16
1.3.7 Uncertainty Analysis.....	17
1.4 Results and Discussion.....	18
1.5 Conclusions	25
Acknowledgments.....	26
References Cited	27
CHAPTER 2	
Mercury Transport Model of the Carson River and Lahontan Reservoir System, Nevada: An Investigation of Total and Dissolved Species and Associated Uncertainty.....	29
Abstract	29
2.1 Introduction	30
2.1.1 Site Description.....	32
2.2 Modeling Approach.....	36
2.2.1 Past Studies of CRLR Mercury Transport Modeling	38
2.2.2 Flow Regimes and Modeled Mercury Loading Mechanisms	40
2.2.3 Methylation and Demethylation	44
2.2.4 Generalized Likelihood Uncertainty Estimate.....	45
2.2.5 Relative Uncertainty	49
2.3 Results	50
2.3.1 Model Calibration and Verification	50
2.3.2 Uncertainty Analysis.....	58

2.4	Discussion	72
2.5	Conclusions	79
	Acknowledgments.....	80
	Appendix A: Notation.....	81
	References Cited	83

CHAPTER 3

Seasonal Variation of Mercury Associated with Different Phytoplankton Size

Fractions in Lahontan Reservoir, Nevada.....		87
	Abstract	87
3.1	Introduction	88
3.2	Site Description	90
3.3	Methods	92
3.3.1	Reservoir Water Column Sampling	92
3.3.2	Mercury Analysis.....	94
3.3.3	Data Analysis	96
3.4	Results	97
3.4.1	Water Column Concentrations and Loads into the Reservoir	97
3.4.2	THg and MeHg Associated with Phytoplankton	99
3.5	Discussion	106
3.6	Conclusions	109
	Acknowledgements.....	110
	References Cited	110

CHAPTER 4

The Importance of Dynamic Mercury Loads on Body Burdens in a Planktivorous Fish (*Orthodon microlepidotus*): a Bioenergetic and Mercury Mass Balance

Perspective		114
	Abstract	114
4.1	Introduction	115
4.2	Site Description	117
4.3	Methods	122
4.3.1	Model Algorithm	122
4.3.2	Model Parameterization and Calibration	126
4.3.2.1	Bioenergetics in the Laboratory - Juvenile Fish	126
4.3.2.2	Dynamic Water Column Concentrations (C_w).....	126
4.3.2.3	Bioenergetics in the Natural Environment.....	129
4.3.2.4	Prey Contamination (C_δ).....	139
4.3.2.5	MeHg Body Burdens	140
4.4	Results and Discussion.....	141
4.5	Conclusions	147
	Acknowledgements.....	149
	References Cited	150
Concluding Remarks.....		157

LIST OF FIGURES

CHAPTER 1

1.1:	The Carson River – Lahontan Reservoir system with the detail showing the 10 river reaches used by Miller et al. (1999) for geomorphic analysis.	8
1.2:	Modeled discharge at the Fort Churchill gage, with water column sampling dates marked.	11
1.3:	Water column mercury concentrations collected June 10, 1995 along the Carson River and Lahontan Reservoir, (a) Calibration of λ_l (Hg^{2+} bank concentrations) to best match observed Hg^{2+} water column concentrations, (b) comparison of modeled and observed MeHg with no calibration.	19
1.4:	80% confidence intervals given uncertainty related to geomorphic change near FCH for (a) Hg^{2+} and, (b) MeHg.	22
1.5:	Upper 80% confidence interval for entire model domain over entire simulation given uncertainty in geomorphic changes to the river channel.	24

CHAPTER 2

2.1:	The Carson River – Lahontan River (CRLR) watershed with inset showing location of the watershed with respect to California and Nevada.	33
2.2:	Details of the CRLR model domain with respect to the (a) river and (b) reservoir.	34
2.3:	Modeled mean daily discharge at the Fort Churchill gaging station.	36
2.4:	Verification of the bank erosion algorithm (equation 2.1) by comparing observed and modeled channel width increases between areal photographs taken in 1991 and 1997, for the 10 river reaches marked in Figure 2.2 and defined by Miller et al. (1999).	51
2.5:	Pre-flood data sets with sites labeled by number.	53
2.6:	Water column mercury concentrations at Weeks Bridge for, (a) THg, (b) DHg, (c) TMeHg and (d) DMeHg.	55
2.7:	Post-flood water column mercury concentrations at Weeks Bridge. (a) percentage of THg that is dissolved, (b) percentage of TMeHg that is dissolved.	56
2.8:	Post-flood regression of predicted and observed concentrations of dissolved species in the reservoir.	59
2.9:	Percentage of observed data captured by the GLUE-defined 95% confidence interval (CI) as a function of species, flow and location.	61
2.10:	Stabilization of GLUE derived parameter means with increased number of realizations (J) for (a) pre-flood simulation, (b) post-flood simulation.	62
2.11:	Examples of likelihood functions produced by the GLUE approach, (a) λ_1 pre-flood simulation, (b) E pre-flood simulation, (c) λ_1 post-flood simulation, (d) E post-flood simulation., (e) λ_1 post-flood simulation $N = 10$, and (f) E post-flood simulation $N = 10$	65
2.12:	FOSM relative uncertainty of each of the parameters tested (a) pre-flood simulation, (b) post-flood simulation.	67

2.13: System-wide ranges in the GLUE 95% CI (R_u) for WY 2004 through WY 2006 (a) THg, log ₁₀ ng/L and (b) TMeHg, ng/L, (c) TMeHg, ng/L and (d) DMeHg, ng/L.....	69
2.14: System-wide ranges in the GLUE 95% CI for WY 2004 through WY 2006 (a) DHg, log ₁₀ (ng/L) and (b) DMeHg, ng/L.....	70

CHAPTER 3

3.1: Lahontan Reservoir with Fisherman's Point (FPO) sampling site marked.....	91
3.2: (a) water column concentrations collected at Weeks Bridge by the USGS and at FPO.....	98
3.3: Chl _a concentrations in µg/L for phytoplankton less than 35 µm and total phytoplankton.....	100
3.4: Mercury accumulation in SPM < 35 µm and total SPM, expressed as mercury concentration per unit mass for (a) THg C_b , (b) MeHg C_b ,	101
3.5: Bioaccumulation (K_d) for SPM < 35 µm and total SPM, (a) THg K_d and (b) MeHg K_d	104
3.6: MeHg K_d for SPM < 35 µm and total SPM as a function of (a) Chl _a , (b) residence time, τ , (c) log-transformed DMeHg loads, W and (d) SPM.	105

CHAPTER 4

4.1: Lahontan Reservoir with basins marked.	118
4.2: Total Hg (THg) contamination as a function of wet weight for three Lahontan Reservoir fish populations: walleye (E&E, 1998), carp (Cooper et al., 1983; E&E, 1998;), and Sacramento blackfish (Cooper et al., 1983; 1985; E&E, 1998; Craft et al., 2005; Kris Urquhart, NDOW, written communication February 25, 2010).	120
4.3: Typical five year C_w (ng/L) sequence into/through Lahontan reservoir based on transport model predictions presented by Carroll et al. (in prep) for years 1997 through 2008.	128
4.4: Cosine approximation of reservoir water temperatures calibrated to FPO data and verified with LDM data.....	132
4.5: Observed annual prey density (mg/L) in Lahontan Reservoir.	135
4.6: First-order second-moment analysis of normalized sensitivity and uncertainty (i.e., sum to 1.0) for bioenergetic parameters based on the 5-year simulation of natural conditions.	138
4.7: Predicted and observed fish weights based on age class.....	138
4.8: Model results compared to observed data with data identified by source and year of sample.	142
4.9: Modeled MeHg body burdens (µg/g) in Sacramento blackfish along the length of Lahontan Reservoir as a function of fish weight (a) dynamic C_w originating from the Carson River, (b) constant $C_w = 1.33$ ng/L.....	143
4.10: Modeled MeHg body burdens (µg/g) in Sacramento blackfish along the length of Lahontan Reservoir as a function of fish weight given altered (and hypothetical) loading scenarios.....	148

LIST OF TABLES**CHAPTER 2**

2.1: Description of parameters used in the CRLR model with traditional calibration values and associated strategies.	46
2.2: Break down of the multi-criteria objective function based on species, location and flow regime.	47
2.3: Mercury transport parameters used to calibrate mercury species as a function of flow regime.	50
2.4: Resultant posterior means (μ) and standard deviations (σ) for the pre-flood and post-flood GLUE analysis for the parameters investigated.	60

CHAPTER 4

4.1: Sacramento blackfish Hg body burdens in Lahontan Reservoir.	121
4.2: Parameters used in the BMMBM with sources defined.	130

INTRODUCTION

The importance of mercury (Hg) as a global pollutant is clear and well documented but many questions still remain in terms of Hg cycling, bioavailability and bioaccumulation. The Carson River-Lahontan Reservoir system (CRLR) in west-central Nevada is listed by the U.S. Environmental Agency (US EPA) as a Superfund site due to its contamination with Hg derived from mining of the Comstock Lode in the later portion of the 19th century. Large amounts of residual Hg reside in the Carson River bank sediments and flood plain deposits and offer a nearly inexhaustible supply of contaminants to the Carson River with downstream transport into Lahontan Reservoir.

Fish populations in Lahontan Reservoir exceed the Federal Action limit for consumption (1 µg/g). Large walleye (*Stizostedion vitreum*), the top predator in Lahontan Reservoir, are observed with total body burdens nearly seven times the Federal Action Limit, and muscle tissue concentrations nine times larger than the recommended limit. Likewise, second consumers such as bathivorous carp (*Cyprinus carpio*) and planktivorous Sacramento blackfish (*Orthodon microlepidotus*) contain Hg above 1 µg/g and may represent a public health problem since these fish are harvested commercially for San Francisco markets.

Four chapters are presented with each representing a distinct and complete document for publication. Therefore, some repetition is encountered between chapters. The first phase of research aims at capturing observed water quality trends in total and dissolved Hg species and estimating uncertainty in the ability of the transport model to predict water column concentrations. The geologic and geochemical controls on total Hg (THg) and total methylmercury (TMeHg) transport through the Carson River have been

successfully modeled (Heim and Warwick, 1997; Carroll et al., 2000; Carroll and Warwick, 2001; Carroll et al., 2004) with a linked and modified version of RIVMOD (Hosseinipour and Martin, 1990) and WASP5/MERC4 (Ambrose et al., 1991). Research presented capitalizes on these earlier studies to quantify the transport of dissolved species, the physical parameters impacting mercury transport into/through Lahontan Reservoir as well as to define uncertainty associated with geomorphological and biogeochemical controls influencing loading and transport through the system.

Specifically, Chapter 1: Evaluating the Impacts of Uncertainty in Geomorphic Channel Changes on Predicting Mercury Transport and Fate in the Carson River system, Nevada, improves on earlier versions of the CRLR transport model by explicitly including the reservoir in the analysis, as well as adding a bank package that accounts for flow history. Monte Carlo simulation investigates uncertainty in geomorphic parameters of bank erosion and overbank deposition and questions if the system fundamentally changed, in terms of Hg transport, as a result of a single, large flow event. Chapter 1 is already published in the *International Journal of Soil, Sediment and Water* (Warwick and Carroll, 2008). Chapter 2: Mercury Transport Model of the Carson River and Lahontan Reservoir System, Nevada: an Investigation of Total and Dissolved Species and Associated Uncertainty, is a capstone paper that revisits transport of total species but with attention given to all flow regimes for years 1991 through 2008, and incorporates dissolved species into the analysis (Carroll et al., in prep). The dissolved fraction is the component that may be bioavailable to plankton and most readily transferred to higher trophic levels. Calibration strategies and uncertainty analysis are investigated to help isolate what constituents of the model are important in describing both total and dissolved

Hg transport and addresses how well those components are understood. In addition, generalized likelihood uncertainty estimate (GLUE) techniques are used to determine if the system fundamentally changed as a result of the massive flood.

The second phase of research looks at bioaccumulation as a function of a temporally variable Hg loading signal. Chapter 3: Seasonal Variation of Mercury Associated with Different Phytoplankton Size Fractions in Lahontan Reservoir, Nevada quantifies seasonal variation of total Hg and MeHg accumulation in phytoplankton as a function of dissolved point source (fluvial) mercury loads, reservoir residence time and algal growth. This chapter is currently in review with *Water, Air and Soil Pollution* (Carroll et al., in review). Lastly, Chapter 4 addresses the importance of a temporal signal in predicting Hg bioaccumulation in fish. To remove complex food web interactions from the analysis, the planktivorous Sacramento blackfish is the investigated species. A bioenergetic and mercury mass balance model (BMMBM) is constructed that accounts for prey availability and adjusts prey contamination as a function of DMeHg water column concentration computed in Chapter 2 and the bioavailability of MeHg in phytoplankton observed in Chapter 3. Analysis compares modeled body burdens using dynamic and constant loading scenarios and looks at model sensitivity to hypothetical lags in river inputs to the reservoir.

References Cited

Ambrose, R.B., Wool, T.A., Martin, J.P. and Schanz, R.W., 1991. WASP5.X: A Hydrodynamic and Water Quality Model: Model Theory, User's Manual and Programmer's Guide. U.S. E.P.A., Athens, Georgia.

- Carroll, R.W.H., Warwick, J.J., Heim, K.J., Bonzongo, J.C., Miller, J.R. and Lyons, W.B., 2000. Simulating Mercury Transport and Fate in the Carson River, Nevada. *Ecological Modeling*, 125:255-278.
- Carroll, R.W.H. and Warwick, J.J., 2001. Uncertainty analysis of the Carson River mercury transport model. *Ecological Modeling*, 137: 211-224.
- Carroll, R., Warwick, J.J., James, A., and Miller, J. 2004. Modeling Erosion and Overbank Deposition during Extreme Flood Conditions on the Carson River, Nevada. *Journal of Hydrology*. 297:1-21.
- Carroll, R.W.H., Memmott, J., Warwick, J.J., Fritsen, C.H., Bonzongo, J.C., and Acharya, K. in review. Temporal variation of mercury associated with different phytoplankton size fractions in Lahontan Reservoir, Nevada. *Water, Air and Soil Pollution*.
- Carroll, R.W.H., Warwick, J.J. and Pohll, G.M. in prep. Mercury transport model of the Carson River and Lahontan Reservoir System, Nevada: An investigation of total and dissolved species and associated uncertainty. Intended Journal - *Ecological Modelling*.
- Heim, K.J. and Warwick, J.J., 1997. Simulating sediment transport in the Carson River and Lahontan Reservoir, Nevada. *Journal of the American Water Resources Association*, 33(1): 177-191.
- Hosseini-pour, E.Z. and Martin, J.L., 1990. RIVMOD: a one-dimensional hydrodynamic sediment transport model: model theory and user's guide. U.S. E.P.A, Athens, Georgia.
- Warwick, J.J. and Carroll, R.W.H. 2008. Evaluating the impacts of uncertainty in geomorphic channel changes on predicting mercury transport and fate in the Carson River system, Nevada. *International Journal of Soil, Sediment and Water*. 1: 1-15. Full text at <http://scholarworks.umass.edu/intljssw/vol1/iss1/4>.

CHAPTER 1

Evaluating the Impacts of Uncertainty in Geomorphic Channel Changes on Predicting Mercury Transport and Fate in the Carson River system, Nevada

John J. Warwick¹ and R.W.H. Carroll²

Abstract

The Carson River is one of the most mercury contaminated fluvial systems in North America. Most of its mercury is affiliated with channel bank material and floodplain deposits, with the movement of mercury through this system being highly dependent on bank erosion and sediment transport processes. Mercury transport is simulated using three computer models: RIVMOD, WASP5, and MERC4. Model improvements include the addition of a bank package that accounts for flow history. The rates at which river stages are rising or falling will, in turn, impart time-dependant and vertically variable MeHg concentrations within the channel banks along the Carson River. Also, Lahontan Reservoir's geomorphic characteristics have been refined along with the explicit tracking of a temporally and spatially varying colloidal fraction. The augmented and refined modeling approach results in more accurate and realistic simulation of mercury transport and fate. An extensive uncertainty analysis, involving characterizing the co-variance of two calibration parameters used to define bank erosion

¹ Executive Director, Desert Research Institute, Division of Hydrologic Sciences Reno, NV 89512 775-673-7379 (ph), John.Warwick@dri.edu

² Assistant Research Hydrologist, Desert Research Institute, Division of Hydrologic Sciences Reno, NV 89512 970-349-0356 (ph), Rosemary.Carroll@dri.edu (Corresponding Author): Current Mailing Address: P.O. Box 4196 Crested Butte, CO 81224

and overbank deposition, will define the degree of expected variation in model predictions relative to limitations posed by available field data.

KEY WORDS: Monte Carlo, mercury modeling, Carson River, Lahontan Reservoir

1.1 INTRODUCTION

The U.S. Environmental Protection Agency (US EPA) designated the Carson River as part of a Superfund site in 1991 due to contamination by mercury. It is estimated that approximately 6.36×10^6 kg (7,000 tons) of residual mercury is now distributed throughout the river's bank sediments and floodplain deposits (Miller et al, 1998; Smith and Tingley, 1998). It has also been found that more than 95% of the mercury transported in the Carson River is affiliated with particulate matter (Bonzongo et al., 1996). During January 1997 a rare, high magnitude flood generated significant geomorphic change and resulted in an estimated 1.81×10^8 kg (200,000 tons) of sediment and 1,360 kg (3,000 lbs.) of mercury to be transported downstream into Lahontan Reservoir (Hoffman and Taylor, 1998). These quantities far exceed the amount of sediment and mercury transported in the decade prior to the flood. Consequently, any useful model of mercury transport in the Carson River system requires an accurate simulation of bank erosion and floodplain sedimentation mechanisms during extreme flood events. The January 1997 flood is the largest recorded event on the Carson River (1911 to present) and provides a unique opportunity to assess sediment cycling and mercury transport as a result of a rare-magnitude event. Modeling procedures use data collected by Miller et al. (1999) on channel widening and overbank deposition as a result of the 1997 flood as well as

mercury data collected by the University of Nevada, Reno (UNR) and the U.S. Geological Survey (USGS) before, during and after the flood.

1.2 SITE DESCRIPTION

The Carson River flows eastward out of the Sierra Nevada Mountains just to the south of the Lake Tahoe Basin. Figure 1.1 shows a map of the Carson River with several reference locations marked. The section of the Carson River under investigation extends from the USGS gaging station near Carson City, Nevada (CCG, point 0 in Figure 1.1 detail) downstream through Lahontan Reservoir. The river's delta is located approximately 80 km from CCG and is located approximately 10 km below the Fort Churchill gaging station (FCH). Miller et al. (1999) conducted an extensive survey of the Carson River in the early spring following the 1997 flood. Both bank erosion and overbank deposition were evaluated using geomorphic techniques of aerial photography (taken in 1991 and 1997) and floodplain mapping. Data were discretized into 10 river reaches (refer to Figure 1.1) defined by valley slope and floodplain width. For a complete discussion on techniques and results of the geomorphic survey read Miller et al. (1999).

Flow in the Carson River is typical of most semi-arid fluvial systems in that it is highly variable. Flow is predominately from snowmelt in the Sierra Nevada with peak discharge generally occurring in the spring with a sustained moderately high hydrograph. Catastrophic floods, such as the January 1997 flood, however, are generated with rain-on-snow events that can occur during the winter months. Peak mean daily discharge during the 1997 flood was estimated at $630 \text{ m}^3/\text{s}$. For comparison, the designated 100-year event occurred in 1986 with a peak discharge of $470 \text{ m}^3/\text{s}$. In contrast, the summer and fall

months are dominated by low flows and these flows can cease all together during extended periods of drought.

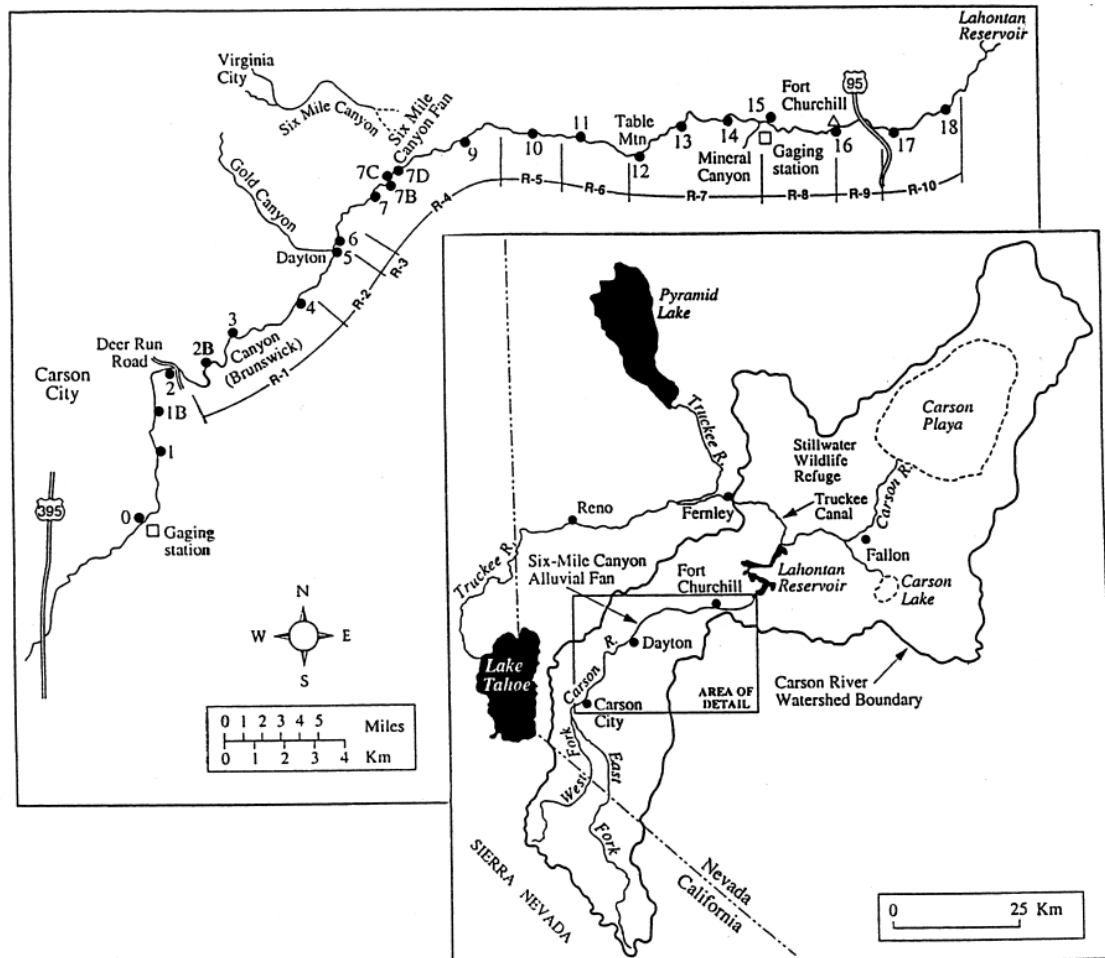


Figure 1.1: The Carson River – Lahontan Reservoir system with the detail showing the 10 river reaches used by Miller et al. (1999) for geomorphic analysis.

1.3 MODELING PROCEDURES

1.3.1 Model Description

Three computer models (RIVMOD, WASP5 and MERC4) were used to simulate the transport of sediment and mercury in the Carson River. RIVMOD (Hosseini-pour and

Martin, 1990) is a U.S. EPA 1-dimensional hydrodynamic and sediment transport routine that simultaneously solves standard fluid equations of continuity and momentum. Finite difference equations are solved by the Newton-Raphson method to determine fluid velocity and depth given unsteady flow conditions. WASP5 (Ambrose et al., 1991) is the U.S. EPA Water Quality Analysis Simulation Program-5 that was developed to simulate the transport and transformation of various water body constituents. Mass balance equations account for all material entering and leaving model segments through direct and diffuse loading, advective and dispersive transport, and any physical or chemical transformation. MERC4 (Martin, 1992) is a subroutine contained within WASP5. It was developed to specifically compute mercury speciation and kinetic transformation. MERC4 is capable of simulating up to four mercury species and three distinct solid types. Five state variables are modeled in this study: inorganic mercury (Hg^{2+}), methylmercury (MeHg), washload, coarse suspended sediment (CSS) and bedload. Elemental mercury (Hg^0), while very toxic, is highly volatile with only very low concentrations detected in the surface waters of the Carson River (Bonzongo et al., 1996) and so was excluded from analysis.

Washload constitutes the smallest fraction (diameter < 0.063 mm) and is considered uniformly distributed from the riverbed to the water surface. Concentrations of CSS (diameter > 0.063 mm) are greatest near the riverbed and diminish upward toward the water surface. This is a direct reflection of the exchange of bed material into suspension and visa-versa (Meade, 1990). Bedload is the third type of solid modeled. It is defined as coarse material that travels by rolling, skipping and/or sliding along the riverbed. In addition to these three sediment fractions, the colloidal material (diameter

less than 0.002 mm) was assumed to occupy a fraction of the washload. Colloids represent fine material that will not settle despite a decrease in stream velocities either on the river's floodplain or within the reservoir. The colloidal upstream boundary condition at the CCG was set to 11% of the total washload based on site data. The modeled fraction of colloidal material was then allowed to vary downstream such that when washload was deposited the fraction of colloids increased. The colloidal fraction increases to 100% of the fine material following sedimentation in the reservoir's delta region.

RIVMOD, WASP5 and MERC4 were originally chosen, linked and modified by Warwick and Heim (1995) and Heim and Warwick (1997) with further modification by Carroll et al. (2000) and Carroll et al. (2004). It is acknowledged an updated WASP7 and mercury module exist, however dynamic linking of WASP5 with RIVMOD as well as extensive code modifications to WASP5 done by previous studies prohibit its use. An attempt has been made to briefly summarize modeling procedures; however, one is encouraged to refer to these previous studies for a complete discussion on model development.

The Carson River - Lahontan Reservoir model contains 307 water column segments starting at the CCG and ending at Lahontan Dam. The river is defined as segments 1 through 203 with segment spacing equal to 0.5 km. Reservoir segments (204 to 307) encompass the entire reservoir during peak capacity and are discretized smaller (0.25 km) to improve numeric stability during summer and fall drawdowns. All water column segments contain a corresponding bed segment for sediment and mercury exchange, but only river segments contain a representative bank element (described in the section Methylation in Bank Segments) for a total of 817 modeled segments. Carroll et al.

(2004) modeled daily flows from 1991 to 1997 to simulate estimated erosion by Miller et al. (1999). Carroll et al. (2004) found no significant geomorphic change occurred during the drought years of 1991, 1992 and 1993. Therefore, this study will only focus only on daily flows beginning October 1, 1993 and extend through the 1998 water year to include University of Nevada, Reno (UNR) and USGS data collected near FCH in the model's analysis (refer to Figure 1.2).

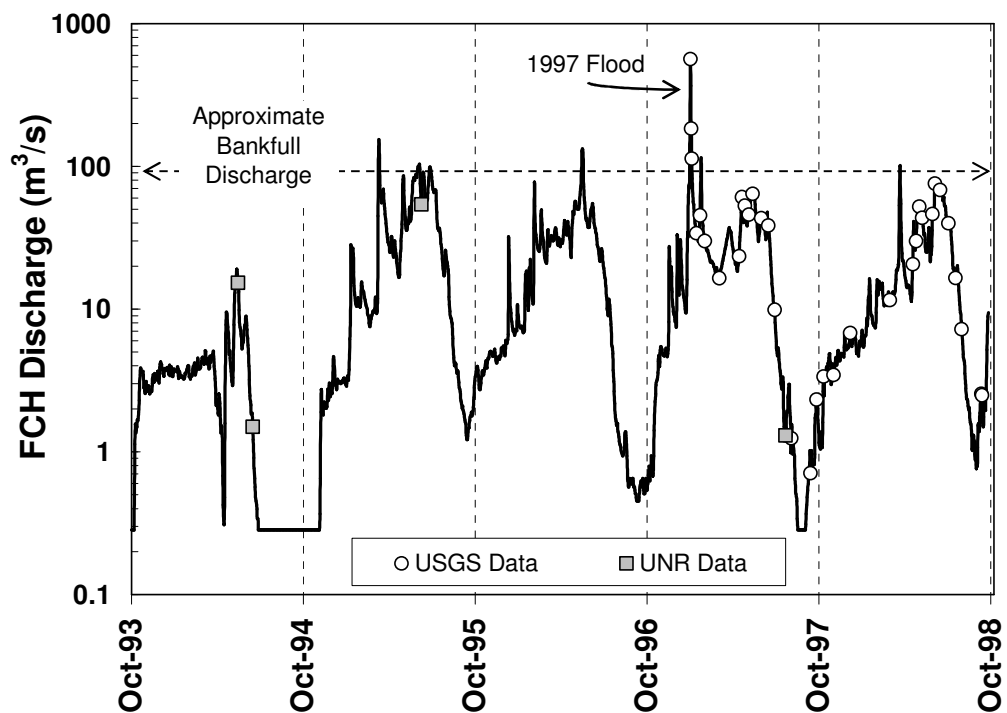


Figure 1.2: Modeled discharge at the Fort Churchill gage, with water column sampling dates marked. (UNR = collected by the University of Nevada, Reno; USGS = collected by the U.S. Geological Survey).

1.3.2 Previous Modifications to RIVMOD

Early alterations to RIVMOD include a revision of the simple rectangular channel geometry to a more complex shape (Warwick and Heim, 1995). Past research along the

Carson River considered cross sectional geometry spatially variable but temporally fixed (Carroll et al., 2000). Subsequent modifications allowed dynamic width adjustment in which the modeled mass eroded was used to update channel width every timestep by assuming the entire vertical face of the bank was susceptible to erosion (Carroll et al., 2004). The divided channel approach was also applied to the momentum equation contained within the RIVMOD numeric code to estimate floodplain depths and velocities during overbank flows (Carroll et al., 2004).

1.3.3 Modeling Bank Erosion and Overbank Deposition

Carroll et al., (2004) developed an empirical relationship in WASP to describe bank erosion during in-channel flows as well as during over-bank flows. These relationships assume the rate of erosion is proportional to the shear stress applied to the bank (Darby and Thorne, 1996) and is indirectly related the average velocity, or square-root of the channel bottom slope. Using Manning's wide channel relationship Carroll et al. (2004) developed the following relationship for bank erosion,

$$MER = \frac{\psi_1 \rho_s \gamma_w n^2 D^{2/3} v^2 L_s}{S_0^{1/2}} + \frac{\psi_2 \rho_s \gamma_w n^2 (D - h) v^2 L_s}{h^{1/3} S_0^{1/2}} \quad (1.1)$$

where MER is the total bank mass eroded (kg) γ_w is the specific weight of water ($\text{kg/m}^2/\text{s}^2$), h is the height of the vertical bank face along the river's edge (m), D is the water depth starting at the vertical face of the channel bank (m), S_f is the friction slope, v is the water velocity (m/s), n is Manning's coefficient, L_s is the segment length (m), and ψ_1 and ψ_2 are constants of proportionality ($\text{m}^2 \text{ s/kg}$). The first term on the right-hand-side of equation 1.1 was used to model mass eroded from the banks when river discharge was below bank-full, while both terms on the right-hand-side of equation 1.1 were used to

model mass eroded during over-bank discharge. Carroll et al. (2004) calibrated ψ_1 using measured water column concentrations of washload material at FCH when flows were below bankfull discharge and calibrated ψ_2 such that total modeled mass eroded (*MER*) from the banks fell within the range presented by Miller et al. (1999). It is only possible to match observed values by allowing significantly more erosion to occur when flows surpass bankfull discharge than when flows are confined to the main channel. Carroll et al. (2004) modeled results show that nearly 87% of bank mass eroded in a 6-year time span occurred during the single 1997 flood event. These results agreed with Miller et al. (1999) who attributed all geomorphic change along the Carson River from 1991-1997 to this single high-magnitude event. Verification of this approach showed the model fell within the 95% confidence interval of the observed mean channel width increase in seven of the 10 reaches (reaches shown in Figure 1.1 detail), with trends well predicted in two of the remaining three reaches.

Overbank deposition was modeled using separate, but related, approaches for CSS and washload (Carroll et al., 2004). CSS was modeled by coupling analytical approaches presented by Thomann and Mueller (1987) and Walling and He (1997) in order to relate the amount of sediment deposited to the distance from the main channel. With no calibration, modeled values of CSS deposition on the floodplain agreed quite well with observed values by matching observed values in five out of 10 reaches (Carroll et al., 2004).

Carroll et al. (2004) modeled washload deposition using a functional relationship developed for the model WEPP (Foster et al., 1995) that relates the rate of washload deposition to the difference between the actual concentration of sediment in the water

column and the theoretical transport capacity (Johnson et al., 2000). The rate of washload deposition R_s^w (kg/s/m²) is given by,

$$R_s^w = \frac{\bar{\beta}V_s^w}{q_f}(G_{main}^w - T_c) \quad (1.2)$$

where V_s^w is the average fall velocity for washload material (m/s) and q_f (m²/s) is the discharge per unit width on the floodplain. Using Stoke's Law and assuming an average washload particle diameter of 0.033 mm (non-colloidal washload 0.002 mm to 0.63 mm), V_s^w equals 0.001 m/s. G_{main}^w is the water column non-colloidal washload (kg/s/m) in the main channel and T_c is the transport capacity (kg/m/s). β is a dimensionless turbulence coefficient and is assumed to decay exponentially with distance from the channel across the floodplain. To estimate T_c , a modified form of the model applied by Johnson et al. (2000) was used (Carroll et al., 2004),

$$T_c = \psi_3 q^2 S_0^{1.66} \quad (1.3)$$

where ψ_3 is a calibration constant (kg s/m⁵) adjusted to match washload water column concentrations at FCH during overbank flows. These functions were able to predict washload concentrations at FCH, but over predicted washload deposited on the floodplain for most modeled reaches and over predicted total washload deposited by a factor of 2.7 (Carroll et al., 2004). Carroll et al. (2004) calibration of ψ_1 , ψ_2 and ψ_3 to model bank erosion and overbank deposition was maintained in this study.

1.3.4 Modeling Lahontan Reservoir

Lahontan Reservoir consists of three distinct basins with water from the Carson River entering the south basin and moving northward through the middle basin and into

the north basin (refer to Figure 1.1). The north basin terminates at Lahontan Dam with inputs from the Truckee Canal occurring at the north side of the dam. Lahontan Reservoir is almost 30 km in length when filled to maximum capacity. Past modeling of the Carson River-Lahontan Reservoir system used 0.5 km model segment lengths throughout the study site, but allowed for a finer discretization of segments (0.25 km) in the region of the reservoir delta. Rediscrretization of the entire reservoir into 0.25 km segments was done to improve model stability during the drought of 1994 when drawdown in the reservoir allowed the delta to migrate into the north basin. Model stability was similarly improved by smoothing reservoir channel bottom slopes. Detailed cross sections of each modeled segment in the reservoir were developed using an updated U.S. Bureau of Reclamation (USBR) bathymetry map. Reservoir segments were redefined using these cross sections and the geometric definitions required by the modified RIVMOD (Carroll et al., 2004). Groundwater inflows/outflows were added to the reservoir to force modeled reservoir stages to match observed values. In particular, this was important to match massive drawdown in the reservoir during the drought of 1994 and allowed for accurate movement of the delta region which is important in simulating sediment and mercury deposition.

1.3.5 Modeling Mercury Transport

Boundary conditions, initial conditions, methylation - demethylation rates, particle reaction coefficients and the diffusion from bottom sediments are discussed in detail by Carroll et al. (2000). Carroll et al. (2000) developed a relationship describing river bank Hg concentrations ($[Hg^{2+}]_{bank}$) as a function of channel bed slope (S_0) (equation 1.4a) in which λ_l ($\mu\text{g}/\text{kg}$) was adjusted to match observed pre-1997 flood water

column concentrations along the Carson River. To accommodate a newly developed bank package where the concentration of MeHg would be computed as time varying based upon bank moisture history, a spatially variable (simple linear function) inorganic mercury bank concentration was imposed as shown in equation 1.4b,

$$[Hg^{2+}]_{bank} = \frac{\lambda_1}{S_0^{0.5}} \quad (1.4a)$$

$$[Hg^{2+}]_{max} = \frac{\lambda_1}{S_0^{0.5}}; [Hg^{2+}]_{bank} = [Hg^{2+}]_{bot} + \frac{([Hg^{2+}]_{max} - [Hg^{2+}]_{bot}) \cdot D}{2h} \quad (1.4b)$$

where $[Hg^{2+}]_{max}$ = maximum inorganic bank mercury concentration ($\mu\text{g}/\text{Kg}$), $[Hg^{2+}]_{bot}$ = measured channel bottom inorganic mercury concentration ($\mu\text{g}/\text{Kg}$) based on data collected by Miller and Lechler (1998) and described by (Carroll et al., 2000), D is water depth beginning at the vertical face of the bank (m) and h = the vertical height of the bank (m). The factor of two in the denominator of equation 1.4b accounts for banks on both sides of the river. It is also assumed that banks related to the low flow inner channel as well as the low to medium flow transition slope (roughly flow depths less than 1 m) have Hg^{2+} bank concentrations similar to channel bottom sediments. For this study, the calibration of λ_1 was accomplished using Hg^{2+} water column data collected during flow conditions just below bankfull (June 10, 1995).

1.3.6 Methylation in the Bank Sediments

Laboratory experiments conducted by Dr. Mark Hines (University of Massachusetts, Lowell) demonstrated that methylation activity was nonexistent when the bank soils were dry but quickly became significant after approximately four days of soil saturation (<http://biogeochemistry.uml.edu/pages/Hg.html>). To implement these findings,

the newly developed bank package tracks the depth of vertical bank that has been saturated for four or more days, computes the average Hg^{2+} concentration in the saturated bank sediments (equation 1.4b), and then computes a MeHg bank concentration based on the computed amount of Hg^{2+} and the methylation-demethylation ratio. Rapid increases in flow will actually cause a “dilution” of in-stream MeHg concentrations since the bank concentrations will not increase by the time of significant erosion. On the other hand, if flow rises more gradually such that a majority of the bank remains saturated for four or more days, then the concentration of MeHg in the banks will be substantial as will be the potential mass loading rate into the river due to bank erosion and possibly bank diffusion. No calibration was performed using MeHg bank concentrations to match water column concentrations.

1.3.7 Uncertainty Analysis

Carroll and Warwick (2001) performed the first comprehensive uncertainty analysis of the Carson River mercury transport model. Specifically, uncertainty in the methylation-demethylation ratio and the diffusion rate of mercury from channel bottom sediments were evaluated in the river channel from the CCG to the FCH region. This study used a similar approach to uncertainty, but focused only on impacts of geomorphic change on mercury transport while incorporating channel widening and dynamic bank methylation rates into the analysis. The Monte Carlo simulation was employed using the computing power of the Desert Research Institute’s Advanced Computing in Environmental Sciences (ACES) program. This is a sophisticated research grid among the three University and Community College System of Nevada campuses. Grid computing power comes from a SGI Altix 3700 from Silicon Graphics with the shared –

memory high performance supercomputer boasting 40 Intel Itanium2 CPUs, 80 GB of RAM and 3 TB of disk space and the Linux kernel. Five hundred simulations were run on ACES (taking three months computing time) simultaneously adjusting the parameters λ_l and ψ_l . Results were then ranked to establish the 80% confidence interval of Hg and MeHg water column concentrations across the modeled domain and over the entire course of the simulation.

1.4 RESULTS AND DISCUSSION

Hg water column concentrations measured June 1995 were calibrated using a λ_l value equal to 6,000 $\mu\text{g}/\text{kg}$. This value is approximately double that presented by Carroll et al. (2000), which is explained by the relationships between equation 1.4a used by Carroll et al. (2000) and equations 1.4b used herein. Figure 1.3a shows that while water column Hg^{2+} concentrations are slightly over-predicted in the upper river reaches, river Hg^{2+} concentrations at FCH (segment 140) and the river's delta region were well predicted. No calibration was attempted to match Hg^{2+} reservoir concentrations. Figure 1.3a suggests that the model may either over-estimate the importance of the overbank flow event earlier in 1995 (refer to Figure 1.2) and its ability to transport Hg^{2+} into the reservoir, or has not moved the pulse of Hg^{2+} through the reservoir quickly enough. Verification of λ_l used pre- and post-1997 flood data collected by UNR (refer to Figure 1.2 for sampling dates and flow regimes). Excellent results suggest equation 1.4b is fairly robust and capable of modeling systematic trends seen in mercury water column concentrations. No calibration was attempted to match MeHg water column data. Modeled MeHg water column concentrations for June 10, 1995 are compared to observed

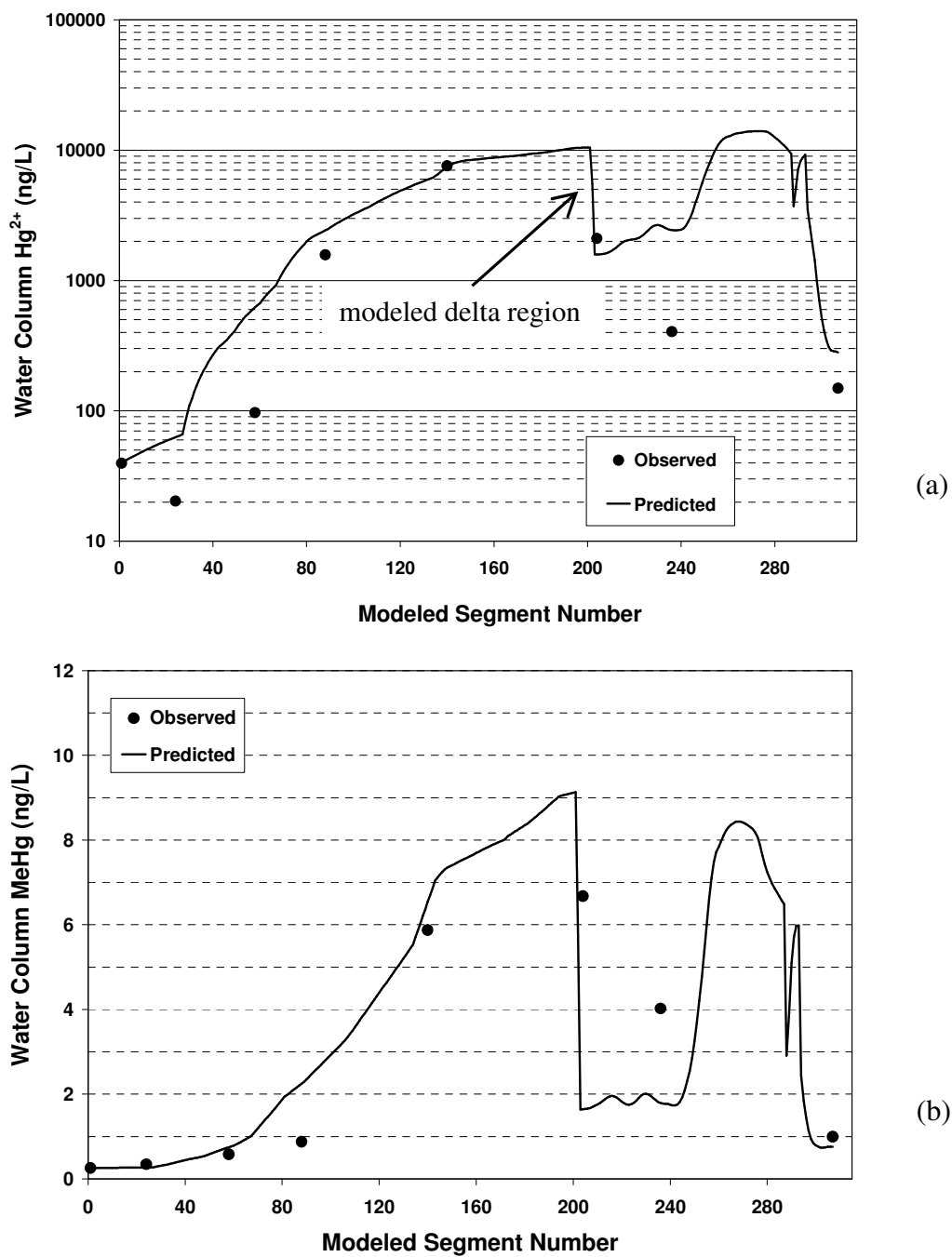


Figure 1.3: Water column mercury concentrations collected June 10, 1995 along the Carson River and Lahontan Reservoir, (a) Calibration of λ_i (Hg^{2+} bank concentrations) to best match observed Hg^{2+} water column concentrations, (b) comparison of modeled and observed MeHg with no calibration.

values in Figure 1.3b. Given no calibration,, modeled results show excellent correlation with observed concentrations. Similar to Hg^{2+} results, MeHg concentrations in the reservoir show a large pulse of MeHg. Lack of data in the reservoir prevents judgment on the existence of this pulse.

The Monte Carlo simulation was conducted running 500 realizations with confidence intervals calculated from ranked results. λ_l was varied $\pm 33\%$ from its calibrated value to assess uncertainty in Hg^{2+} and MeHg bank concentrations and their subsequent impact on water column concentrations due to bank erosion and bank diffusion processes. A triangle distribution was used with a mean (maximum probability of occurring) equal to the calibrated value (6,000 $\mu\text{g}/\text{kg}$) and the upper and lower bounds set to a probability of zero. On the other hand, a half-triangle distribution was used to define ψ_2 , with maximum probability set to the calibrated value (8,000 $\text{m}^2\cdot\text{s}/\text{kg}$) and 4,000 $\text{m}^2\cdot\text{s}/\text{kg}$ set to zero probability. This lower bound was established by matching the minimum estimated total mass eroded (*MER*) by Miller et al. (1999). Maximum values of each probability distribution function (*PDF*) were computed such that the area under each *PDF* equaled 1.0. Note that *MER*, as determined by ψ_2 and the amount of fine material deposited on the floodplain, as defined by the transport capacity (ψ_3), are indirectly related to each other. The relationship between these variables was developed (equation 1.5) by adjusting ψ_3 to match the highest observed washload concentration (2,250 mg/L at 514 m^3/s) given different values for ψ_2 . The resultant strong correlation ($r^2 = 0.99$) allows for excellent auto-calibration during the Monte Carlo simulation.

$$\Psi_3 = 1.96 \times 10^6 - 13.694(\Psi_2 - 40,000) \quad (1.5)$$

Setting the maximum limit of the ψ_2 distribution to the original calibrated value excludes the upper bound of *MER* as defined by Miller et al. (1999). This was done because Carroll et al. (2004) found the model over predicted washload deposition on the floodplain (i.e., transport capacity (ψ_3) was too small). To bias the Monte Carlo realizations toward less over-bank deposition, it was necessary, according to equation 1.5, to bias the model toward less bank erosion (i.e., smaller values of ψ_2).

Figure 1.4 shows that the resultant 80% confidence interval for expected variation due to bank erosion near FCH does not encapsulate all available data. Marked in Figure 1.4 are data collected during a flash flood event in Mineral Canyon (refer to Figure 1.1). Elevated Hg^{2+} and MeHg concentrations in the Carson River during this event are not related to modeled processes in the Carson River and, while shown in Figure 1.4, are excluded from analysis. Figure 1.4a shows bank erosion processes dominate Hg^{2+} inputs during spring melt (and rain-on-snow events) with peak Hg^{2+} concentrations occurring during over-bank discharge events. Hg^{2+} data collected prior to, and during, the 1997 flood fall within the estimated bounds. This includes the USGS sample flood, however, Hg^{2+} concentrations show a decreasing trend and the modeled 80% confidence interval falls below many Hg^{2+} concentrations during phases of spring discharge. In fact, with each overbank discharge event, the range in Hg uncertainty diminishes. The decrease in modeled Hg^{2+} concentrations and the narrowing of uncertainty with time is the result of shallower modeled depths due to channel width increases. The inability of the model to explain Hg concentrations following the flood implies an over prediction of bank erosion during the 1997. On the other hand, data not

encompassed by the 80% confidence interval during periods of low discharge most likely reflect uncertainty in channel bottom diffusion rates and not geomorphic processes.

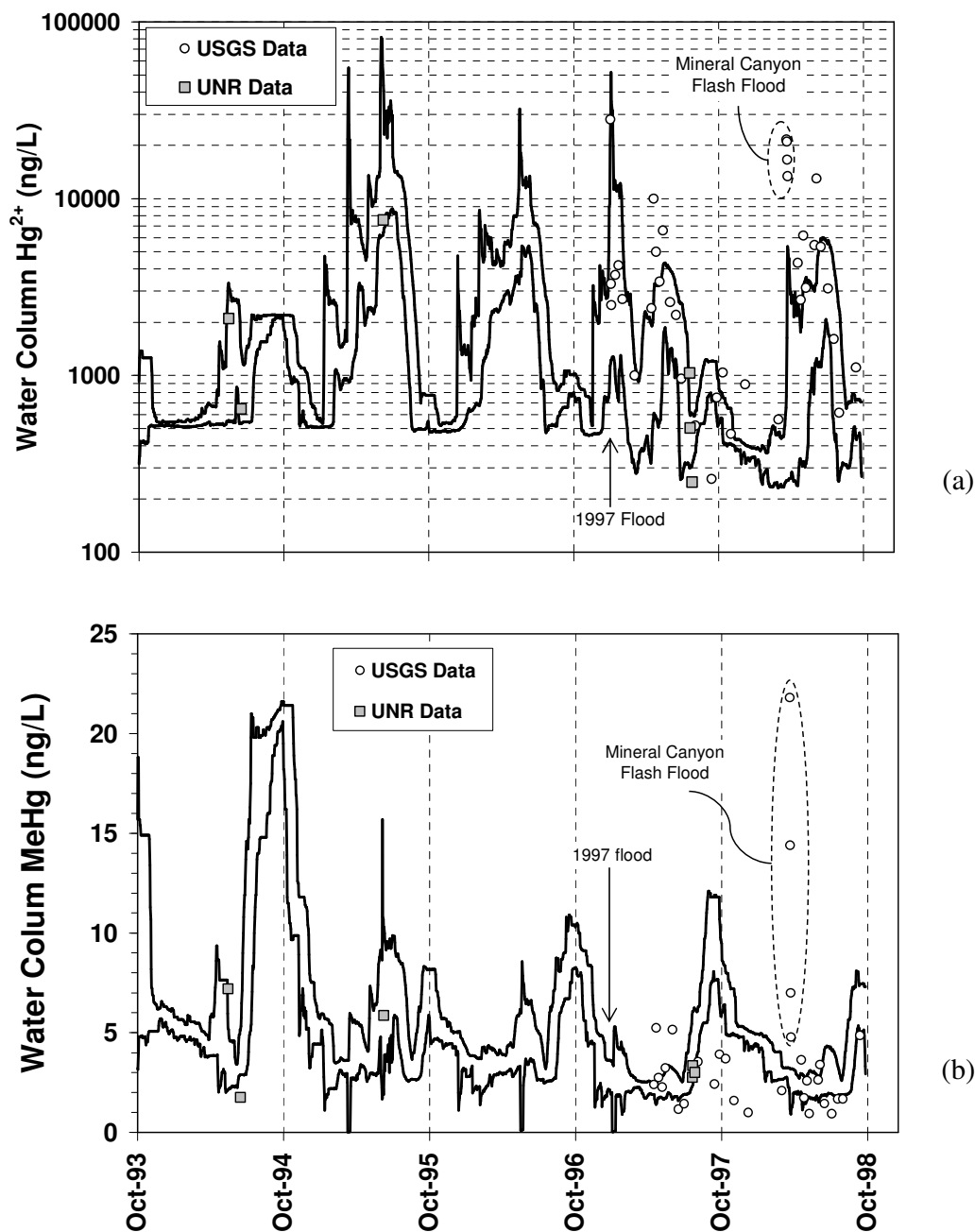


Figure 1.4: 80% confidence intervals given uncertainty related to geomorphic change near FCH for (a) Hg^{2+} and, (b) MeHg. Model results compared to data collected by UNR and the USGS.

Unlike inorganic mercury, modeled MeHg in the river's water column appears dominated by diffusion and not necessarily bank erosion processes. This is evident during the drought of 1994 when MeHg experiences its highest water column concentrations (Figure 1.4b) and the greatest range in the 80% confidence interval. The large range in uncertainty modeled in 1994 is a reflection of uncertainty in λ_l , the associated MeHg bank concentrations and resultant bank diffusion since significant bank erosion does not occur before or during 1994. In contrast, the second largest range in MeHg uncertainty occurs during the first over-bank flow event in 1995. This demonstrates that while diffusion appears more important, bank erosion is still a viable mechanism for MeHg loading to the river with significant impacts on MeHg water column concentrations. The 1997 flood event, which is so important to loading of Hg^{2+} , actually dilutes MeHg due to the flashy nature of the flood and the lag in peak MeHg bank concentrations relative to bank erosion. Similar to Hg^{2+} , however, modeled MeHg uncertainty decreases over time such that MeHg loading via bank erosion or bank diffusion diminishes with each successive over-bank flow event as a result of increased channel widths.

System-wide upper 80% bounds of uncertainty due to bank erosion processes are presented in Figure 1.5. The 1997 flood occurred on day 1193 in the simulation and model segment 304 represents the furthest upstream extent of Lahontan Reservoir. Settling of contaminated sediment at the reservoir delta causes a rapid decrease in mercury concentrations (Hg^{2+} and MeHg) and allows quick delineation of the delta region. During the drought of 1994 the reservoir (day 350 to 400) reverted back to river-status as it was nearly drained. Hg^{2+} and MeHg concentrations were relatively high

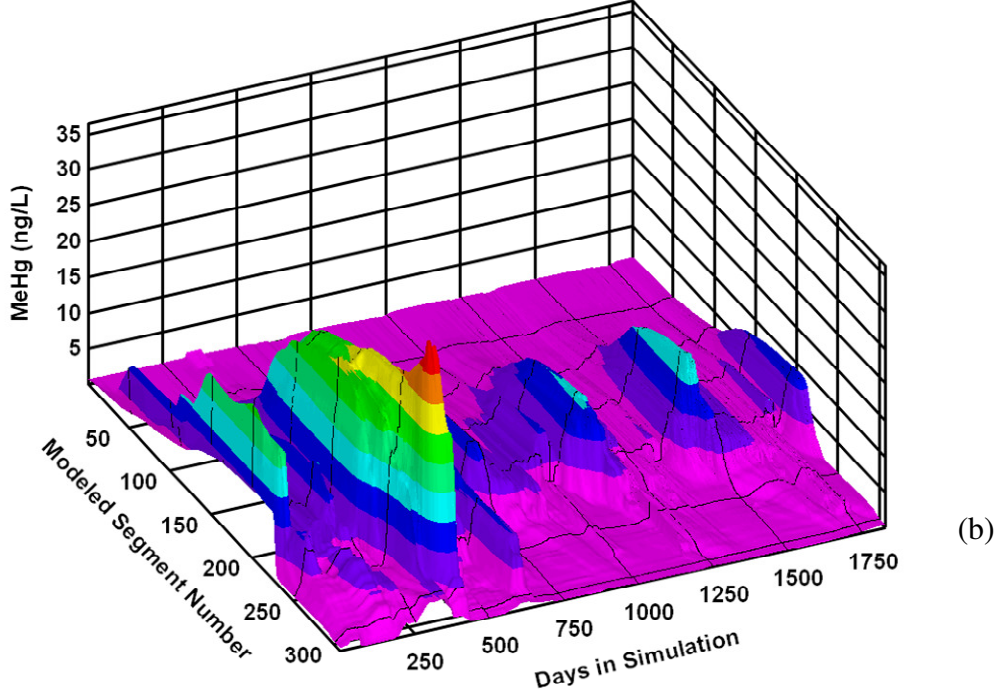
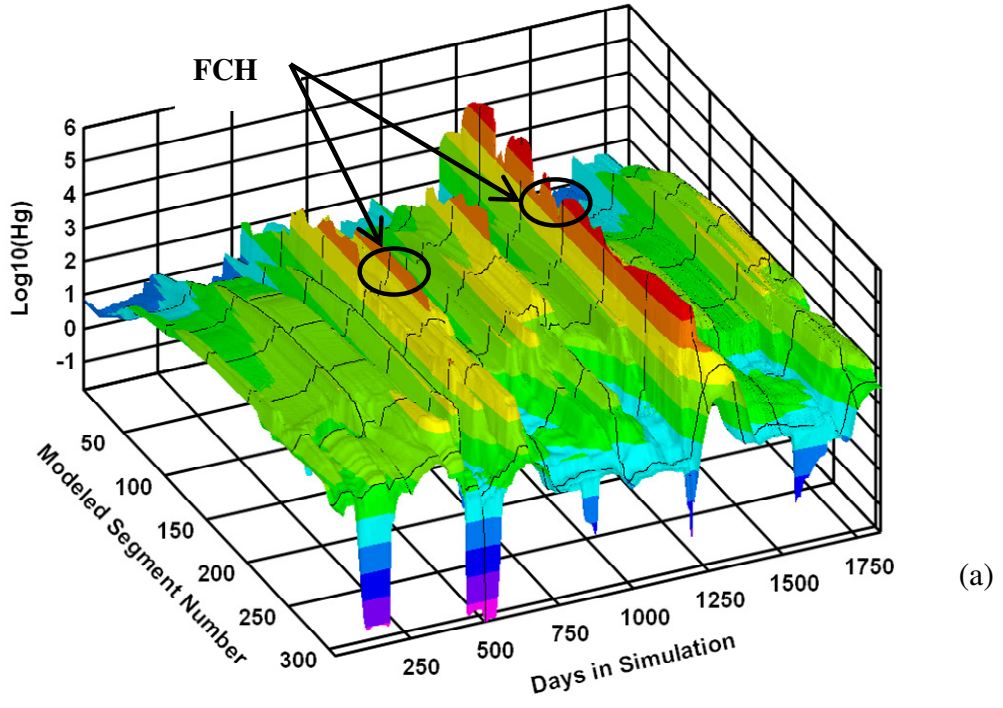


Figure 1.5: Upper 80% confidence interval for entire model domain over entire simulation given uncertainty in geomorphic changes to the river channel. (a) Hg^{2+} , (b) MeHg. Note that Hg^{2+} is plotted in log10-units.

throughout the reservoir during the drought since water column velocities remained high and sedimentation was limited. MeHg concentrations throughout the system were highest during the drought of 1994 with diffusion dominated loading (Figure 1.5b). MeHg concentrations during the 1997 flood were much lower as the result of dilution.

System-wide Hg^{2+} results (Figure 1.5a) agree, in part, with those presented for FCH in Figure 1.5a, such that erosion is important during 1995 when flows first go over bank, and to a lesser degree in 1996. However, system-wide, the 1997 flood appears the dominate Hg^{2+} loading event into the reservoir and not 1995 as suggested by FCH results. During the 1997 flood the Hg^{2+} upper 80% confidence interval is significantly elevated throughout most of the system, including the reservoir where velocities remained high despite the reservoir reaching its maximum capacity. The discrepancy between FCH results and system-wide results has to do with the very shallow channel bottom slope (S_0) defined at FCH and its indirect relationship to MER defined by equation 1.1. The FCH site, marked in Figure 1.5a, shows a significant dip in Hg^{2+} concentrations during the 1997 flood relative to steeper river segments above and below its location. A similar dip is not evident in 1995 during peak flows. FCH illustrates that segments with shallow river bottom slopes place greater emphasis on earlier over-bank flow events than steeper river segments.

1.5 CONCLUSIONS

In summary, uncertainty related to modeled geomorphic processes of bank erosion and overbank deposition describe observed variation in Hg^{2+} water column concentrations prior to and during the 1997 flood. The model places relatively greater

uncertainty in modeled behavior on earlier over-bank discharge events than later events. This is most evident in river reaches that have shallow channel slopes, which experience the greatest increases in channel widths during the earliest modeled over-bank flow events. Despite this limitation, the model is able to capture all of the measured variation in the Hg^{2+} concentrations during the 1997 flood arguably the largest Hg^{2+} loading event ever recorded in the Carson system. However, a change in the system appears to occur during the 1997 flood that is not adequately modeled since uncertainty in modeled parameters alone cannot explain Hg^{2+} variation following the flood.

MeHg loading appears dominated by diffusion as opposed to geomorphic changes to the river channel. Diffusion from river banks is indirectly included in the uncertainty analysis via the amount of Hg^{2+} (and subsequent MeHg) in the river banks. Bank diffusion appears as an important mechanism for MeHg loading as evidenced by the large amount of MeHg uncertainty in during the drought of 1994. However, its influence diminishes with time because of increased channel widths and the resultant decrease in river depths. Uncertainty in geomorphic channel change, including Hg^{2+} and MeHg bank concentrations, are not enough to capture observed variation in MeHg water column concentrations at FCH. Future work will need to include uncertainty in diffusion rates as well as methylation and demethylation rates to encompass all observed variability.

Acknowledgments

This work was partially funded by the National Science Foundation (EAR-9712857) and the Nevada Institute of Water Resources Research (NIWRR) contract number 06HQGR0098. The U.S. Geological Survey (USGS) contributed federal money while the Desert Research Institute provided matching support. The authors wish to thank

Ms. Karen Thomas (USGS Carson City) for sharing data and associated explanations from field observations.

References Cited

- Ambrose, R.B., Wool, T.A., Martin, J.P. and Schanz, R.W., 1991. WASP5.X: A Hydrodynamic and Water Quality Model: Model Theory, User's Manual and Programmer's Guide. U.S. E.P.A., Athens, Georgia.
- Bonzongo, J.C., Heim, K.J., Warwick, J.J. and Lyons, W.B., 1996. Mercury Levels in Surface waters of the Carson River-Lahontan Reservoir system, Nevada: influence of historic mining activities. *Environ Pollution*, 92(2): 193- 201.
- Carroll, R.W.H., Warwick, J.J., Heim, K.J., Bonzongo, J.C., Miller, J.R. and Lyons, W.B., 2000. Simulating Mercury Transport and Fate in the Carson River, Nevada. *Ecological Modeling*, 125:255-278.
- Carroll, R.W.H. and Warwick, J.J., 2001. Uncertainty analysis of the Carson River mercury transport model. *Ecological Modeling*, 137: 211-224.
- Carroll, R., Warwick, J.J., James, A., and Miller, J., 2004. Modeling Erosion and Overbank Deposition During Extreme Flood Conditions on the Carson River, Nevada. *Journal of Hydrology*. 297:1-21.
- Darby, S.E. and Thorne, C.R., 1996. Numerical simulation of widening and bed deformation of straight sand-bed rivers. I: Model development. *Journal of Hydraulic Engineering*, 122(4): 184-193.
- Foster, G.R., Flanagan, D.C., Nearing, M.A., Lane, L.J., Risse, L.M., and Finkner, S.C. 1995. Chapter 11: Hillslope erosion component. *In* USDA-Water Erosion Prediction Project (WEPP) Technical Documentation, NSERL Report No. 10, National Soil Erosion Research Laboratory, USDA-ARS-MWA, W. Lafayette, IN.
- Heim, K.J. and Warwick, J.J., 1997. Simulating sediment transport in the Carson River and Lahontan Reservoir, Nevada. *Journal of the American Water Resources Association*, 33(1): 177-191.
- Hoffman, R.J. and Taylor, R.L., 1998. Mercury and suspended sediment, Carson River basin, Nevada- loads to and from Lahontan Reservoir in flood year 1997 and deposition in reservoir prior to 1983. FS-001-98, USGS

- Hosseini-pour, E.Z. and Martin, J.L., 1990. RIVMOD: a one-dimensional hydrodynamic sediment transport model: model theory and user's guide. U.S. E.P.A, Athens, Georgia.
- Johnson, B.E., Julien, P.Y., Molnar, D. K., and Watson, C.W., 2000. The two-dimensional upland erosion model CASC2D-SED. *Journal of the American Water Resources Association* 36(1): 31-42.
- Martin, J.L., 1992. MERC4: A mercury transport and kinetics model: model theory and user's guide. U.S. E.P.A., Athens, Georgia.
- Meade, J.R., 1990. Movement and storage of sediment in rivers of the United States and Canada. In: M.G. Wolman and H.C. Riggs (Editors), *Surface water hydrology. The geology of North America*. Geological Society of America, Boulder, CO, pp. 255-280.
- Miller, J.R. and Lechler, P.J., 1998. Mercury partitioning within alluvial sediments of the Carson River valley, Nevada: implications for sampling strategies in tropical environments. In: J.W. et al. (Editor), *Geochemistry of tropical environments*. Springer-Verlag, pp. 211-233.
- Miller, J.R., Lechler, P.J., and Desilets, M., 1998. The role of geomorphic processes in the transport and fate of mercury in the Carson River basin, west-central Nevada. *Environmental Geology*, 33(4): 249-262.
- Miller, J.R., Barr, R., Grow, D., Lechler, P., Richardson, D., Waltman, K. and Warwick, J., 1999. Effects of the 1997 flood on the transport and storage of sediment and mercury within the Carson River valley, west-central Nevada. *Journal of Geology*, 107(3): 313.
- Smith, G.H. and Tingley, J.V., 1998. *The history of the Comstock Load, 1850-1997*. Nevada Bureau of Mines and Geology in association with the University of Nevada Press.
- Thomann, R.V. and Mueller, J.A., 1987. *Principles of Surface Water Quality Monitoring and Control*. Harper Collins Publishers, Inc, New York, NY, 549 pp.
- Walling, D.E. and He, Q., 1997. Investigating spatial patterns of overbank sedimentation of river floodplains. *Water, Air and Soil Pollution*, 99: 9-20.
- Warwick, J.J. and Heim, K.J., 1995. Hydrodynamic modeling of the Carson River and Lahontan Reservoir, Nevada. *Water Resources Bulletin*, 31(1): 67-77.

CHAPTER 2

Mercury Transport Model of the Carson River and Lahontan Reservoir System, Nevada: An Investigation of Total and Dissolved Species and Associated Uncertainty

Rosemary W.H. Carroll³, John J. Warwick⁴ and Greg M. Pohl³

Abstract

Four flow regimes are defined to capture significant mechanisms of mercury (Hg) loading for total and dissolved species. During extremely low flows, only gradient driven diffusion of Hg from the bottom sediments is modeled. At low flows, diffusion loading is augmented with turbulent mixing of channel bed material. Hg loading into the river during medium to higher flows is driven by bank erosion process, while Hg cycling during overbank flows is controlled by both bank erosion and floodplain deposition. Methylation and demethylation (M/D) occur in the channel and reservoir bed sediments as well as in channel bank sediments and are described by first order kinetic equations, with bank M/D adjusted for moisture history. Results for multi-criteria based GLUE simulations are compared to traditional (i.e., manual) calibration output. Model evaluation is done using conditions prior to, and after a substantial flood to determine if systematic changes occurred to Hg cycling as a result of the flood. Uncertainty is compared to observed variability in water column

³ Corresponding Author. Assistant Research Hydrologist, Division of Hydrologic Sciences, Desert Research Institute, 2215 Raggio Parkway, Reno, NV 89512 Rosemary.Carroll@dri.edu.

⁴ Vice President of Research, Desert Research Institute, Reno, NV 89512. John.Warwick@dri.edu

³Program Director, UNR Graduate Program of Hydrologic Sciences; Associated Research Professor, Desert Research Institute, Reno NV USA Greg.Pohl@dri.edu

concentrations based on species, flow regime and location in the system, and discussed in the context of GLUE applicability and relative uncertainty defined by first order – second moment analysis.

KEY WORDS: mercury, methylmercury, river transport model, GLUE, relative uncertainty

2.1 INTRODUCTION

The U.S. Environmental Protection Agency (US EPA) designated the Carson River and Lahontan Reservoir (CRLR) as a superfund site in 1991 for its contamination by mercury (Hg) as a result of historic mining practices. It is estimated that 6.36×10^6 Kg (7,000 tons) of residual Hg is distributed throughout the river bank sediments and floodplain deposits (Miller et al., 1998; Smith and Tingley, 1998) and offers a nearly inexhaustible source of contamination to the river/reservoir system. It has also been found that nearly 95% of the Hg transported through the Carson River is bound to sediments (Bonzongo et al., 1996a; 1996b). Consequently past modeling studies of the CRLR have focused on total inorganic Hg (THg) and total methylmercury (TMeHg), most of which is cycled through the river via sediment transport process of bank erosion and overbank deposition during higher flow events (Carroll et al., 2000; 2001). More recent modeling efforts of the Carson River have characterized geomorphic change caused by an extreme flood (Carroll et al., 2004) and its impact on Hg transport; with indication that a systematic change in Hg transport might have occurred as a result of this single event (Warwick and Carroll, 2008).

Prior modeling efforts along the CRLR system have focused less attention on the dynamic loading mechanisms of dissolved species (DHg and DMeHg). Yet it is the dissolved, or more specifically the solution phase (Tessier and Turner, 1995), species that may be bioavailable to plankton and transferred to higher trophic levels. The dissolved fraction is often defined as that fraction of Hg that remains after passing through a 0.45 μm filter. Several studies have found that significant portions of the Hg passed through a filter remained bound to colloids (Guentzel et al., 1996; Stordal et al., 1996) and therefore the dissolved fraction is not an exact surrogate for bioavailability. However, quantifying loading mechanisms of dissolved species is one step toward understanding and managing ecologic health of the system.

Loading of dissolved species is incorporated into the CRLR transport model presented by Warwick and Carroll (2008). Calibration strategies and uncertainty analysis are investigated to help isolate what components of the model are important in describing both total and dissolved Hg transport and how well those components are understood. In general, the goal of any uncertainty analysis is threefold. It is to find the best model to predict future events given the observed data that are available for model calibration, to quantify error associated with future prediction, and to quantify the impact of input parameter uncertainty to help guide model development (Stedinger et al, 2008). It is recognized that the complexity and over-parameterized nature of the CRLR transport model will exclude the idea of any single parameter group existing to uniquely define observed behavior. Instead, it is more probable that different parameter sets can produce equally good, or acceptable, model behavior. Beven and Binley (1992) introduced the generalized likelihood uncertainty estimate

(GLUE) as a methodology for model calibration and uncertainty analysis that incorporates this concept of equifinality in parameter sets. GLUE uses Monte Carlo simulation, or repetitive random selection of parameter groups, and evaluates model performance based on a likelihood function defined by the model user.

The primary objective of this study is to produce a fully dynamic transport model of total and dissolved Hg species for the CRLR system at all flow regimes. In the construction and utilization of this model several questions are asked in an effort to grasp what components of Hg transport are well understood and subsequently well characterized, and what components in the model remain poorly modeled and/or highly uncertain. These questions include:

- Can the CRLR transport model capture Hg concentrations and trends in total and dissolved species?
- Is the GLUE methodology an appropriate method to calibrate and evaluate uncertainty along the CRLR?
- Did the system fundamentally change as a result of a massive flood?
- How does uncertainty change based on species, flow and location, and what model input parameters contribute most to prediction uncertainty?

2.1.1 Site Description

The Carson River flows eastward out of the Sierra Nevada Mountains just to the south of the Lake Tahoe Basin through a series of alleviated valleys and canyons until reaching the Carson Playa, a large hydrologically closed basin in the Carson Desert. Figures 2.1 and 2.2 illustrate the extent of the Carson River watershed (8084 km²) with several U.S. Geological Survey (USGS) and University of Nevada, Reno

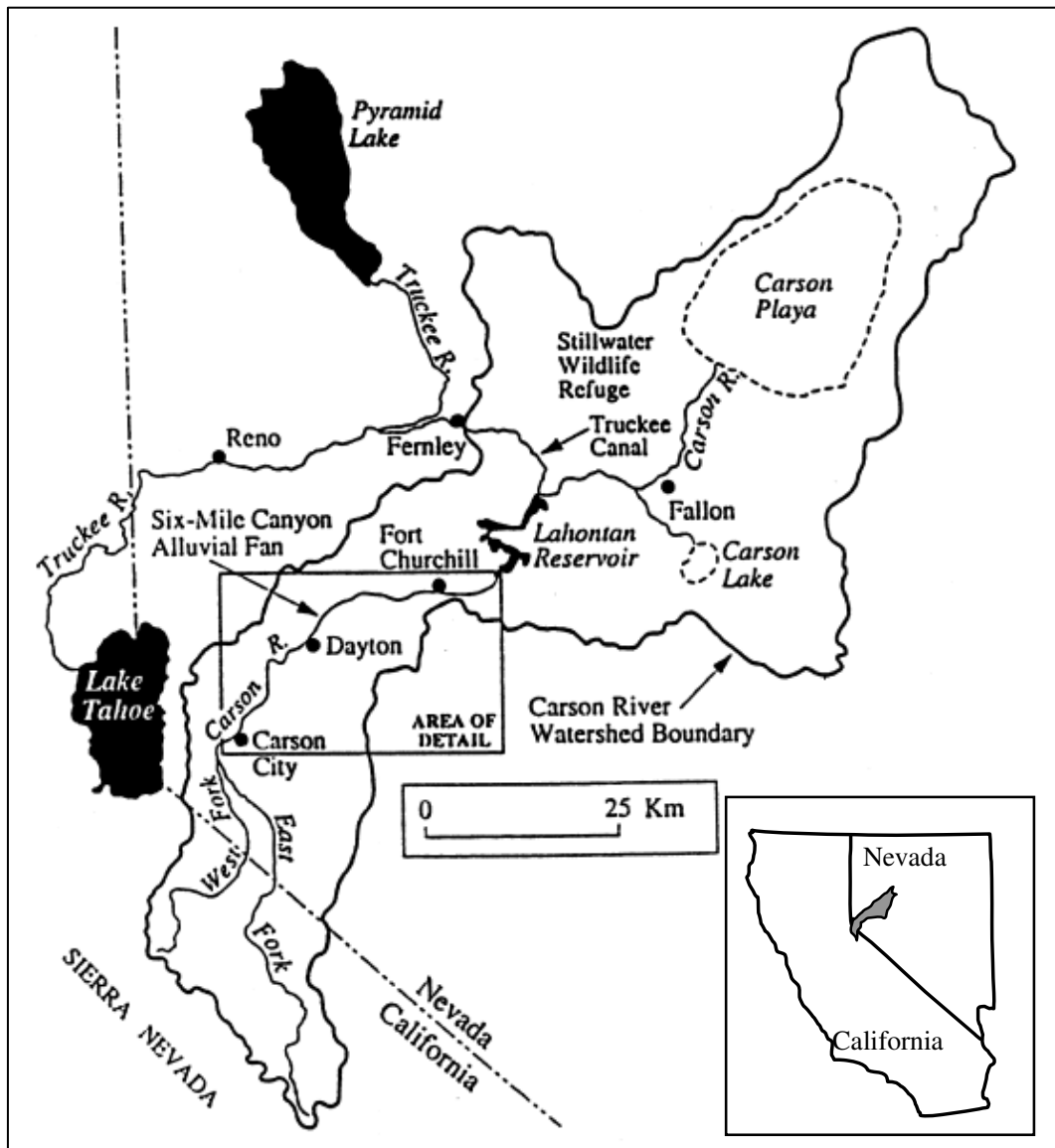


Figure 2.1: The Carson River – Lahontan River (CRLR) watershed with inset showing location of the watershed with respect to California and Nevada. The section of the river outlined with a box (from Carson City to Lahontan Reservoir) is detailed in Figure 2.2.

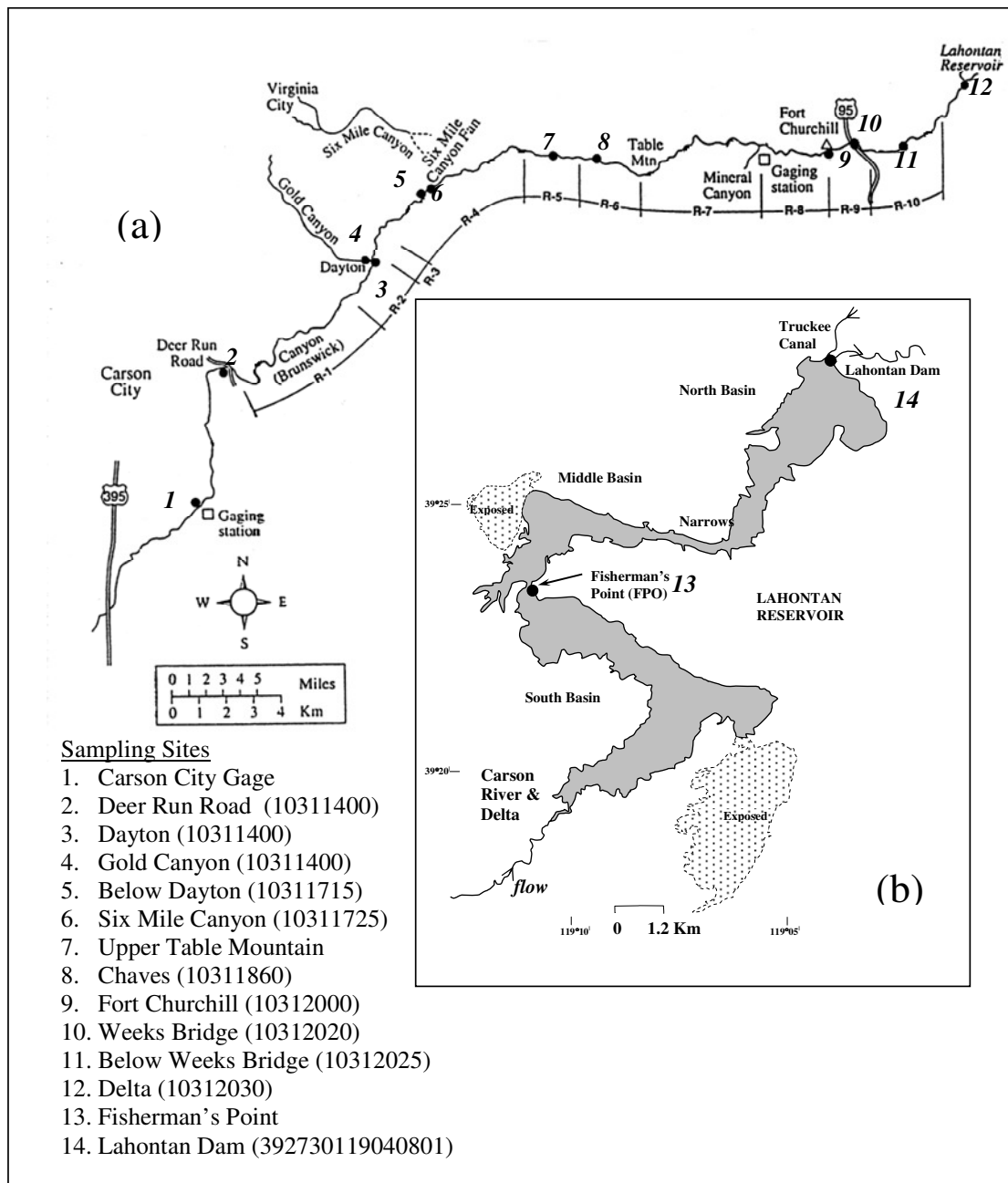


Figure 2.2: Details of the CRLR model domain with respect to the (a) river and (b) reservoir. Sampling sites marked as 1 to 14 with USGS gage numbers provided where appropriate. The 10 river reaches defined by Miller et al. (1999) are identified in (a).

(UNR) sampling locations marked. The section of the basin under concern extends from the USGS gaging station near Carson City (site 1 in Figure 2.2) down to Lahontan Dam (site 14). Lahontan Reservoir was constructed in 1915 and is used to irrigate fields in Lahontan Valley and is managed as a warm water fishery. Lahontan Reservoir consists of three distinct basins with water from the Carson River entering the south basin and moving northward through the middle basin and into the north basin. The north basin terminates at Lahontan Dam with inputs from the Truckee Canal occurring at the north side of the dam. Narrow channels connect each of the basins and are marked as Fisherman's Point, connecting the south and middle basins (site 13) and the Narrows, connecting the middle and north basins.

Flow in the Carson River is typical of most semi-arid fluvial systems in that it is highly variable. Flow is predominately from snowmelt in the Sierra Nevada with peak discharge occurring in the spring with a sustained moderately high hydrograph. Large floods, however, are generated with rain-on-snow events that occur during the winter months (e.g., the 1997 flood). The summer and fall months are dominated by low flows and these flows can cease all together during extended periods of drought. The modeled hydrograph at Fort Churchill (site 9) is given in Figure 2.3 with the 1997 flood marked for reference. Two separate model simulations are conducted in this study. The pre-flood simulation extends from February 1991 until February 1997 and includes the 1997 flood. Pre-flood dates are determined by arial photographs that help constrain changes channel morphology caused by the flood (Carroll et al., 2004). The post-flood simulation begins in February 1997 and continues through December

2008 to encompass a wide range of flow scenarios partnered with data collected by the USGS.

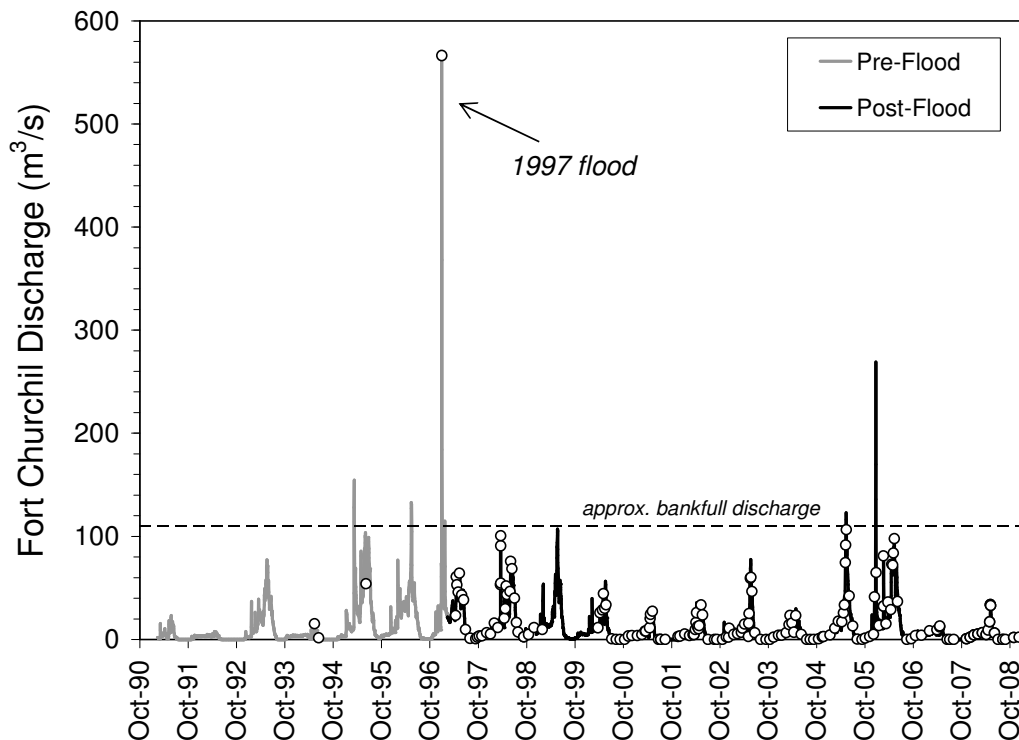


Figure 2.3: Modeled mean daily discharge at the Fort Churchill gaging station (site 9, Figure 1). The January 1997 flood is the largest recorded event on the Carson River given a 100 year record. Model runs are sectioned into pre-flood and post-flood. White circles = water quality sampling dates.

2.2 MODELING APPROACH

Three computer models (RIVMOD, WASP5 and MERC4) simulate the transport of sediment and Hg in the Carson River. RIVMOD (Hosseini-pour and Martin, 1990) is a US EPA 1-dimensional hydrodynamic and sediment transport routine that simultaneously solves standard fluid equations of continuity and momentum. Finite difference equations are solved by the Newton-Raphson method to determine fluid velocity and depth given unsteady flow conditions. WASP5

(Ambrose et al., 1991) is the US EPA Water Quality Analysis Simulation Program-5 that was developed to simulate the transport and transformation of various water body constituents. Mass balance equations account for all material entering and leaving model segments through direct and diffuse loading, advective and dispersive transport, and any physical or chemical transformation.

MERC4 (Martin, 1992) is a subroutine contained within WASP5. It was developed to specifically compute mercury speciation and kinetic transformation. MERC4 is capable of simulating up to four mercury species and three distinct solid types. Five state variables are modeled in this study: inorganic mercury, MeHg, washload, coarse suspended sediment (CSS) and bedload. Washload constitutes the smallest fraction (diameter < 63 μm) and is considered uniformly distributed from the riverbed to the water surface. Concentrations of CSS (diameter > 63 μm) are greatest near the riverbed and diminish upward toward the water surface. USGS sampling techniques obtain a flow weighted mean of CSS for use in the one-dimensional CRLR transport model. Bedload is the third type of solid modeled. It is defined as coarse material that travels by rolling, skipping and/or sliding along the riverbed. A full description of bedload transport modeling strategies is provided by Carroll et al., 2000.

RIVMOD, WASP5 and MERC4 were originally chosen, linked and modified by Warwick and Heim (1995) and Heim and Warwick (1997), with further modification by Carroll et al. (2000), Carroll et al. (2004) and Warwick and Carroll (2008). It is acknowledged an updated WASP7 and Hg module exist, however dynamic linking of WASP5 with RIVMOD as well as extensive code modifications

to WASP5 done by previous studies prohibit its use. While an attempt has been made to briefly summarize modeling procedures that are explicitly used in this research, one is encouraged to refer to previous studies for a complete discussion on model development.

2.2.1 Past Studies of CRLR Mercury Transport Modeling

Early alterations to RIVMOD include a revision of the simple rectangular channel geometry to a more complex shape (Warwick and Heim, 1995). Cross sectional geometry was assumed spatially variable but temporally fixed and the divided channel approach was applied to estimate floodplain depths and velocities during overbank flows (Carroll et al., 2000). Carroll et al. (2004) modified RIVMOD to compute dynamic width adjustment in which the modeled mass eroded updated the channel width every timestep by assuming the entire vertical face of the bank was susceptible to erosion.

Carroll et al. (2004) developed an empirical relationship in WASP to describe bank erosion during in-channel and overbank flows as well as overbank deposition of CSS and washload material. A brief review is provided here since calibration strategies are slightly different than presented in the original publications. The rate of bank erosion is proportional to the shear stress applied to the bank (Darby and Thorne, 1996) and is indirectly related the average velocity, or square-root of the channel bottom slope. Using Manning's wide channel assumption, the relationship for bank erosion is,

$$MER = \frac{\psi_1 \rho_s \gamma_w n^2 D^{2/3} v^2 L_s}{S_0^{1/2}} + \frac{\psi_2 \rho_s \gamma_w n^2 (D-h) v^2 L_s}{h^{1/3} S_0^{1/2}} \quad (2.1)$$

where MER is the total bank mass eroded (kg) γ_w is the specific weight of water ($kg/m^2/s^2$), h is the height of the vertical bank face along the river's edge (m), D is the water depth starting at the vertical face of the channel bank (m), S_0 is the channel bottom slope, v is the water velocity (m/s), n is Manning's coefficient, L_s is the segment length (m) in the downstream direction, and ψ_1 and ψ_2 are constants of proportionality ($m^2 \cdot s/kg$). The first term on the right-hand-side of equation 2.1 is used to model mass eroded from the banks when river discharge is below bankfull ($D = h$), while both terms on the right-hand-side of equation 2.1 are used to model mass eroded during overbank discharge. ψ_1 is adjusted to best match observed washload concentrations at site 9 when flows are below bankfull discharge and ψ_2 is adjusted to match the observed total mass eroded between February 1991 to February 1997 (Miller et al., 1999). Carroll et al. (2004) used a spatially homogenous cross sections as an initial condition for calibration.

Warwick and Carroll (2008) implemented a spatially variable inorganic Hg bank concentration ($[Hg]_{bk}$) shown in equation 2.2,

$$[Hg]_m = \frac{\lambda_1}{S_0^{0.5}} \quad (2.2a)$$

$$[Hg]_{bk} = [Hg]_b + \frac{([Hg]_m - [Hg]_b)D}{2h} \quad (2.2b)$$

where λ_1 ($\mu g/kg$) is a calibration parameter adjusted to match THg water column concentrations during higher flow regimes, $[Hg]_m$ is the maximum inorganic bank mercury concentration ($\mu g/Kg$), $[Hg]_b$ is the measured channel bed inorganic mercury concentration in the model bed segment coincident with a bank segment ($\mu g/Kg$). It is also assumed that banks related to the low flow inner channel as well as the low to

medium flow transition slope (roughly flow depths less than 1 m, refer to Carroll and Warwick, 2001) have $[Hg]_{bk}$ equal to channel bottom sediments.

Laboratory experiments found methylation activity nonexistent when the bank soils are dry but quickly became significant after approximately four days of soil saturation (Dr. Mark Hines, University of Massachusetts, Lowell, <http://biogeochemistry.uml.edu/pages/Hg.html>). Consequently, the bank package developed by Warwick and Carroll (2008) tracks the depth that the vertical bank is saturated for four or more consecutive days and establishes the average inorganic mercury concentration used to generate MeHg in the bank sediments based off of this depth (equation 2.2b). TMeHg in the bank sediments is calculated from the fraction of pore water inorganic Hg available for methylation which is based on the computed THg in the banks, user defined adsorption coefficients, and the methylation and demethylation rates given for bank segments. Rapid increases in flow cause a dilution of in-stream TMeHg concentrations since TMeHg bank concentrations do not increase sufficiently by the time of significant erosion. On the other hand, if river flows rise more gradually, such that a majority of the bank sediments are saturated for four or more days, then the concentration of TMeHg in the banks is substantial and TMeHg mass loading rates into the river are large.

2.2.2 Flow Regimes and Modeled Mercury Loading Mechanisms

To capture significant mechanisms of Hg loading for total and dissolved species at all flow regimes the following flow categories and associated loading mechanisms are defined below.

Extremely Low Flow: Extremely low flows occur when the channel flow velocity is less than a critical velocity (v_c) of 0.18 m/s, as determined by Hjulstrom (1935) for the minimum velocity required to erode and transport the observed course bottom sediment (diameter = 130 μm) found along the Carson River (Carroll et al., 2000). Critical velocity corresponds to a discharge of approximately equal to 3 m^3/s . For extremely low flows, only gradient driven diffusion of mercury from the bottom sediments is modeled. Diffusion is defined in WASP5 with equation 2.3,

$$\frac{\partial M}{\partial t} = \frac{E A \eta}{d \eta} \left[\frac{C_b}{\eta} - C_w \right] \quad (2.3)$$

where M is total mass (g), t is time (s), A is interfacial area between the channel bottom and overlying water column (m^2), η is porosity, C_b and C_w are the dissolved chemical concentrations in the channel bed sediments and overlying water column, respectively (mg/L or g/m^3), d is the characteristic mixing distance (m) between the bed and the water column, E is the diffusion coefficient (m^2/s). Positive flux is mass loading into the water column and negative flux is mass movement into the bed sediment pore water.

The surface area (A) is dependent on the cross sectional geometry and the hydraulic characteristics calculated in RIVMOD. The characteristic mixing distance is defined as the length in the upper surface of the bed segment that allows a chemical gradient to form between the bed pore water to the sediment-water interface. This value is set at 0.05 m everywhere (Gandhi et al., 2007). A diffusion coefficient (E) in water for most common organic solvents, including Hg, generally ranges from $1.00 \times 10^{-11} \text{ m}^2/\text{s}$ to $1.0 \times 10^{-9} \text{ m}^2/\text{s}$ (Cussler, 1976; Reid et al., 1977).

Low Flow: Low flow is defined when velocities are greater than or equal to v_c , but flows are still low enough that bank erosion is not significant (estimated 3 m³/s to 10 m³/s). Channel bed movement occurs such that diffusive mass loads in equation 2.3 are augmented with THg and TMeHg loads derived from turbulent mixing of the bed material as described with equation 2.4a and 2.4b, respectively.

$$\frac{\partial M_{THg}}{\partial t} = B_f [v - v_c] A C_b^T (1 - f_b) \quad (2.4a)$$

$$\frac{\partial M_{TMeHg}}{\partial t} = B_f [v - v_c] A C_b^T \quad (2.4b)$$

where M is total mass (g) of mercury leaving the channel bed and entering the overlying water column, v is the modeled flow velocity of the water column segment (m/s), B_f is a velocity correction factor (dimensionless) and C_b^T is the concentration of the total species in the bottom sediments (mg/L, or g/m³). Particulate loading of Hg is adjusted $(1 - f_b)$ where f_b (dimensionless) is the fraction of DHg in the bed segment. An increase in f_b increases the relative contribution of DHg in the water column compared to particulate sources. Including f_b is necessary to reduce the level of predicted DHg dilution and better fit observed data.

Medium & High Flows: Mercury loading into the river during medium and high flow events is dominated by bank erosion processes, but flows remain within the river's channel. Bankfull discharge is approximately 110 m³/s. The modeling approach presented by Warwick and Carroll (2008), and presented in section 2.2.1, is maintained in this study. The only modification made to the model is the inclusion of DHg loading into the river with bank erosion. Observed DHg shows concentrations increase during medium to high flows and supports this conceptual model. To mirror

f_b in the river bed, an additional term (ϕ_b , dimensionless) defines the fraction of THg that is dissolved in the river banks.

$$\frac{\partial M_{THg}}{\partial t} = MER \cdot [Hg]_{bk} \cdot (1 - \phi_b) \cdot 10^{-6} \quad (2.5)$$

M is mass loading from the banks (g), MER (Kg) and $[Hg]_{bk}$ ($\mu g/kg$) are computed via equations 2.1 and 2.2b, respectively. A factor of 10^{-6} is added to be dimensionally correct.

Overbank Flows: Mercury cycling during overbank flows is dominated by bank erosion as well as floodplain deposition. Calibration strategies done in past studies that relate to both bank erosion and overbank deposition during overbank flows (Warwick and Carroll, 2008) are maintained in this research. However, massive amounts of modeled THg entering the river during overbank flows necessitated a new approach to dealing with Hg associated with eroded sediment and the relative amount of DHg in relationship to these contaminated particles. Contaminated sediment particles are allowed to settle on the floodplain (or in reservoir) when velocities are slow enough.

In the model, designated adsorption coefficients partition Hg almost entirely to washload material, which is not always the case given the history of Hg contamination along the CRLR system. Instead, THg originates from the Comstock mining operation and includes Hg associated with mill tailings and amalgam grains, not just fine sediment. Miller et al. (1999) observed Hg concentrations associated with overbank CSS deposits (as a result of the 1997 flood) are approximately one-fourth those measured in fine grained deposits. To adjust for Hg associated with CSS, Stokes settling velocities are augmented by a correction factor (σ_f) with the

assumption that mercury laden particles are slightly heavier than uncontaminated sediment and will settle at a faster rate. A σ_f greater than 1.0 computes a settling velocity greater than uncontaminated washload, while a σ_f equal to 13.0 allows contaminated fines to settle at the same rate as CSS. A similar algorithm is not implemented for MeHg since MeHg is the byproduct of sulfur reducing bacteria transforming Hg in sediment pore waters after deposition. Therefore, MeHg is associated with fine particles only.

2.2.3 Methylation and Demethylation

Methylation of DHg and demethylation of DMeHg occurs in the channel and reservoir bed sediments as well as the channel bank sediments and are described by the first order kinetic equation 2.6:

$$\frac{\partial[C_p]}{\partial t} = f_{temp} K_{20}[C_r] \quad (2.6)$$

where $[C_p]$ and $[C_r]$ are the dissolved concentrations of the product and the reactant within the model segment respectively (mg/L), t is time (day), K_{20} the reaction rate (day^{-1}) and f_{temp} is a temperature multiplier to correct for temperatures deviating from 20° C (dimensionless). The temperature multiplier is given by the following relationship:

$$f_{temp} = Q_{10}^{\frac{T-20}{10}} \quad (2.7)$$

where T is the ambient water temperature (°C) and Q_{10} is a temperature coefficient. The K_{20} and Q_{10} allow one to solve for the methylation/demethylation (M/D) ratio throughout the year based on temperature. Q_{10} is defined with CRLR sediment

samples as 2.03 and 2.32 for methylation and demethylation, respectively (Heim, 1996). The ratio of methylation to demethylation K_{20} collected within the CRLR channel bottom sediments is provided in Table 2.1 with the assumption that bank sediment rates are equal to those in the channel bed sediments. The upper reservoir is defined as the delta region and the southern basin. The lower reservoir encompasses the middle and north basins of the reservoir (refer to Figure 2.2).

2.2.4 Generalized Likelihood Uncertainty Estimate

The GLUE methodology (Beven and Binley, 1992) is used with model performance based on the root mean squared error (*rmse*) objective function for all Hg water column data collected along the CRLR system. These data are divided into different criteria based on species, flow regime and location, with criteria and the number of observed data per criteria given in Table 2.2. The reservoir is only evaluated in terms of dissolved species since the model does not account for sediment resuspension or algal growth and Hg assimilation in estimating total species concentrations. To avoid bias toward any single criteria, and to promote a balanced aggregate of all criteria, the multi-criteria objective function presented by Blasone et al. (2008) is incorporated into the GLUE approach,

$$F_j(\vec{\theta}_j) = \sum_{i=1}^{ncrit} \frac{Q_i(\vec{\theta}_j)}{(Q_i)_{\min}} \quad (2.8)$$

where *ncrit* is the total number of criteria used in the objective function based on those criteria with data, $F_j(\vec{\theta}_j)$ is the aggregate objective function for the j^{th} randomly selected parameter vector $\vec{\theta}$, $Q(\vec{\theta}_j)$ is the *rmse* for the i^{th} criteria given the

Table 2.1: Description of parameters used in the CRLR model with traditional calibration values and associated strategies.

	Parameter	units	Description	Value	Calibration	verification
Geomorphic	ψ_1	m ² s/Kg	constant of proportionality for bank erosion	150	washload conc at site 9	none ^a
	ψ_2	m ² s/Kg	constant of proportionality for bank erosion	140,000	total MER into reservoir from 1991 to 1997	channel width changes 1991 to 1997
Mercury Transport	σ_f	none	adjusts Stoke's settling velocity of Hg laden washload on the floodplain and in the reservoir	7.8	mean THg during 1997 flood site 10	none ^b
				5,000 (pre)	THg at medium flow site 9	THg at high flow site 9
	λ_1	µg/Kg	maximum THg concentrations in the river banks	19,000 (post)	minimize post-flood THg rmse ^c at site 10	post-flood trend in THg with respect to flow site 10
	B_f	none	velocity correction factor for turbulent mixing of bed material	1x10 ⁻⁹	THg pre-flood low flow site 9	THg post-flood low flow site 10
	f_b	none	fraction of dissolved THg in bed sediments	0.03	DHg post-flood low flow site 10	Percent THg dissolved site 10
	ϕ_b	none	fraction of dissolved THg in bank sediments	0.002	DHg post-flood med-high flow site 10	Percent THg dissolved site 10
	d_{riv}	m	diffusional distance in river sediments	0.05	literature ^d	post-flood DMeHg site 10
	d_{res}	m	diffusional distance in reservoir sediments	0.05	literature ^d	post-flood DMeHg site 13 & 14
	E	m ² /s	diffusion coefficient	1.5x10 ⁻¹¹	minimize post-flood DMeHg rmse site 10	post-flood trend in DMeHg with respect to flow site 10
Biogeochemical^e	M/D _{bed & bank}	none	channel bed and bank sediments	0.00915	observed ^f	pre- and post-flood DMeHg & TMeHg
	M/D _{up}	none	upper reservoir sediments	0.01160	observed ^g	pre- and post-flood DMeHg & TMeHg
	M/D _{low}	none	lower reservoir sediments	0.00160	observed ^g	pre- and post-flood DMeHg & TMeHg

^aall washload data used in calibration rating curve

^boverbank data only collected during 1997 flood

^croot mean squared error

^dratio of methylation to demethylation K₂₀ rate coefficients

^eGandhi et. al., 2007

^fHeim, 1996

^gGandhi et. al., 2007; M. Marvin-DiPasquale (unpublished data)

Table 2.2: Break down of the multi-criteria objective function based on species, location and flow regime. The number of samples is provided for each criteria. If the number of samples is zero for a given criteria, then that criteria is not included in the global function.

Criteria	Species	Location	Flow	# of Data	
				Pre-Flood	Post-Flood
1	THg	River	Ext Low	6	65
2	THg	River	Low	0	67
3	THg	River	Med-High	17	123
4	THg	River	Overbank	3	0
5	DHg	River	Ext Low	6	64
6	DHg	River	Low	0	66
7	DHg	River	Med-High	11	115
8	DHg	River	Overbank	0	0
9	TMeHg	River	Ext Low	6	51
10	TMeHg	River	Low	0	68
11	TMeHg	River	Med-High	10	121
12	TMeHg	River	Overbank	0	0
13	DMeHg	River	Ext Low	6	52
14	DMeHg	River	Low	0	67
15	DMeHg	River	Med-High	10	120
16	DMeHg	River	Overbank	0	0
17	DHg	Reservoir	NA	6	9
18	DMeHg	Reservoir	NA	5	9
G	Global	All	All	86	997

parameter set $\vec{\theta}$. $(Q_i)_{\min}$ is the minimum computed rmse for the i th criteria given all realizations. The resultant likelihood function for $\vec{\theta}_j$, given total realizations (J), is compared to the vector of observed data \vec{Y} with,

$$L_j(\vec{Y}|\vec{\theta}_j) = \frac{1}{c} \cdot \left(\frac{1}{F_j(\theta_j)} \right)^N \quad (2.9)$$

The constant c normalizes the likelihood function such that $\sum_{j=1}^J L_j(\vec{Y}|\vec{\theta}_j) = 1$.

Within equation 2.9, N is a subjective shape factor often used in a GLUE likelihood function to tighten or widen estimated confidence intervals (CI). As N approaches 0, the likelihood function yields equal likelihoods (or weights) for all realizations ($1/J$) and GLUE is analogous to traditional Monte Carlo analysis. As N approaches infinity, the best fitting realization obtains a likelihood value of 1.0, and all other realizations receive a weight of 0, and the problem is equivalent to an inverse solution. For this study, N is set equal to 1 to mimic Blasone et al. (2008) and establish a conservative approach in CI estimates used in other studies (e.g., Morse and Pohll, 2003). The resultant likelihood function in equation 2.9 then modifies the input parameter's prior distribution (L^0) using Bayes Theorem to produce a posterior input distribution defined by observed data,

$$L_j(\bar{\theta}_j|\bar{Y}) = \frac{L_j(\bar{Y}|\bar{\theta}_j)L_j^0(\bar{\theta}_j)}{\kappa} \quad (2.10)$$

$$\kappa = \sum_{j=1}^J L_j(\theta_j|Y)L_j^0(\theta_j) \quad (2.11)$$

where κ is a normalizing constant to ensure the posterior CDF equals unity. The 95% CI is computed by summing the ranked likelihood values to 0.025 and 0.975 for the lower and upper bound, respectively. GLUE estimated mean (μ_l) and standard deviation (σ_l) for the l^{th} input parameter in j^{th} realization (or parameter set) are computed using the likelihood function as follows,

$$\mu_l = \sum_{j=1}^J [L_j(\bar{Y}|\bar{\theta}_j) \cdot \theta_{j,l}] \quad (2.10)$$

$$\sigma_l = \sum_{j=1}^J [L_j(\bar{Y}|\bar{\theta}_j) \cdot (\theta_{j,l} - \mu_l)^2] \quad (2.11)$$

To test for statistical differences between pre- and post-flood estimated means, normality is assumed ($J > 30$) and the t-test is used,

$$t_k = \frac{|\mu_{k,pre} - \mu_{k,post}|}{\sqrt{\frac{\sigma_{k,pre}^2}{J_{pre}} + \frac{\sigma_{k,post}^2}{J_{post}}}} \quad (2.12)$$

The null hypothesis is that no statistical difference occurs between means estimated before the flood and those estimated after the flood. The hypothesis is rejected at a significance level of 95%, or $\alpha = 0.05$.

2.2.5 Relative Uncertainty

Relative uncertainty (U) is computed for each input parameter (θ_l) using the first-order second-moment (FOSM) approach,

$$U_{i,l}(\vec{Y}|\theta_l) = \sigma_l^2 \left(\frac{dQ_{i,l}}{d\theta_l} \right)^2 \quad (2.13)$$

Input parameters are evaluated independently by adjusting the calibrated value presented in Table 2.1 by $\pm 1\%$ and using the GLUE derived standard deviation. Linearity is required for first-order analysis. The small percentage adjustment in parameter values is an attempt to maintain linearity in model response by limiting the range in which it's asked to perform. Relative uncertainty is computed for all data, or the global criteria, as well as for each subset of data defined in Table 2.2.

2.3 RESULTS

2.3.1 Model Calibration and Verification

Parameters of interest are listed and described in Table 2.1 with a description of traditional calibration strategies and verification provided. Table 2.3 couples transport parameters and Hg species as a function of flow regime used in the calibration process. Observed M/D values are used in the model and no calibration is performed for MeHg species. While similar strategies to Carroll et al. (2004) are employed for the geomorphic/sediment transport calibration of ψ_1 and ψ_2 , homogenous cross sections are replaced by observed channel widths as initial conditions.

Table 2.3: Mercury transport parameters used to calibrate mercury species as a function of flow regime. NC = no calibration.

Species	Flow Regime	Parameter
THg	extremely low	NC
	low	B_f
	medium to high	λ_1
	overbank	σ_f
DHg	extremely low	E
	low	f_b
	medium to high	ϕ_b
	overbank	NC
TMeHg	extremely low	NC
	low	NC
	medium to high	NC
	overbank	NC
DMeHg	extremely low	NC
	low	NC
	medium to high	NC
	overbank	NC

Updated values for ψ_1 and ψ_2 are provided in Table 2.1. Verification of the approach is provided in Figure 2.4 and compares modeled and observed channel width changes from 1991 to 1997 for the 10 individual river reaches (refer to Figure 2.2, detail of the river). Nine of the 10 reaches are accurately modeled, and bank erosion trends in the downstream direction are replicated with a 99% level of significance based on a spearman rank coefficient (r_s) equal to 0.83. Modeled behavior of reach six is the only reach with notable difference compared to the observed mean. Miller et al. (1999) found that the largest increases in channel width

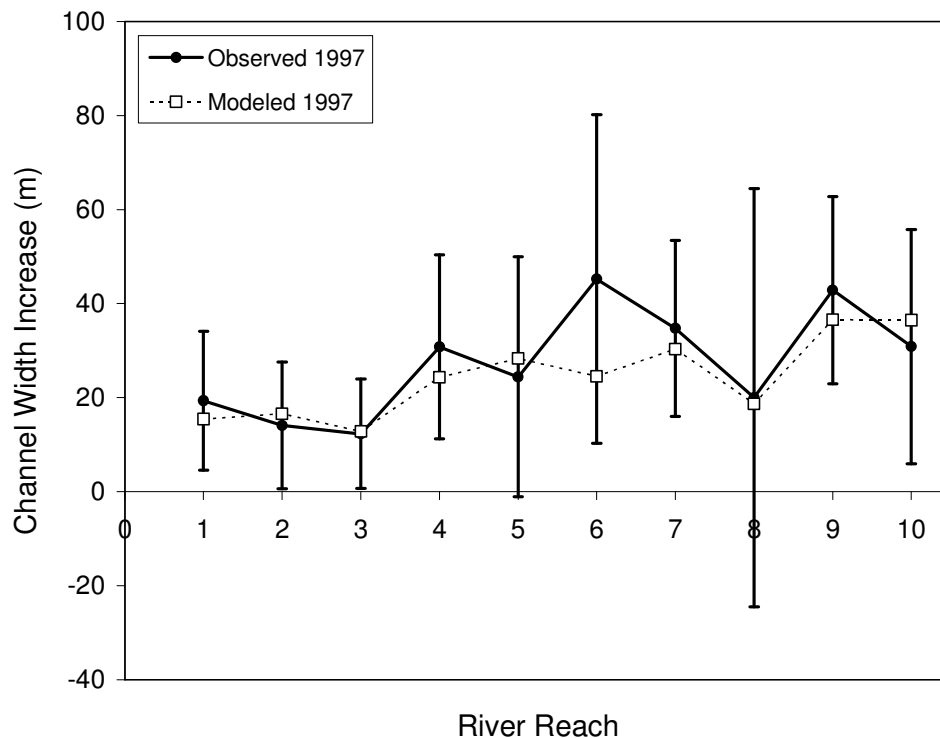


Figure 2.4: Verification of the bank erosion algorithm (equation 2.1) by comparing observed and modeled channel width increases between areal photographs taken in 1991 and 1997, for the 10 river reaches marked in Figure 2.2 and defined by Miller et al. (1999). Output represents the mean width increase for a given reach. Error bars represent \pm sd of the observed mean.

occur in reaches with shallower slopes and, to a lesser degree, larger floodplain widths. The statistical significance in the later is reduced due to reach 6, which experienced large channel width increases despite a relatively narrow valley floor. While reach 6 is the exception in geomorphic change compared to observed trends in other river reaches, the modeled value still falls within a standard deviation of the observed mean and deemed acceptable.

Mercury transport calibration of B_f , λ_l , and σ_f is done to best match THg collected during low (Figure 2.5a), medium (Figure 2.5c) and overbank flows, respectively, using data collected prior to and during the 1997 flood. Verification of these parameters is shown with a high flow THg data set (Figure 2.5d), as well as for all pre-flood TMeHg data (Figure 2.5b, 2.5d and 2.5e). Calibrated THg concentrations are modeled with a *rmse* equal to 2,900 ng/L, which is equal to half the observed standard deviation. With no calibration, the *rmse* for TMeHg equals 1.77 ng/L, which is also equivalent to half the observed standard deviation. In all cases, downstream trends in observed THg and TMeHg are reproduced. Concentrations increase in the downstream direction with a precipitous drop in total species as the river enters the reservoir and sediment deposition occurs. Observed dilution at site 14 is captured by including the Truckee Canal in the model with USGS observed THg (25 ng/L) and TMeHg (0.42 ng/L) concentrations lower than those modeled in the reservoir.

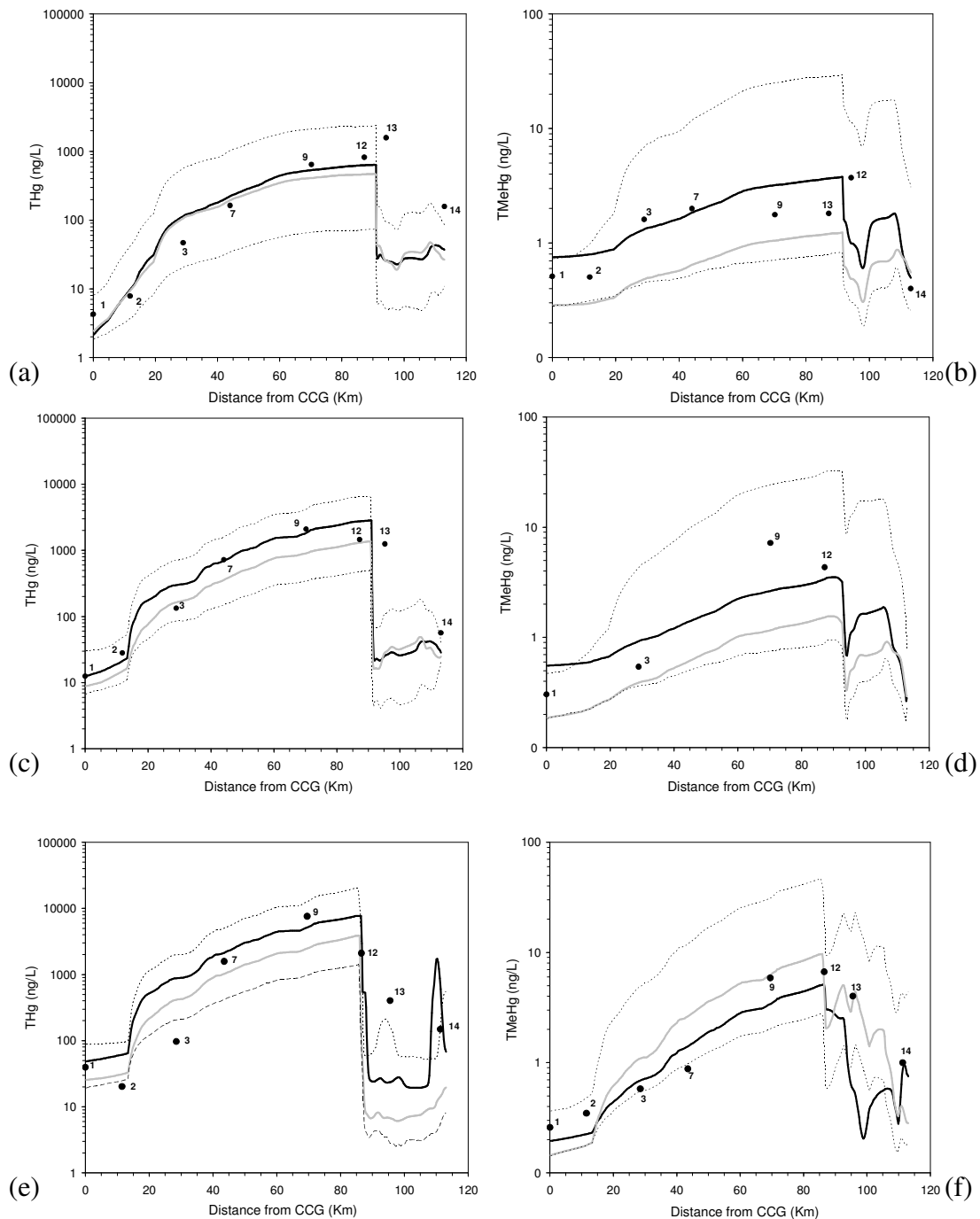


Figure 2.5: Pre-flood data sets with sites labeled by number. CCG = Carson City Gage. (a) THg, B_f calibration, low flow June 1994, (b) TMeHg, no calibration, low flow June 1994, (c) THg, λ_l calibration, medium flow May 1994, (d) TMeHg, no calibration, medium flow May 1994, (e) THg, no calibration, high flow June 1995, (f) TMeHg, no calibration, high flow June, 1995. Black circles = observed, thick dark line = modeled with traditional calibration strategies, gray thick line = best realization in GLUE, thin dashed lines = GLUE derived 95% confidence intervals.

Following the 1997 flood, the USGS began a regular sampling campaign of total and dissolved species along the Carson River, with the greatest number of samples collected at Weeks Bridge (site 10). These relatively extensive data sets are used in the calibration and verification of dissolved species. Specifically, E , f_b and ϕ_b (refer to Table 2.1 and Table 2.2) are adjusted to best match observed DHg during extremely low, low and medium-high flows (Figure 2.6b). The calibrated value for ϕ_b is one order of magnitude lower than f_b and supports a higher rate of adsorption in the finer bank materials compared to coarser channel bed sediments. While the modeling approach replicates observed DHg behavior for flows contained within the river's channel, it appears to break apart when flows exceed bankfull. During overbank events, bank erosion increases substantially. This in turn produces large bank derived inputs of DHg based on ϕ_b . While no data exists to contradict model results, it is likely that modeled DHg concentrations are too large to be reasonable.

In addition to dissolved species, post-flood attention is given to maximum THg in the bank sediments, since the pre-flood λ_l value is found not sufficiently large enough to predict post-flood THg water column concentrations (Warwick and Carroll, 2008). Traditional recalibration of λ_l minimized the *rmse* of post-flood THg predictions at site 10 (Figure 2.6a). The recalibrated λ_l increases from a pre-flood value of 5,000 $\mu\text{g}/\text{Kg}$ to 19,000 $\mu\text{g}/\text{Kg}$. The four-fold increase may reflect a greater quantity of post-flood data and a more accurate estimate of λ_l . However, the large increase in λ_l may also represent a change in the system following the flood in terms of THg exposed in the channel bank sediments as a result of geomorphic change during the flood. Results in the uncertainty analysis will examine the idea further.

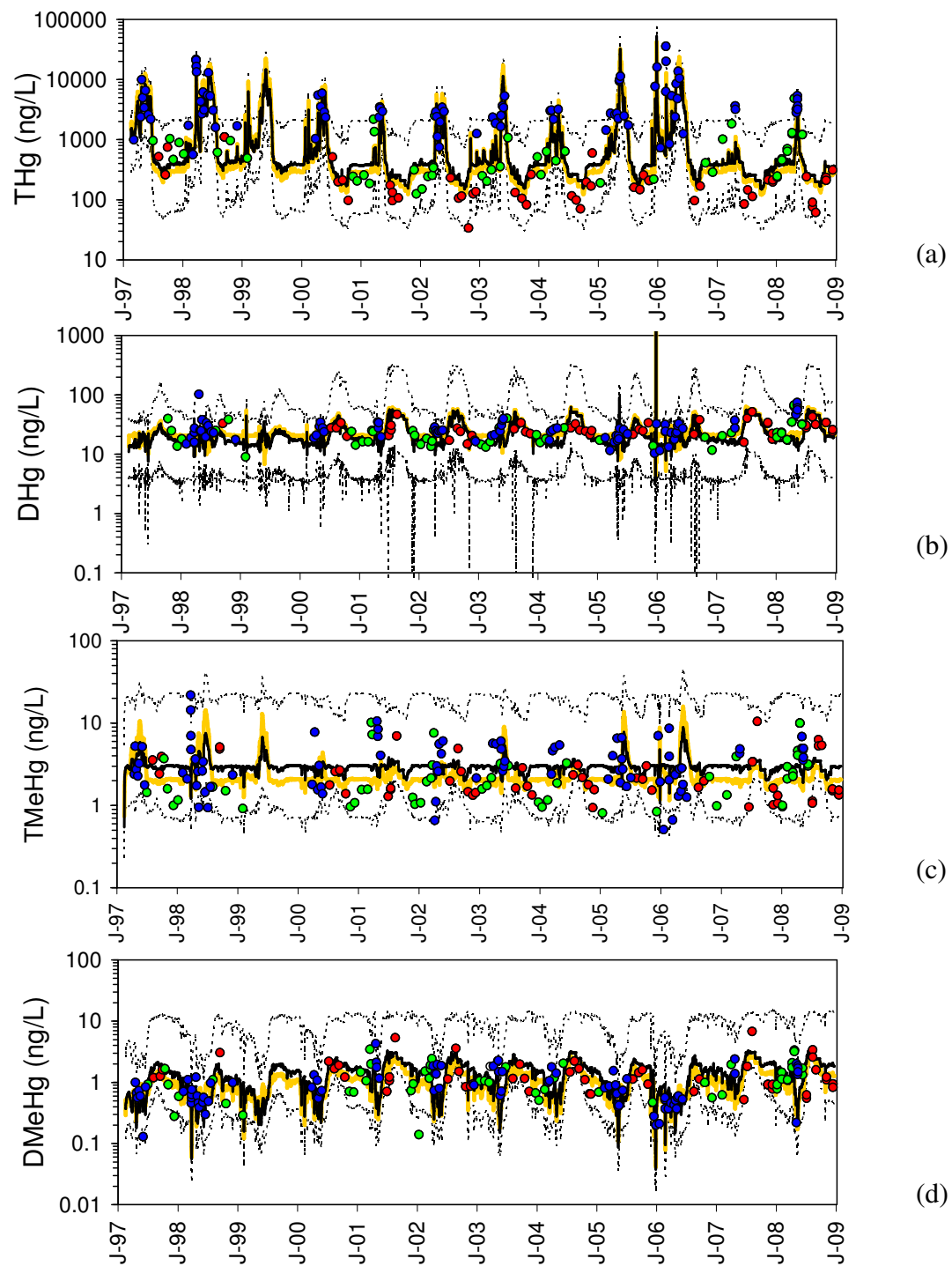


Figure 2.6: Water column mercury concentrations at Weeks Bridge for, (a) THg, (b) DHg, (c) TMeHg and (d) DMeHg. Red circles = observed data extremely low flow; green circles = observed data low flow; blue circles = observed data medium-high flow, thick black line = modeled calibration/verification, thick orange line = best GLUE, thin dashed lines = GLUE derived 95% CI. Flow provided in Figure 2.3.

Modeled water column THg concentrations are well modeled ($rmse = 3,500$ ng/L) for observed concentrations spanning several orders of magnitude (34 ng/L to nearly 36,000 ng/L). Likewise, the CRLR transport model is able to match observed THg trends with respect to flow by producing ($r_s = 0.97$, $p \ll 0.01$). In addition, the percent DHg is a function of f_b , ϕ_b and σ_f and the model replicates observed behavior in terms of the percent of THg that is dissolved (Figure 2.7a). Modeled percentages decrease substantially during higher flow events reaching as low as 0.01% with percentages increasing with decreased flow up to 30%.

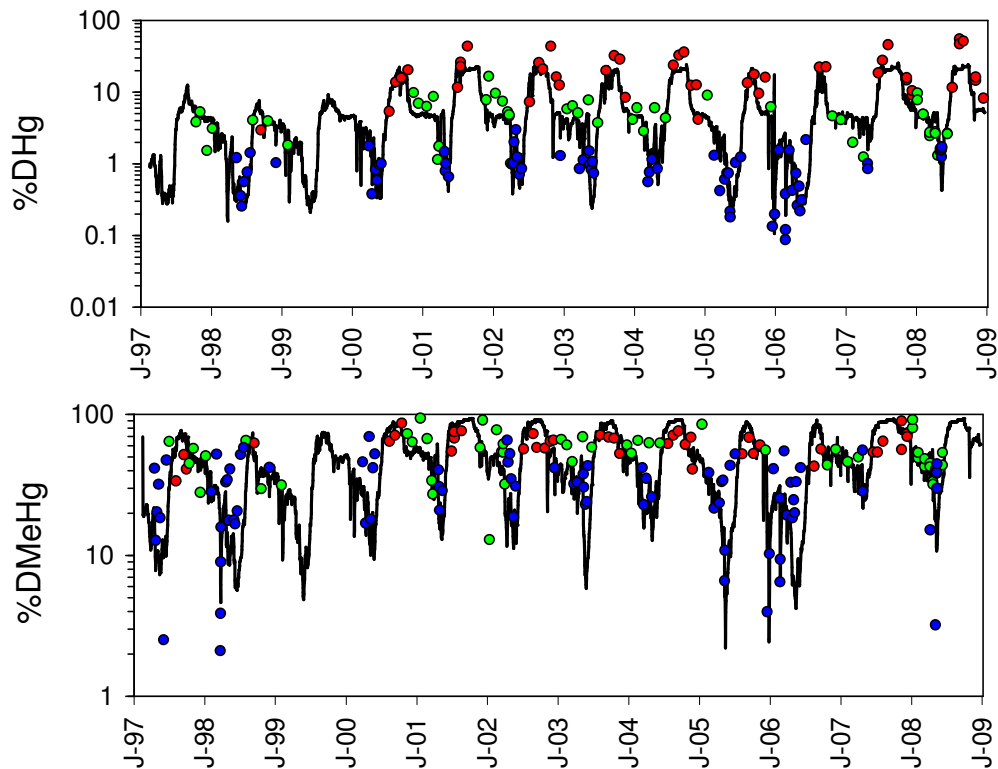


Figure 2.7: Post-flood water column mercury concentrations at Weeks Bridge. (a) percentage of THg that is dissolved, (b) percentage of TMeHg that is dissolved. Red circles = observed data extremely low flow; green circles = observed data low flow; blue circles = observed data medium-high flow, thick black line = model verification. Associated river flows provided in Figure 2.3.

Observed TMeHg is difficult to predict (Figure 2.6c) with tremendous scatter in observed data (majority of data 1.0 to 11.0 ng/L) witnessed during all flow regimes. The largest concentrations, however, are generally observed during medium-high spring flow events. Lack of a definitive trend in observed data makes it difficult to narrow mechanisms responsible for loading and transport of TMeHg. It is hypothesized that the timing of sample collection with respect to a rising hydrograph versus a falling hydrograph may be responsible for some of the observed scatter (Karen Thomas, USGS, Carson City, Nevada, communication February 2009). With no model calibration with respect to TMeHg species, results at site 10 fall in the midst of the data scatter by predicting relatively consistent concentrations equal to 3 ng/L. Increases in concentration occur during spring melt when the rising water levels are slow enough to ensure bank saturation for more than four consecutive days and allow M/D_{bank} to reach its full potential for a given depth of flow and erosion rate. Similar to TMeHg, no calibration is performed with respect to DMeHg. Modeled DMeHg (Figure 2.6d) mimics observed trends with respect to flow ($r_s = 0.72$, $p < 0.01$) and replicates observed concentrations with an *rmse* value of 0.97 ng/L, which is approximately equal to one standard deviation in observed behavior. DMeHg concentrations are highest in the summer when flows are lowest. Concentrations decrease with a rising hydrograph. The percentage of dissolved TMeHg is a function of modeled sediment adsorption coefficients described by Carroll et al. (2000) and are not modified to account for faster settling rates. However, Figure 2.7b confirms that adsorption coefficients are appropriate, with modeled percentages relatively low

during high flows (2 to 40%) and increasing up to 90% during extremely low flow conditions.

No calibration for any modeled species is done in the reservoir. Few data exist, with most data collected at either site 13 (Fisherman's Point) or site 14 (Lahontan Dam). All post-flood reservoir data was collected during the summer of 2006, with data at site 14 collected at three discrete depths. Observed values represent either the mean of duplicate samples or a volume weighted average for samples collected with depth in the reservoir. Figure 2.8 is a regression of predicted concentrations against observed values. Observed variability is represented with ± 1 standard deviation about the mean, while model uncertainty is represented with the GLUE derived 95% confidence interval along the y-axis. With no calibration, model predictions fall in the same order of magnitude as observed values, but regression slopes are flat, such that the model over predicts when observed concentrations are low, but under predict when concentrations are high. Inability to match trends in reservoir concentrations is mitigated, somewhat, by large observed variability in data. In addition, effect of parameter uncertainty can include more of the data, with modeled variability dependent on river processes and reservoir residence. This is discussed in more detail in the following sections.

2.3.2 Uncertainty Analysis

A list of parameters included in the GLUE analysis is given in Table 2.4. Along with model parameters already discussed in Table 2.1, water column boundary concentrations at the site 1 (Carson City Gage, Figure 2.2) are included in the GLUE

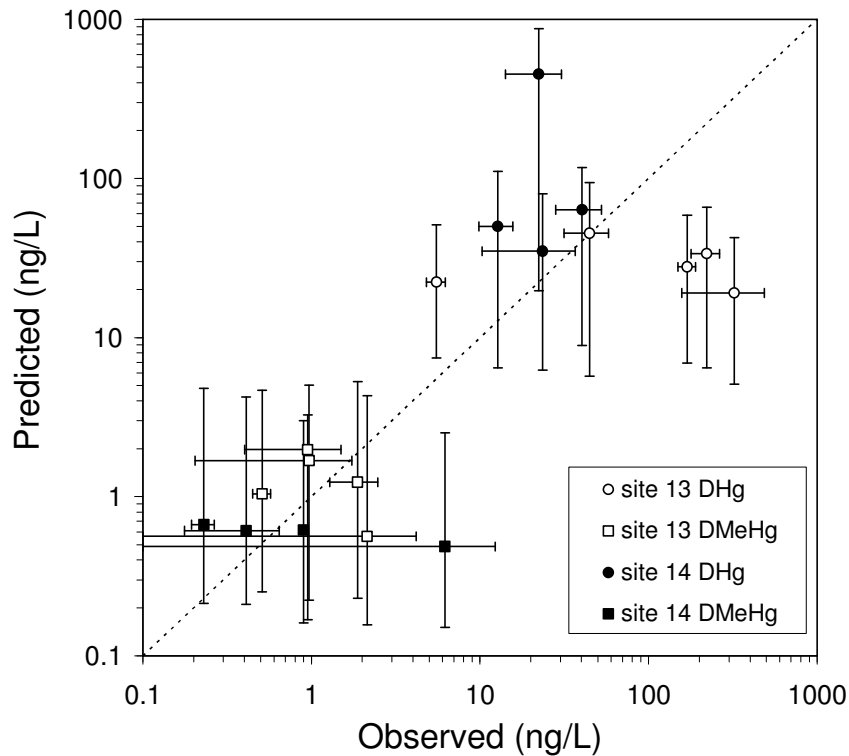


Figure 2.8: Post-flood regression of predicted and observed concentrations of dissolved species in the reservoir. All samples collected during the summer of 2006. Error bars along the x-axis represents observed variability (± 1 sd). Error bars along the y-axis represent the GLUE derived 95% confidence interval.

analysis. Error terms are added as the fraction of predicted boundary concentration based on previously implemented rating curves (Carroll et al., 2000). This is done to establish level of significance of boundary conditions compared to other model parameters. Prior input distributions are assumed uniform to show no preference for a given value within the specified range. Those input parameters that span several orders of magnitude (e.g., d_{riv} , d_{res} , E , B_f) are assigned log-uniform distributions. The uniform distribution is well justified (Romanowicz et al., 1996).

Table 2.4: Resultant posterior means (μ) and standard deviations (σ) for the pre-flood and post-flood GLUE analysis for the parameters investigated. Δ = the percent change in parameter mean between simulations, t = test statistic for the difference in sample mean, α = maximum probability in making an error in rejecting the null hypothesis (i.e., sample means are the same), and associated significance level that pre- and post-flood means are different. Geo = geomorphic parameter group. Prior distribution means also provided.

Geo		prior μ	Pre-Flood ^a		Post-Flood ^b		Δ (%)	t	α	sig level (%)
			μ	σ	μ	σ				
	ψ_2	136,500	106,459	29,968	112,203	32,129	5	3.95	0.00	100
Mercury Transport	λ_1	22,750	15,746	10,254	22,866	12,949	45	12.95	0.00	100
	d_{RIV}	0.010	0.023	0.025	0.0218	0.026	-4	0.72	0.47	53
	d_{RES}	0.010	0.0198	0.022	0.0221	0.025	12	2.08	0.04	96
	S_f	10.4	10.7	1.5	10.5	1.5	-3	3.92	0.00	100
	E	1.50E-11	2.98E-11	0.000	2.53E-11	0.000	-15	2.97	0.00	100
	B_f	1.00E-09	1.73E-09	0.000	1.38E-09	0.000	-20	3.89	0.00	100
	f_b	0.0074	0.012	0.013	0.014	0.015	0.1	2.11	0.03	97
	ϕ_b	0.0007	0.0011	0.0013	0.0014	0.001	0.02	3.67	0.00	100
BC site 1 ^c	THg_0	0.35	0.36	0.56	0.36	0.53	0	0.14	0.89	11
	$TMeHg_0$	0.05	0.01	0.28	-0.01	0.29	-1	1.03	0.30	70
	$FDHg_0$	0.00	0.07	0.56	0.07	0.53	0	0.13	0.89	11
Biogeochemical	M/D_{Bed}	0.02902	0.01874	0.01222	0.01758	0.01169	-6	2.09	0.04	96
	M/D_{bank}	0.02902	0.02059	0.01184	0.01887	0.01219	-8	3.07	0.00	100
	M/D_{up}	0.02944	0.02059	0.01311	0.02094	0.01292	2	0.58	0.56	44
	M/D_{low}	0.00334	0.00290	0.00174	0.00295	0.00173	2	0.65	0.52	48

^anumber of realizations is 1000

^bnumber of realizations is 850

^cfraction increase(+) or decrease(-) from boundary condition rating curve

Figure 2.9 shows that 80% of the observed behavior falls within the estimated 95% CI for the pre-flood simulation and 87% of the observed data is contained in the post-flood CI. It is expected that a 95% CI should encapsulate 95% of the data, suggesting the computed CI is slightly too narrow. Using the global objective function (i.e., includes all criteria with data), both simulations produce nearly equal percentages of data falling above and below the 95% CI. The primary distinction in pre- and post-flood simulations occurs in the reservoir. For the pre-flood simulation

only 45% of the data fall within the computed CI, with all the remaining data falling below the estimated lower bound. In contrast, the post-flood simulation is able to capture more than 72% of the observed reservoir data, with the majority of error falling above the CI. The change in prediction bias is not known, but may reflect a low quantity of data in the reservoir to constrain the model.

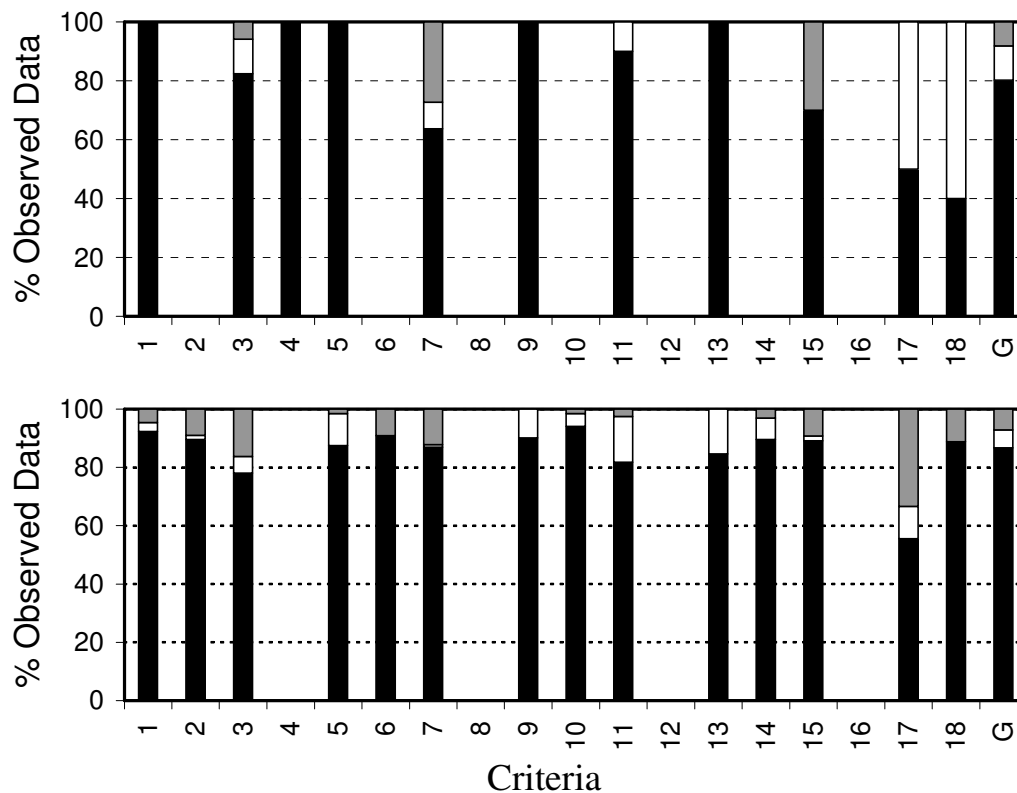


Figure 2.9: Percentage of observed data captured by the GLUE-defined 95% confidence interval (CI) as a function of species, flow and location. (a) pre-flood GLUE simulation, (b) post-flood GLUE simulation. Refer to Table 3 for a definition of data criteria, and the number of data in each category. Black = contained in 95% CI, white = data falls below 95% CI and gray = data falls above 95% CI

Convergence to μ is tracked in Figure 2.10 as a function of the number of realizations (J) based on the normalized mean (μ^*), where μ^* is defined as the ratio of μ at a given number of realizations to the final computed μ given all realizations. The pre-flood simulation has difficulty converging to less than $\pm 2.5\%$ its final mean value. However, most oscillations in μ^* are constrained to $\pm 5\%$ by 500 realizations.

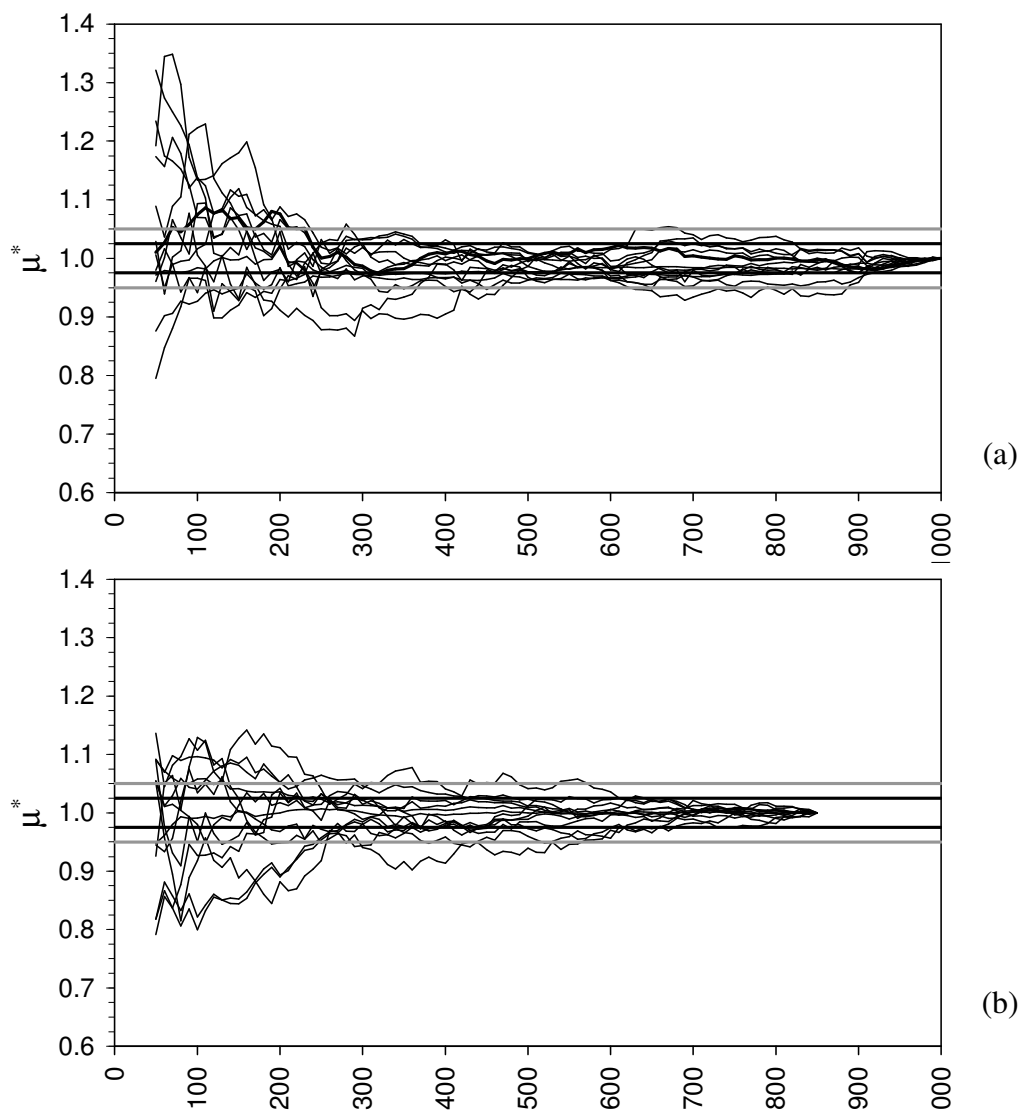


Figure 2.10: Stabilization of GLUE derived parameter means with increased number of realizations (J) for (a) pre-flood simulation, (b) post-flood simulation. Each thin line represents an individual parameter. Thick black lines = $\pm 2.5\%$ the final mean value. Thick gray lines = $\pm 5\%$ the final mean value.

Exceptions include d_{riv} , d_{res} , M/D_{bed} and B_f which require approximately 900 realizations to stay within $\pm 5\%$ the final mean value. Mean values for the post-flood simulation showed greater stability with values converging to $\pm 5\%$ the final μ_k by 500 realizations, and to $\pm 2.5\%$ by 680 realizations. Greater oscillation in pre-flood μ estimates compared to post-flood estimates is caused by insufficient pre-flood data necessary to constrain parameters related to dissolved species at extremely low flow and low flow conditions.

Prior distribution means as well as GLUE derived posterior means and standard deviations are provided in Table 2.4 for the pre- and post-flood simulations. The percent change in posterior means between simulations (Δ), resultant t-statistic and significance level are also provided. Results show that river transport and biogeochemical parameters are different between the two simulations, while boundary condition concentrations at and reservoir related M/D rates are statistically the same. Given pre-flood means fluctuate between $\pm 5\%$, it is likely that small Δ values are not indicative of actual change, but actually are indicative of the pre-flood model's inability to converge on a stable mean value. However, larger Δ values, specifically, λ_l and E , may indicate a possible shift in mean value. What is debatable is if this shift is the result of physical change in the system or numeric technique (e.g., choice of objective function, number of observed points, etc.). It is argued that E can not physically change since it is a property of the size and mass of the solute and the viscosity of the solvent. Therefore, a change in E between pre- and post-flood simulations is related to numeric technique and not systematic change.

Conversely, a 45% increase in THg bank concentrations (λ_1) may be related to a physical change in the system as a result of the 1997 flood. The erosion effects of the 1997 flood are dramatic. Miller et al. (1999) documents the removal of bridge embankments and approach ramps, the damage to irrigation facilities, the local removal of fence lines constructed along the pre-flood channel, the destruction of the FCH gaging station previously located on the valley floor well beyond the channel margins, the localized erosion of man-made levees constructed for flood control and the abundance of riparian trees with exposed root structures previously covered. Examination of aerial photographs shows that portions of the Carson River experienced width increased up to 280% of pre-flood conditions and in several locations the channel avulsed to cut off meanders. Greatest channel change occurred in the flatter regions of the river basin, where floodplains are widest (Miller et al., 1999) and where deposition of contaminated sediment from the Comstock Load is expected to be large (Carroll et al., 2000). Under these circumstances it is argued that the river exposed higher concentrations of contaminated bank sediment in the lower sloped regions of the river and require a higher λ_1 value following the flood in comparison to pre-flood estimates.

Examples of likelihood values as functions of THg bank concentration (λ_1) and diffusion rate (E) are provided in Figure 2.11. The pre-flood simulation shows greater sensitivity to λ_1 than did the post-flood simulation with a sharp, well defined peak at 9,000 $\mu\text{g}/\text{Kg}$ (Figure 2.11a). It is the highly biased nature of the pre-flood λ_1 likelihood distribution that is able to reduce the prior λ_1 mean of 22,750 $\mu\text{g}/\text{Kg}$ to

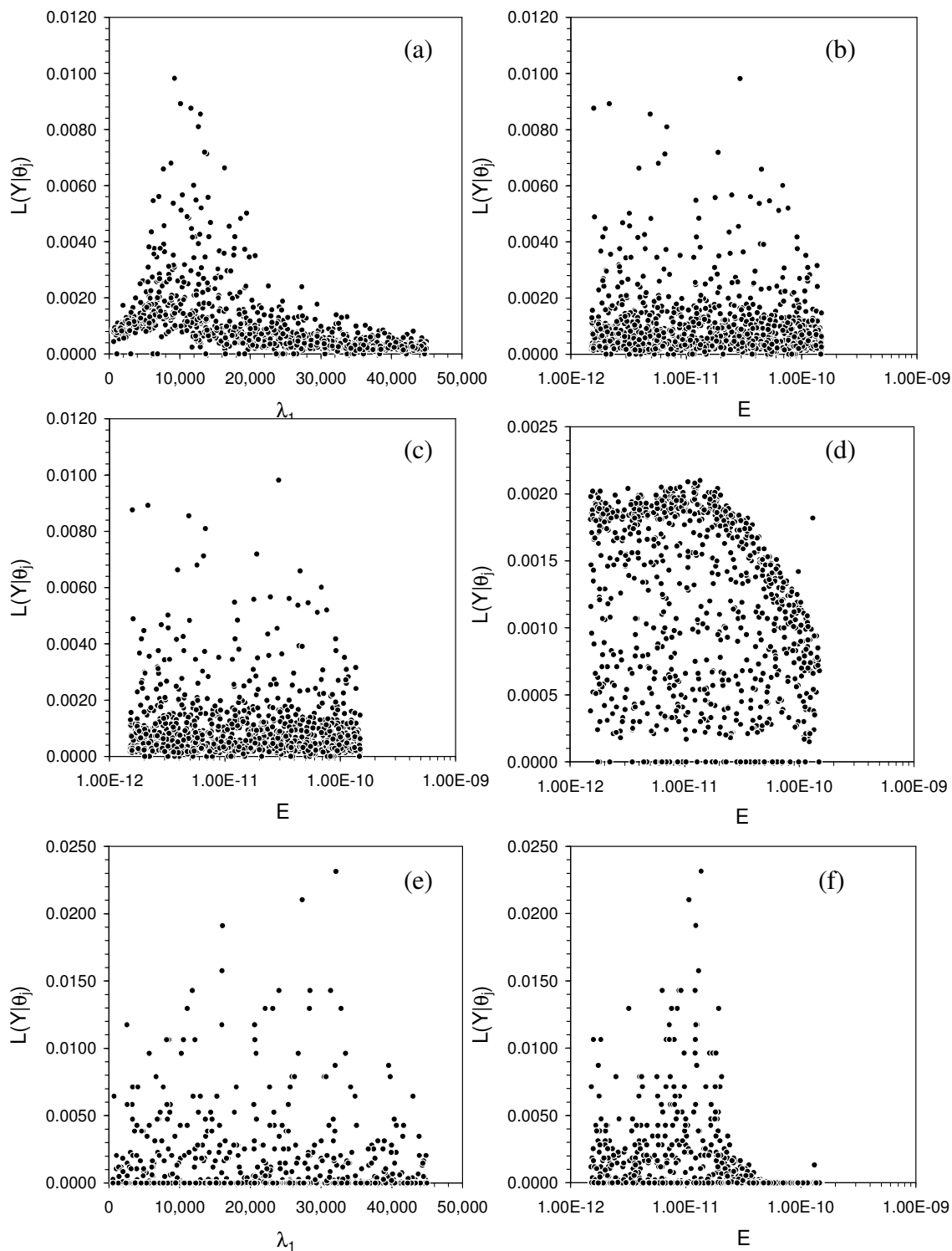


Figure 2.11: Examples of likelihood functions produced by the GLUE approach, (a) λ_1 pre-flood simulation, (b) E pre-flood simulation, (c) λ_1 post-flood simulation, (d) E post-flood simulation., (e) λ_1 post-flood simulation $N = 10$, and (f) E post-flood simulation $N = 10$.

15,746 $\mu\text{g}/\text{Kg}$. In contrast, the post-flood λ_l likelihood values show no preference within the sampled range (Figure 2.11c) and produce no change to the prior distribution mean. Lack of any bias in the post-flood λ_l may negate the idea of physical change in the system and one can counter-argue that the posterior λ_l mean is only a function of a subjectively chosen prior distribution. However, increasing N to 10 (Figure 2.11e) increases post-flood sensitivity to λ_l but still maintains a posterior mean approximately equal to the prior distribution mean. The equality of prior and posterior means is therefore coincidental, or the relic of an appropriately chosen input distribution and does not negate the notion of physical change in the system as a result of the flood.

Post-flood simulation shows a greater sensitivity to the diffusion rate E (Figure 2.11d) and this sensitivity increases with an increase in N . Likelihood estimates depict little preference for $E < 2.0 \times 10^{-11} \text{ m}^2/\text{s}$ and a marked decrease in values when E is greater than $2.0 \times 10^{-11} \text{ m}^2/\text{s}$. The sharp edge along the upper range of E is not evident in the pre-flood simulation and, consequently, the estimated mean for E in the pre-flood simulation is shifted to larger values.

Relative uncertainty for the pre-flood and post-flood simulation is provided in Figure 2.12. At the global scale (G), pre-flood parameter uncertainty (Figure 2.12a) is dominated by λ_1 , and to a much lesser extent by σ_f , ϕ_b and ψ_2 . Breaking the analysis into different subsets of the data based on species, flow regime and location, the parameters defining uncertainty at the global level are primarily associated with THg at higher flows. Uncertainty associated with other flow regimes and other species show greater dependence on loading from the bottom sediments (B_f) and

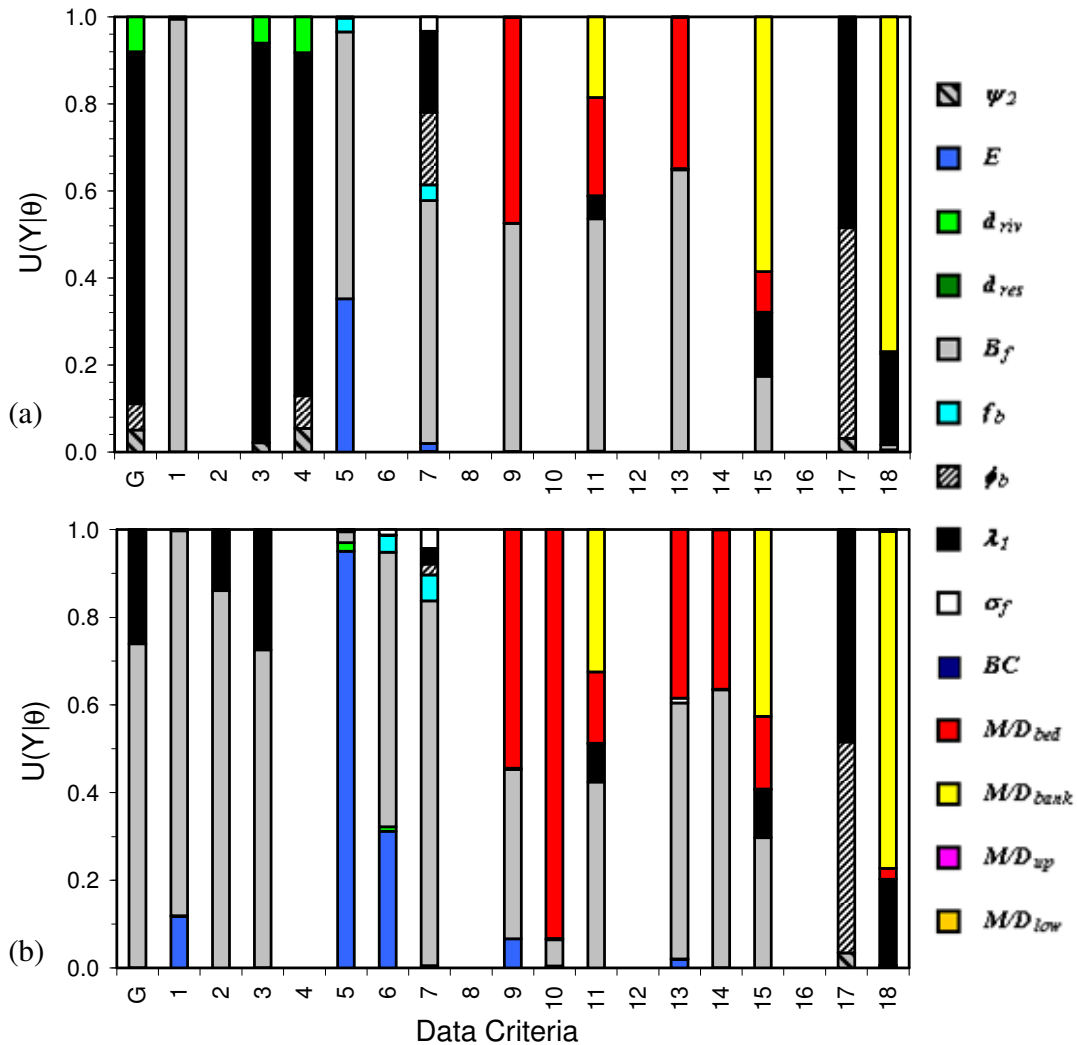


Figure 2.12: FOSM relative uncertainty of each of the parameters tested (a) pre-flood simulation, (b) post-flood simulation. Criteria defined in Table 2.2

biogeochemistry (M/D). For MeHg species, roughly half of the uncertainty in model prediction is caused by uncertainty in biogeochemical parameters. This increases to approximately 70% for DMeHg during higher flow regimes. Pre-flood uncertainty pertaining to both DHg and DMeHg in the reservoir is related to bank erosion processes (λ_1 , ϕ_b , ψ_2 , M/D_{bed}) and not to diffusion from benthic sediments in the reservoir (M/D_{up} , M/D_{low} , d_{res}). In this regard, model prediction in the reservoir is

highly dependent on properly defining river loads and less reliant on properly parameterizing reservoir benthic inputs.

Figure 2.12b shows FOSM analysis for the post-flood simulation. Results are similar to the pre-flood simulation, but with greater emphasis on B_f than λ_l . The switch in emphasis from a dominance of a higher flow parameter (λ_l) to a lower flow parameter (B_f) is, again, related to the large quantity of low flow data collected following the flood.

The results for the best post-flood GLUE realization as well as the 95% CI at site 10 are plotted in Figures 2.5 and 2.6 to compare with the calibrated/verified model output. The term “best” is quantified as that Monte Carlo realization that produced the largest likelihood value given $N = 1$. In general, auto-calibration via GLUE replicates traditional calibration strategies for most of the data sets, especially for the post-flood simulation in which a greater number of data are available.

The GLUE derived 95% CI are large in comparison to model values, with ranges at Weeks Bridge approximately one order of magnitude for all species, however, CI capture less than 95% of the data and can be regarded too narrow at the global scale. Increasing N to 10 will give greater weight to those realizations which perform better, but will further reduce the CI and exclude more than 40% of the data from the CI.

The range in computed uncertainty (R_u) is shown in Figures 2.13 and 2.14 for total and dissolved species respectively, and focuses attention only on water years (WY) 2004 to 2006. This three year span provides a dry, wet, and average WY, respectively, with an overbank event occurring in January 2006 as the result of a rain

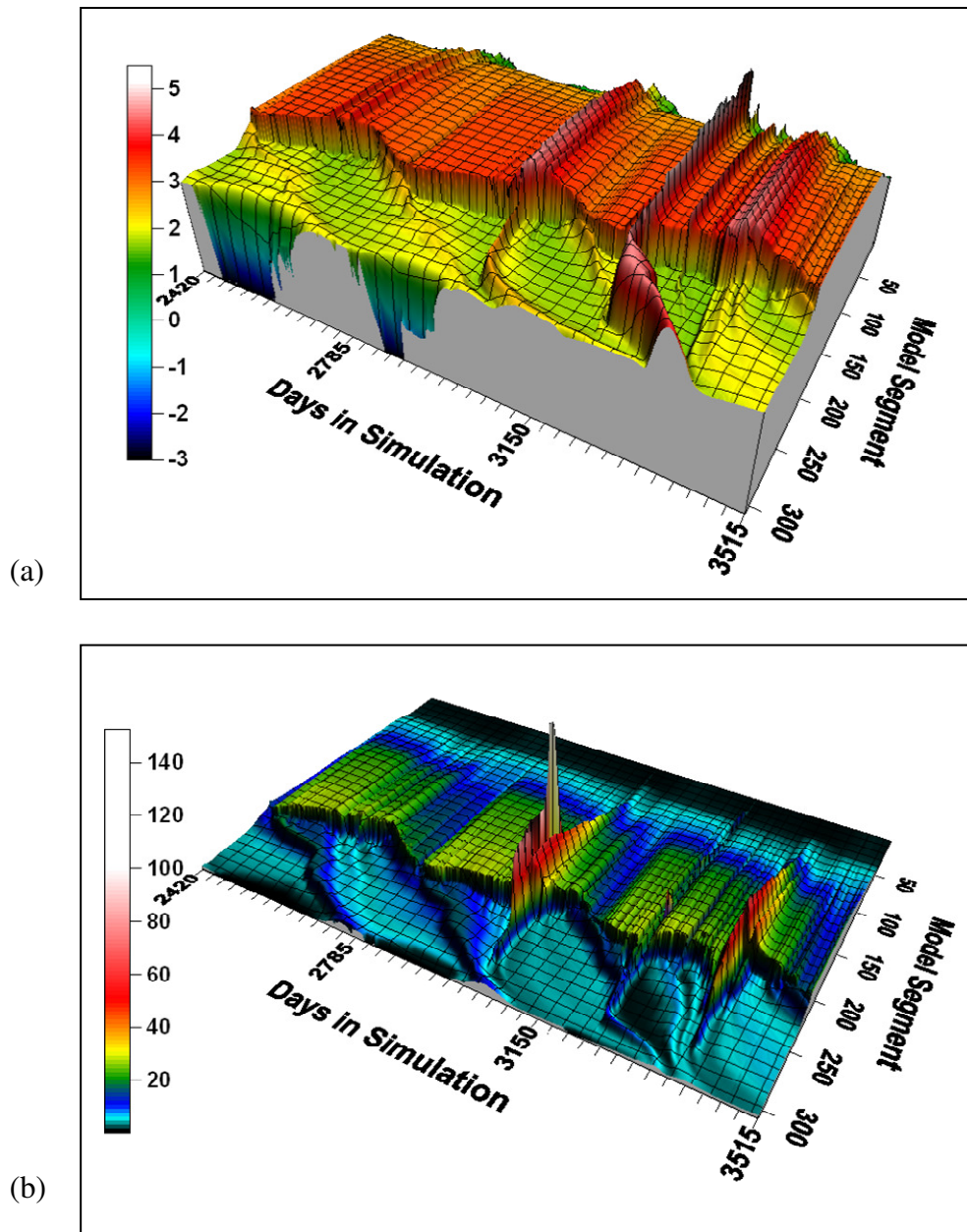


Figure 2.13: System-wide ranges in the GLUE 95% CI (R_u) for WY 2004 through WY 2006 (a) THg, \log_{10} ng/L and (b) TMeHg, ng/L, (c) TMeHg, ng/L and (d) DMeHg, ng/L. For reference, day 2420 corresponds to October 1, 2003 and day 5315 is September 30, 2006. The maximum upstream location of the reservoir is model segment 204.

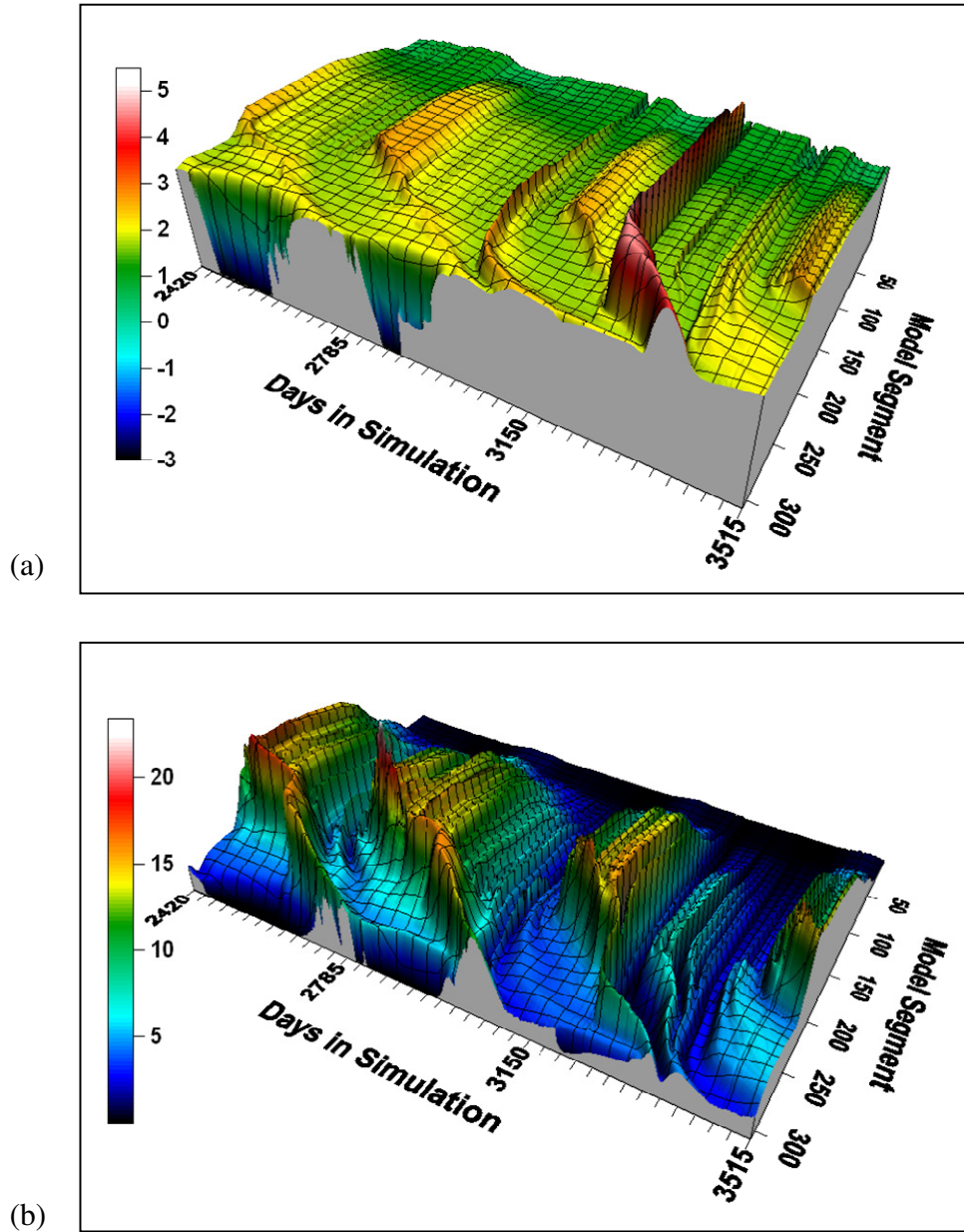


Figure 2.14: System-wide ranges in the GLUE 95% CI for WY 2004 through WY 2006 (a) DHg, log(ng/L) and (b) DMeHg, ng/L. For reference, day 2420 corresponds to October 1, 2003 and day 5315 is September 30, 2006. The maximum upstream location of the reservoir is model segment 204.

on snow event. Results show that total species have larger uncertainty in the river than in the reservoir as a result of sediment deposition in the reservoir. The model supports a migrating delta region with sedimentation beginning where velocities slow substantially based on reservoir stage. In Figure 2.13, this is evidenced by a non-stationary transition zone separating large uncertainty in the river from relatively low uncertainty in the reservoir.

For total species, R_u generally increases with flow. This is particularly apparent for THg in Figure 2.13a. TMeHg uncertainty mirrors THg with respect to flow but R_u predictions are complicated by bank moisture history. With reference to flow in the river provided in Figure 2.3, WY 2005 experienced higher than average flows during spring runoff. The gradual, but substantial, rise in the hydrograph in WY 2005 produces the largest modeled range in uncertainty for the post-flood simulation. In contrast, the overbank event in WY 2006 produces a collapse in R_u despite very large flows. Consequently, spring melt hydrographs have a greater potential for bank sediments to reach their maximum M/D rate. In this situation, the choice of M/D_{bank} will impact predicted water column concentrations substantially and generate larger R_u values. If the rise and fall of the hydrograph is rapid and short lived then bank sediments are not saturated long enough to reach the maximum M/D rate and the influence of M/D_{bank} on water column TMeHg concentrations is mitigated.

Dissolved species tend to have a greater uncertainty at very low flows and slower reservoir velocities (Figure 2.14). DMeHg R_u is largest during the summer of 2004 (dry year) and lowest during spring runoff events and the overbank event in

2006. DHg generally follows the same trend as DMeHg, but deviates from DMeHg behavior during above average spring runoff (e.g., WY 2005) and overbank events. During high flow events bank erosion transports DHg into the river and is directly related to uncertainty defining the fraction of dissolved THg in the bank materials (ϕ_b).

Predicted uncertainty in the reservoir for all species is relatively low compared to peak R_u values in the river. In all cases, ranges of uncertainty derived from the river propagate through the reservoir as a function of reservoir residence time. Figure 2.13 and Figure 14 highlight the FOSM analysis that uncertainty predictions in the reservoir are characterized by uncertainty in mercury loading mechanisms in the river and not loading from reservoir benthic sediments. In addition, uncontaminated water from the Truckee Canal just above the dam at model segment 307, influences R_u . Years with larger canal inflows (e.g., 2004) can cause water to move upstream from Lahontan Dam and dilute portions of the reservoir's North basin. Large canal inflows reduce uncertainty in water quality predictions just above the dam.

2.4 DISCUSSION

This research set out to answer four questions. Combining two of the four questions: can the CRLR transport model adequately reproduce total and dissolved species along the entire system and over diverse flow regimes, and if not, how can relative uncertainty in parameter input (and model structure) help refine the calibration process and/or conceptual model? In general, results suggest that concentrations and trends in modeled species are well represented. THg loading and transport is highly constrained in the calibration process, but reproduces a wide range

of concentrations over diverse climatic conditions with acceptable accuracy.

Sediment transport processes dominate THg transport as reported (Carroll et al., 2000; 2004; Warwick and Carroll, 2008). Research presented offers only slight modifications to modeling strategies already published.

In contrast, while steady state models have addressed dissolved species in the reservoir (Diamond et al., 2000; Gandhi et al., 2007), very little focus has been given to dissolved species under transient conditions spanning the entire river-reservoir system. DHg loading and transport is found complex and difficult to model unless several additional input parameters (f_b , ϕ_b and σ_f) are introduced. The historical context of THg in the system is partly responsible for this complexity because of its association with mill tailings and amalgam grains. To obtain reasonable water column concentrations it is necessary to designate uncontaminated and contaminated sediment and to augment settling velocities of fine material. While these additional parameters allow relatively good predictions of DHg at low and medium flows, and THg during overbank flows, the model still fails to capture reasonable DHg concentrations during overbank flows. Improvement of the DHg conceptual model may be warranted. Relative uncertainty in parameters describing DHg transport, suggest improvement may be obtained by better quantifying diffusion rates and the turbulent mixing coefficient B_f . It may even be possible to discard f_b and ϕ_b completely by revisiting E and B_f and still maintain the same degree of prediction in DHg while improving overbank water column results. However, it is more likely that the non-linearity of DHg loading with increased flow is associated with agitated wetting of typically very dry soils in the upper bank sediments, the

sorption/desorption properties of these soils and the potential influence of colloidal contributions during the initial phase of rising flows. Future work will need to investigate these possibilities.

Despite the potential problems encountered with DHg transport, un-calibrated DMeHg water column concentrations are modeled exceptionally well using observed M/D rates, bank moisture history and reported adsorption coefficients. None the less, relative uncertainty in M/D rates in the channel bottom sediments and bank sediments remains large for organic species. This is, in part, due to a lack of preference for any given M/D rate in the global likelihood function which is dominated by λ_l (pre-flood) and B_f (post-flood). Uncertainty, however, at the individual criteria level could be reduced by narrowing the range of acceptable rates.

Reservoir dissolved concentrations are not sensitive to diffusion loads originating from the reservoir benthic sediments in the context of parameters adjusted defining this loading mechanism. These parameters include d_{res} , M/D_{up} and M/D_{low} . Instead, bank erosion processes in the river, defined by THg in the banks (λ_l), the fraction of DHg in the banks (ϕ_b) and potential M/D_{banks} , represent the greatest uncertainty in describing loading and transport of dissolved species through the reservoir. The CRLR transport model therefore assigns greater importance to external loading of dissolved species from the Carson River compared to internal sources of benthic sediments. Specifically, the CRLR transport model suggests that DMeHg loading upstream of the delta region is substantial. Results confirm earlier studies (Gandhi et al., 2007; Diamond et al., 2000; Hoffman and Taylor, 1998; Ecology and Environment, 1998) that also found river loads able to describe observed DMeHg

water column concentrations in the reservoir. Limits to DMeHg benthic flux, specifically in the south basin, are observed by (Kuwabara et al., 2002) despite large quantities of contaminants in the south basin bottom sediments (Miller et al., 1995) and large potential for methylation (Marvin-DiPasquale et al., 2001). Limits to flux are attributed to un-reactive mineralogy in the basin (Diamond et al., 2000), toxic inhibitory effects on microbial activity (Chen et al., 1996), and/or degradation in the water column (Marvin-DiPasquale et al., 2001).

In contrast to DMeHg flux estimates, the possibility of larger DHg fluxes occurs in the south basin (Kuwabara et al., 2002), and these benthic sediments may be an important source to the reservoir. However, the model reduces the importance of DHg flux in order to match observed data, to imply that, similar to DMeHg, the movement of DHg across the sediment-water interface is some how limited. Review of Figure 2.8 shows that the CRLR model is not able to capture DHg in the region of site 13, which is located at the downstream end of the southern basin of the reservoir where the potential for benthic flux is greatest. Is the model's inability to capture DHg an under estimation of the importance of DHg flux from the south basin sediments based on the chosen likelihood function? It may be, but the largest observed DHg water column concentrations at site 13 occur in the spring when river fluxes are high and the potential for benthic flux is correspondingly low. Therefore, error in DHg prediction at site 13 likely reflects error in river transport and/or reservoir velocities and is not necessarily from under estimating benthic fluxes.

The other two questions asked in this study are: is the GLUE methodology an appropriate method to calibrate and evaluate uncertainty along the CRLR, and did the

system physically change as a result of a massive flood? GLUE derived posterior means find a large increase in bank sediment THg as a result of a large flood. The increase is physically possible given the observed erosion of channel banks by Miller et al. (1999). However, the result is dependent one's faith in the GLUE methodology.

The strength of GLUE resides in its simplistic approach to evaluating non-linear systems, including those that have no obvious, unique solution (Stedinger et al., 2008). However, the requirement of the user to specify thresholds of model acceptability and/or effective observation error is a subjective proposition that is not constrained by any specific, or commonly accepted, statistical guidelines. Therefore, the approach is open to criticism. Specifically, Stedinger et al. (2008) discusses that if a statistically valid approach is not implemented in GLUE via a properly chosen likelihood function, then the approach is only a weighted sensitivity analysis that looks at the influence of parameter uncertainty and neglects the importance of model and measurement error in the analysis. Classical approaches, however, rely on first-order approximations or a linearization of modeling processes. With complex hydrological models, linearization is invalid, at least over the range of modeled responses represented. In addition, most hydrologic problems are too difficult to pose in a statistically formal manner. It is for this reason that approaches like GLUE have been created that abandon traditional statistical inferences in the hope of capturing complex behavior (Kuczera and Parent, 1998).

While it is recognized that the *ad hoc* approach of GLUE is not perfect in the classical statistical sense, it is an approach that may cope more adequately with nonlinearity in model structure and incorporate model structural errors in the

uncertainty analysis even if the approach lacks any formal and explicit inclusion of model errors in the objective function (Beven and Binley, 1992). Beven (2006) states that the GLUE modeling approach is more akin to, “mapping of the landscape into a space of feasible models (structures as well as parameter sets)” and that, “the dominant uncertainty lies in how to map the real system into that space of feasible models”. Posterior distributions are estimated directly from model output via a set of acceptable solutions, rather than from a model coupled with an additive residual model that assumes the model is correct (Romanowicz and Beven, 2006).

If one accepts GLUE, almost from a philosophical point of view, then the GLUE derived information for the CRLR should capture uncertainty in model input as well model structure. For the CRLR system, the 95% CIs are approximately one-order of magnitude wide, and while this may appear high, the CI still captures less than 95% of the data. Overall, the number of CRLR data above the CI is equal to those below. Looking at individual criteria, it appears that inorganic species are under predicted by the model (data falls above the CI), while organic Hg is over predicted (data falls below the CI). However, exceptions to these cases occur and it is difficult to parse out where the model, and/or where the GLUE approach could do better to include 95% of the data.

The issue of data bias in the estimation of the CI does arise. Data bias refers to the type and quantity of data used in the objective function. As already noted, model predictions in the reservoir shift from over prediction in the pre-flood simulation, to under prediction in the post-flood simulation. There is no doubt that a larger quantity of reservoir data spanning different seasons and reservoir operations (i.e., residence

time) are needed to better define the conceptual model in the reservoir and help constrain acceptable runs in the GLUE analysis. Questions do arise as to the ability of the chosen objective function to properly represent individual components of the model, specifically the reservoir. Several studies (Beven et al., 2000; Beven and Freer, 2001; Romanowicz and Beven, 2006) have found that the choice objective function does impact the shape of the posterior input distributions, but has less impact on estimated CI. On the other hand, the choice, quality and quantity of data, as well as a suitable method for scaling the likelihoods (e.g., N) give the modeler control over the CI.

Increasing the scaling parameter N will reduce the CI by placing more weight on the best realization. Adjusting N based on the number of observations (e.g., $N = 0.5N_{obs}$) has been done (Feyen et al., 2001; Morse and Pohl., 2003), but is found to over condition the optimal parameter set if a large number of observations exist, and may have difficulty converging. Per instruction by Beven and Binley (1992), several studies adjust N to capture the requisite number of data as defined by the CI (Franks et al, 1999; Beven and Freer, 2001; Morse and Pohl., 2003) with conservative values ($N = 1$) found most appropriate in many instances. However, Stedinger et al. (2008) are critical of $N < 10$ for small data sets, showing that uncertainty intervals can diverge and become too wide when N is small. A value of $N = 1$, they suggest, is absurd for the rainfall-runoff model and objective functions they test.

Despite the misgivings presented by Stedinger et al. (2008), CRLR model results incorporate the conservative $N = 1$. Increasing N is shown in Figure 2.11 to more clearly define acceptable/unacceptable model results, but decreases the size of

the CI such that less than 40% of the post-flood observed data are accounted by the CI. For the pre-flood simulation an $N=10$ over conditions favorable realizations, such that only 1% of the 1000 realizations are considered acceptable. Further decreasing $N<1$ is not done given the criticism of small N values. Inability of the model to capture 95% of the data, even with a conservative $N=1$ and a large number of input parameters included in the analysis (each with wide prior ranges), suggests that complex error structures exist in the CRLR transport model, possibly related to heteroscedasticity, non-stationarity and/or correlation. In the future, it will be necessary to look more explicitly at model structural errors and incorporate into the GLUE methodology.

2.5 CONCLUSIONS

Regardless of the noted limitations in the GLUE approach, model predictions of water quality using the GLUE auto-calibration strategy is found comparable to a traditional (i.e., manual) calibration approach, especially when large amounts of data exist. Input parameter posterior means indicate that a sizable increase in THg concentrations in the river banks occurred as a result of a massive flood in 1997. This is supported by observed geomorphic changes caused by the flood in portions of the river basin where more THg is expected to have been deposited during channel aggradation in the 19th century (Miller et al., 1999; Carroll et al., 2000). The size and statistical significance of this change is not obscured by including a large number of parameters in the analysis, further implying that it is a physical phenomenon and not solely a relic of numeric technique. Uncertainty in model input (and possibly model structure) translates to uncertainty in predicted water column concentrations on the

order of one-order of magnitude, with total species having the greatest uncertainty during higher flows and dissolved species garnering more uncertainty during low flow events. Relative parameter uncertainty is computed using first-order second moment analysis based on Hg species, flow and location. In general, uncertainty in the river could be reduced by better quantifying turbulent mixing from the bottom sediments during low flow conditions, and better constraining the upper and lower ranges of methylation and demethylation in the river bed and bank sediments.

Diffusion rate uncertainty has large implications for DHg, but this uncertainty does not translate to the entire system. Uncertainty in dissolved species in the downstream reservoir is not influenced by parameter uncertainty describing reservoir benthic loads. Instead, uncertainty in the reservoir is dominated by uncertainty in higher flow loading mechanisms upstream in the river.

Acknowledgments

Funding for this project came from the Nevada Institute of Water Resources Research (NIWRR) contract number 06HQGR0098. The USGS contributed federal money while the Desert Research Institute provided matching support. Additional thanks is given to Karen Thomas with the USGS in Carson City, Nevada for sharing data and ideas. A special thanks to Paul Neeley for his invaluable IT assistance during Monte Carlo performed on the SunFire x4600 servers (each with 8 AMD quad-core Opteron 8356 CPU's and 96 GB RAM each with 4 AMD Opteron CPUs and 8 GB) and running the GNU/Linux operating system, CentOS 5.3 distribution.

Appendix A: Notation

A	interfacial area between the channel bottom and overlying water column (m^2)
B_f	velocity correction factor for turbulent mixing and resuspension of total species during low flow conditions (dimensionless)
C_b	dissolved chemical concentration in the channel bed sediments ($mg/L, g/m^3$)
C_b^T	total chemical concentration in the channel bed sediments ($mg/L, g/m^3$)
C_p	concentration of product in methylation or demethylation reactions (mg/L)
C_r	concentration of reactant in methylation or demethylation reactions (mg/L)
C_w	dissolved chemical concentration in water column segment (mg/L)
c	normalizing constant to ensure GLUE likelihoods sum to unity (dimensionless)
D	water depth starting at the vertical face of the channel bank (m)
d	characteristic mixing length (m)
d_{riv}	characteristic mixing length in channel bottom sediments (m)
d_{res}	characteristic mixing length in reservoir bottom sediments (m)
Δ	change in posterior means between pre and post-flood simulations (%)
E	diffusion coefficient (m^2/s)
F	objective function used in GLUE analysis (dimensionless)
f_b	fraction of THg that is dissolved in the bed sediments (dimensionless)
ϕ_b	fraction of THg that is dissolved in the bank sediments (dimensionless)
f_{temp}	temperature multiplier to correct methylation and demethylation for temperatures deviating from 20°C (dimensionless)
γ_w	specific weight of water ($kg/m^2/s^2$)
η	porosity (dimensionless)
$[Hg]_m$	maximum inorganic bank mercury concentration ($\mu g/Kg$)
$[Hg]_b$	inorganic channel bed mercury concentration ($\mu g/Kg$)
$[Hg]_{bk}$	inorganic bank mercury concentration ($\mu g/Kg$)
h	height of the vertical bank face along the river's edge (m)
i	individual data criteria ($i = 1$ to 18) defined in Table 2.3
J	total number of realizations in Monte Carlo
j	individual Monte Carlo realization
K_{20}	reaction rate associated with methylation or demethylation (per day)
κ	normalizing constant to ensure posterior likelihoods sum to unity (dimensionless)
L^0	prior input distribution
L_s	model segment length (m)
$L_j(\vec{Y} \vec{\theta}_j)$	likelihood function for the j^{th} parameter set θ given observed data vector Y
$L_j(\vec{\theta}_j \vec{Y})$	posterior likelihood function computed with Bayes Theorem
l	individual input parameter
λ_l	scales maximum bank inorganic mercury bank concentration as a function of slope ($\mu g/kg$)

M	chemical mass (mg),
MER	total bank mass eroded (kg)
μ	input parameter mean
μ^*	normalized input parameter mean at a given number of realizations to final parameter mean
M/D_{bank}	methylation-demethylation K20 ratio in the river bank sediments
M/D_{bed}	methylation-demethylation K20 ratio in the river channel bed sediments
M/D_{low}	methylation-demethylation K20 ratio in the river channel bed sediments
M/D_{up}	methylation-demethylation K20 ratio in the river channel bed sediments
N	shape/scaling factor used in GLUE likelihood function (dimensionless)
n	Manning's coefficient (dimensionless)
ρ_s	density of bank material (Kg/m^2)
$\bar{\theta}$	set of input parameters
Q_{10}	temperature coefficient to solve methylation or demethylation based on temperature (dimensionless)
Q	root mean squared error defined in GLUE objective function (ng/L)
$(Q_i)_{min}$	minimum root mean squared error for a given data criteria i (ng/L)
R_u	relative uncertainty
r_s	spearman rank correlation coefficient (dimensionless)
S_0	channel bottom slope (dimensionless)
σ	input parameter standard deviation
σ_f	correction of Stokes settling velocity for contaminated fine particles
t	time (s)
U	relative uncertainty computed with first-order second moment
v	water velocity (m/s)
v_c	critical velocity required to erode and transport the observed course bottom sediment
\bar{Y}	set of observed data used to condition the GLUE likelihood function
ψ_1	constant of proportionality to describe bank erosion for in-channel flow ($m^2 s/kg$).
ψ_2	constant of proportionality to describe bank erosion for overbank flow ($m^2 s/kg$).

References Cited

- Ambrose, R.B., Wool, T.A., Martin, J.P. and Schanz, R.W., 1991. WASP5.X: A Hydrodynamic and Water Quality Model: Model Theory, User's Manual and Programmer's Guide. U.S. E.P.A., Athens, Georgia.
- Beven, J. 2006. A manifesto for the equifinality thesis. *Journal of Hydrology*. 320:18-36.
- Beven, K.J. and Binley, A.M. 1992. The future of distributed models: model calibration and uncertainty prediction. *Hydrol. Processes*. 6: 279-298. doi:10.1002/hyp.3360060305.
- Beven, J.K., and Freer, J. 2001. Equifinality, data assimilation, and uncertainty estimation in mechanistic modeling of complex environmental systems. *Journal of Hydrology*. 249: 11-29.
- Beven K.J., Freer J., Hankin B., and Schulz, K. 2000. The use of generalized likelihood measures for uncertainty estimation in high order models of environmental systems. In: Fitzgerald WJ, Smith RL, Walden AT, Young PC, editors. *Nonlinear and nonstationary signal processing*. Cambridge: Cambridge University Press. p. 115–51.
- Blasone, R-S., Madsen, H., and Rosbjerg, D. 2008. Uncertainty assessment of integrated distributed models using GLUE with Markov chain Monte Carlo sampling. *Journal of Hydrology*. 353: 18-32.
- Bonzongo, J.C., Heim, K.J., Chen, Y., Lyons, W.B., Warwick, J.J., Miller, G.C. and Lechler, P.J. 1996a. Mercury pathways in the Carson River - Lahontan Reservoir System, Nevada, USA. *Environmental Toxicology and Chemistry*. 15(5): 677-663.
- Bonzongo, J.C., Heim, K.J., Warwick, J.J. and Lyons, W.B., 1996b. Mercury Levels in Surface waters of the Carson River-Lahontan Reservoir system, Nevada: influence of historic mining activities. *Environ Pollution*, 92(2): 193- 201.
- Carroll, R.W.H. and Warwick, J.J., 2001. Uncertainty analysis of the Carson River mercury transport model. *Ecological Modeling*, 137: 211-224.
- Carroll, R., Warwick, J.J., James, A., and Miller, J. 2004. Modeling Erosion and Overbank Deposition During Extreme Flood Conditions on the Carson River, Nevada. *Journal of Hydrology*. 297:1-21.
- Carroll, R.W.H., Warwick, J.J., Heim, K.J., Bonzongo, J.C., Miller, J.R. and Lyons, W.B., 2000. Simulating Mercury Transport and Fate in the Carson River, Nevada. *Ecological Modeling*, 125:255-278.

- Chen Y., Bonzongo J.C., Miller G.C. 1996. Levels of methylmercury and controlling factors in surface sediments of the Carson River system, Nevada. *Environ. Pollut.* 92:281-287
- Cussler, E.L. 1976. *Multicomponent Diffusion*. Elsevier, Amsterdam.
- Darby, S.E. and Thorne, C.R., 1996. Numerical simulation of widening and bed deformation of straight sand-bed rivers. I: Model development. *Journal of Hydraulic Engineering*, 122(4): 184-193.
- Diamond, M., Ganapathy, M., Peterson, S., and Mach, K. (2000). Mercury dynamics in the Lahontan Reservoir, Nevada: Application of the QWASI Fugacity /Aquivalence multispecies model. *Water, Air and Soil Pollution*. 117: 133-156.
- Ecology and Environment, Inc. 1998. *Ecological Risk Assessment Carson River Mercury Site*. Prepared for the U.S. Environmental Protection Agency, ARCS Region 9 and 10. ZS3490_D4700.
- Feyen, L., Beven, K.J., De Smedt, F., and Freer, J. 2001. Stochastic capture zone delineation within the generalized likelihood uncertainty estimation methodology: conditioning on head observations. *Water Resources Research*. 37(3):625-638.
- Franks, S.W., Beven, K.J., and Gash, J.H.C. 1999. Multi-objective conditioning of a simple SVAT model. *Hydrology and Earth System Sciences*. 3(4): 477-489.
- Gandhi, N., Bhavsar, S.P., Diamond, M.L., and Kuwabara, J.S. 2007. Development of a mercury speciation, fate and biotic uptake (Biotranspec) model: Application to Lahontan Reservoir (Nevada, USA). *Environmental Science and Technology*. 26 (11): 2260-2273.
- Guentzel, J.L, Landing, W.M., Gill, G.A. and Pollman, C.D. 1995 Atmospheric deposition of mercury in Florida: The FAMS project (1992–1994). *Water Air and Soil Pollution*. 80: 393–402.
- Heim, K.J. and Warwick, J.J., 1997. Simulating sediment transport in the Carson River and Lahontan Reservoir, Nevada. *Journal of the American Water Resources Association*, 33(1): 177-191.
- Heim, K.J. 1996. Modeling the fate of mercury in the Carson River and Lahontan Reservoir, Nevada. Thesis 3762 (Ph.D.) - University of Nevada, Reno.
- Hjulstrom, F. 1935. Studies in the morphological activity of rivers as illustrated by the river Fyris. *Geol. Inst. Uppsala Bull* 25: 221528.

- Hoffman, R.J. and Taylor, R.L., 1998. Mercury and suspended sediment, Carson River basin, Nevada- loads to and from Lahontan Reservoir in flood year 1997 and deposition in reservoir prior to 1983. U.S. Geological Survey, FS-001-98.
- Hosseinipour, E.Z. and Martin, J.L., 1990. RIVMOD: a one-dimensional hydrodynamic sediment transport model: model theory and user's guide. U.S. E.P.A, Athens, Georgia.
- Kuczera, G., and Parent, E. 1998. Monte Carlo assessment of parameter uncertainty in conceptual catchment models: the Metropolis algorithm. *Journal of Hydrology*. 211:69-85.
- Kuwabara, J.S., Marvin-Dipasquale, M., Praskings, W., Topping, R.R., Carter, J.L., Fend, S.V., Parchaso, R., Krabbenhoft, D.P., and Gustin, M.N. 2002. Flux of dissolved forms of mercury across the sediment-water interface in Lahontan Reservoir, Nevada. U.S. Geologic Survey Water-Resources Investigation Report 02-4138. U.S. Department of the Interior.
- Martin, J.L., 1992. MERC4: A mercury transport and kinetics model: model theory and user's guide. U.S. E.P.A., Athens, Georgia.
- Marvin-DiPasquale, M., Agee, J., Krabbenhoft, D., and Oremland, R.S., 2001, Methylmercury Formation and Degradation in Sediments of the Carson River System: U.S. Geological Survey, Administrative Report prepared for U.S. EPA (Region IX).
- Miller, J.R., Lechler, P.J., Rowland, J., Desilets, M., and Hsu, L-C. 1995. An integrated approach to the determination of the quantity, distribution, and dispersal of mercury in Lahontan Reservoir, Nevada, USA. *J. Geochem. Explor.* 52:45-55
- Miller, J.R., Lechler, P.J., and Desilets, M., 1998. The role of geomorphic processes in the transport and fate of mercury in the Carson River basin, west-central Nevada. *Environmental Geology*, 33(4): 249-262.
- Miller, J.R., Barr, R., Grow, D., Lechler, P., Richardson, D., Waltman, K. and Warwick, J., 1999. Effects of the 1997 flood on the transport and storage of sediment and mercury within the Carson River valley, west-central Nevada. *Journal of Geology*, 107(3): 313.
- Morse, B.S., and Pohl, P. 2003. Stochastic capture zone analysis of an arsenic-contaminated well using the generalized likelihood uncertainty estimator (GLUE) methodology. *Water Resources Research*. 39(6):1151. doi:10.1029/2002WR001470.

- Reid, R.C., Praunsnitz, J.M., and Sherwood, T.K. 1977. *The Properties of Gases and Liquids*, Third Edition. McGraw-Hill. NY. p. 578
- Romanowicz, R.J., and Beven, K.J. 2006. Comments on the generalized likelihood uncertainty estimation. *Reliability Engineering and System Safty*. 91:1315-1321.
- Romanowicz, R.J., Beven, K.J., and Tawn, J. 1996. Bayesian calibration of flood inundation models, in *Floodplain Processes*. Edited by M.G. Anderson, D.E. Walling and P.D. Bates. pp. 333-360. John Wiley, Hoboken, N.J.
- Smith, G.H. and Tingley, J.V., 1998. *The history of the Comstock Load, 1850-1997*. Nevada Bureau of Mines and Geology in association with the University of Nevada Press.
- Stedinger, J.R., Vogel, R.M., Lee, S.U., and Batchelder, R. 2008. Appraisal of the generalized likelihood estimation (GLUE) method. *Water Resources Research*. (44): 1-17. W00B06, doi:10.1029/2008WR006822.
- Stordal, M.C., Gill, G.A., Wen, L.-S., and Santschi, P.H. 1996. Mercury phase speciation in the surface waters of selected Texas estuaries: Importance of colloidal forms. *Limnology and Oceanography*. 41(1): 52-61.
- Tessier, A., and Turner, D.R. (eds). 1995. *Metal speciation and bioavailability in aquatic systems*. Wiley, Chichester.
- Warwick, J.J. and Carroll, R.W.H. 2008. Evaluating the impacts of uncertainty in geomorphic channel changes on predicting mercury transport and fate in the Carson River system, Nevada. *International Journal of Soil, Sediment and Water*. 1: 1-15. Full text at <http://scholarworks.umass.edu/intljssw/vol1/iss1/4>
- Warwick, J.J. and Heim, K.J., 1995. Hydrodynamic modeling of the Carson River and Lahontan Reservoir, Nevada. *Water Resources Bulletin*, 31(1): 67-77.

CHAPTER 3

Seasonal Variation of Mercury Associated with Different Phytoplankton Size Fractions in Lahontan Reservoir, Nevada

Rosemary W.H. Carroll⁵, Jeramie Memmott⁶, John J. Warwick⁷, Christian H. Fritsen⁸,
Jean-Claude J. Bonzongo⁹ and Kumud Acharya¹⁰

Abstract

Sampling was conducted during 2006 in Lahontan Reservoir, Nevada to quantify seasonal variation of total mercury (THg) and methylmercury (MeHg) accumulation in different phytoplankton size fractions as a function of dissolved point source (fluvial) mercury loads, reservoir residence time and algal growth. Carson River dissolved mercury inputs into the reservoir were extremely dynamic with spring loads two-orders of magnitude larger than summer loads. Chlorophyll *a* (Chl_a) measurements showed two periods of algal growth. A small amount of algal growth occurred March to May. A second more substantial bloom occurred in the late summer, which was dominated by large, filamentous algae. THg concentrations and accumulation in total suspended particulate matter (SPM) were highest when fluvial inputs of mercury contaminated sediment were large and were not associated with

⁵ Corresponding author, Assistant Research Hydrologist, Division of Hydrologic Sciences, Desert Research Institute, 2215 Raggio Parkway, Reno, NV 89512 Rosemary.Carroll@dri.edu.

⁶ Field/Lab Technician, Division of Earth and Ecosystem Sciences, Desert Research Institute, 2215 Raggio Parkway, Reno, NV 89512 Jeramie.Memmott@dri.edu

⁷ Executive Director of Hydrologic Sciences, Desert Research Institute, 2215 Raggio Parkway, Reno, NV 89512 John.Warwick@dri.edu

⁸ Associate Research Professor, Division of Earth and Ecosystem Sciences, Desert Research Institute, 2215 Raggio Parkway, Reno, NV 89512. Chris.Fritsen@dri.edu

⁹ Assistant Professor, Environmental Engineering Sciences, University of Florida, 320 Black Hall, Gainesville, FL 32611-6450. bonzongo@ufl.edu

¹⁰ Associate Research Professor, Division of Hydrologic Sciences, 755 E. Flamingo Road, Las Vegas, NV 89119. Kumud.Acharya@dri.edu

living biomass. However, THg associated with smaller sized particles was more ambiguous with THg concentrations increasing during phytoplankton growth, but trends were statistically insignificant. MeHg accumulation for the small size fraction was indirectly related to fluvial loads of dissolved MeHg and strongly associated with living biomass in the later portion of the summer when algal growth occurred and reservoir residence times were long. Data also suggest that MeHg accumulated minimally in large phytoplankton and samples of total SPM MeHg will skew results toward under predicting MeHg accumulation in smaller phytoplankton.

KEY WORDS: mercury, loading, phytoplankton, eutrophic reservoir

3.1 INTRODUCTION

Trophic enrichment of mercury (Hg) is relatively uniform across a range of food webs conditions (benthic versus pelagic versus stream), ecological settings (marine versus freshwater) and exposure conditions (point source versus atmospheric deposition) (Kidd et al., 1995; Pickhardt et al., 2005; Stewart et al., 2008; Chasar et al., 2009). Since enrichment factors between trophic levels are fairly consistent, difference in top predator fish can often be attributed to differences in Hg availability and accumulation efficiency at the base of the food web (Stewart et al., 2008; Chasar et al., 2009). Stewart et al. (2008) found pelagic systems more effective at accumulating Hg compared to benthic systems. Phytoplankton represent the base of pelagic food webs and have been found to bioaccumulate Hg 10^4 to 10^5 times more than successive trophic transfers (Watras et al., 1998; Moye et al., 2002; Pickhardt and Fisher, 2007). Therefore, small changes in phytoplankton bioaccumulation may

have significant implications on overall Hg bioaccumulation in the system as a whole (Mason et al., 1996).

The inverse relationship between algal growth rate and bioaccumulation presented by Mason et al. (1996) helps explain growth dilution and is supported by several studies which found that higher phytoplankton densities and/or growth rates resulted in less Hg accumulation in both plankton communities as well as at higher trophic levels (Karimi et al., 2007; Chen and Folt, 2005; Pickhardt et al., 2005; Pickhardt and Fisher, 2007). Bloom dilution however, can occur for different reasons; rapid growth such that the growth rate becomes larger than the rate of Hg sequestration, preferential partitioning of Hg to non-living particles (Laurier et al., 2003; Schäfer et al., 2006; Luengen and Flegal, 2009) or limited supply of dissolved Hg species such that uptake depletes water column concentrations during early portions of a bloom (Luengen and Flegal, 2009). Size of the algae, as depicted by Mason et al. (1996), may also influence Hg uptake efficiency. Those with greater surface area to volume are expected to accumulate Hg more rapidly. Work by Pickhardt and Fisher (2007) found this to be true for MeHg, however MeHg was not established as a passive, diffusional process. Instead MeHg uptake was metabolically controlled, as exemplified by much larger accumulation of MeHg in live diatoms compared to dead cells. Moye et al. (2002) also found MeHg uptake dependent on active cellular metabolism, but unlike Pickhardt and Fisher (2007), MeHg uptake efficiency is not always size dependent. Instead, species-specific membrane permeability was speculated as an important parameter in describing uptake efficiency.

Pickhardt and Fisher (2007) found inorganic Hg insensitive to cell size. They suggest that accumulation of inorganic Hg is a function of binding to the ubiquitous organic film found on all particles, living and non-living. Likewise, Luengen and Flegal (2009) show that total Hg (THg), a surrogate for inorganic Hg, preferentially binds to non-living matter (material from broken and decaying cells or organically coated clay particles) with phytoplankton THg concentrations relatively low compared to other types of suspended material.

Given the potential importance of Hg bioaccumulation through the pelagic pathway, this study is focused on relative uptake of THg and MeHg in different size fractions of phytoplankton in a reservoir with highly dynamic fluvial inputs of dissolved THg (2 to 140 g/d). The system examined is a eutrophic reservoir in northern Nevada impacted by historic mining. It is hypothesized that phytoplankton abundance along with the size of the phytoplankton and the timing of mercury loads could impact Hg uptake efficiency into the lower food web.

3.2 SITE DESCRIPTION

The Carson River-Lahontan Reservoir system (CRLR) in west-central Nevada (Figure 3.1) is listed by the U.S. Environmental Protection Agency (US EPA) as a Superfund site due to its contamination with mercury derived from mining of the Comstock Lode in the later portion of the nineteenth century (NVD980813646). Lahontan Reservoir was constructed in 1915 and is used to irrigate fields in Lahontan Valley and is managed as a warm water fishery. Lahontan Reservoir consists of three distinct basins with water from the Carson River entering the south basin and moving

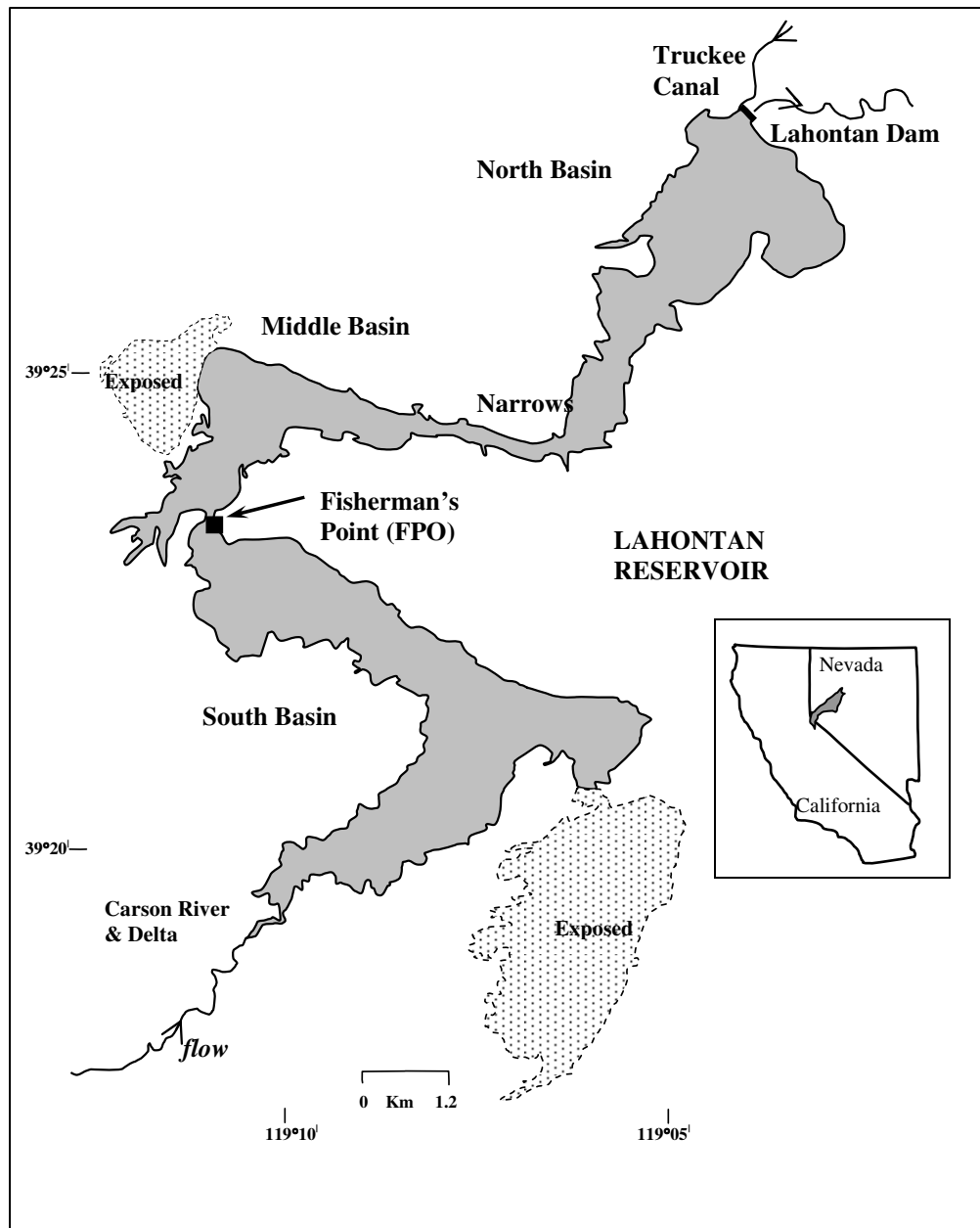


Figure 3.1: Lahontan Reservoir with Fisherman's Point (FPO) sampling site marked. The Carson River enters the southern basin of the reservoir. The USGS sampling site at Weeks Bridge is located 8 km upstream from the Carson River's delta. Upper inset shows location of the Carson River – Lahontan Reservoir (CRLR) watershed with respect to the western United States.

northward through the middle basin and into the north basin. The north basin terminates at Lahontan Dam. Narrow channels connect each of the basins and are marked as Fisherman's Point (FPO), which connects the south and middle basins, and the Narrows, which connects the middle and north basins. The dominant source of dissolved THg (DHg) and dissolved MeHg (DMeHg) into the reservoir is the Carson River (Gandhi et al., 2007; Diamond et al., 2000).

Phytoplankton provide most of the primary production in Lahontan Reservoir due to a limited littoral zone and drastic water level fluctuations in the reservoir. Cooper et al. (1983) observed that 99 percent of the phytoplankton sampled in the reservoir were Cyanophyta, with *Aphanizomenon flos-aquae* dominating the assemblage. Cyanophyta peaked in the hot summer months (10^6 cells/ml) with the magnitude and duration of the bloom increasing from the south basin to the north basin. These large, filamentous cyanobacteria decreased to negligible population levels (< 1 cell /ml) in the winter months in all three reservoir basins. Diatoms, on the other hand, had concentrations several orders of magnitude lower than cyanobacteria but maintained relatively high populations in the fall and winter months (100 – 200 cells/ml). Populations of diatoms were lowest in the north basin of the reservoir and highest in the middle and south basins.

3.3 METHODS

3.3.1 Reservoir Water Column Sampling

Samples for water column chemistry and phytoplankton biomass were obtained at FPO. This location represents a compromise of being close enough to the delta to preserve a well-defined mercury pulse entering from the Carson River, but far

enough from the delta to ensure slower velocities and reduce the risk of the delta migrating northward past the sampling location during reservoir drawdown in the summer months. The choice of FPO minimized sampling logistics because of its narrow cross section (approx. 100 m) and its accessibility by boat. Water column samples were collected every six weeks beginning early March 2006 to capture peak spring runoff. Sampling continued into late September to catch a possible secondary peak of smaller phytoplankton and to observe potential influences of internal cycling of mercury on accumulation in phytoplankton.

Vertical measurements of temperature, pH, oxidation-reduction potential, specific conductivity, *in vivo* fluorescence, photosynthetically active radiation (PAR), turbidity, and dissolved oxygen were obtained with a YSI 6600 sonde at three equidistant locations across the FPO cross section for use in later modeling studies. Maximum depth of the reservoir at FPO was approximately 13 m along the right bank and at the center profile but only 2.5 m along the left bank. During all sampling surveys, water was collected from a total of 10 discrete locations along the reservoir cross section at FPO with sample depths dependent on reservoir stage.

Discrete water samples were collected using a Teflon tube and peristaltic pump. Those collected for Chlorophyll *a* (Chl*a*), suspended particulate matter (SPM), and SPM-associated mercury concentrations (algal material not separated from SMP in the filtering process) were stored in opaque, high-density polyethylene (HDPE) 1 L bottles and transported on ice back to the Desert Research Institute (DRI) analytical facilities. At DRI, all 10 discrete samples were combined in a 14-L, Teflon, U.S. Geological Survey (USGS) Water Quality Modified Churn Splitter to form composite

samples for analysis. The Teflon tubing, HDPE bottles and the churn were all pre-cleaned with 10 percent HNO₃ for 48 or more hours and thoroughly rinsed with milliQ. Tubing and bottles were also thoroughly rinsed with reservoir water prior to sample collection. Additional water was collected at each discrete sample location and placed in one liter, opaque, HDPE bottles to measure Chl_a, and a partial suite of nutrients for each location to determine their spatial variation and to compare their variability with composite samples mixed in the churn. Water column mercury samples were collected using equivalent quantities from each discrete location and combined in an acid-washed Teflon bottle using the clean hands-dirty hands protocol (US EPA, 1996).

Filtering for SPM, THg and MeHg analysis and subsequent freezing at -80 °C was done within three to eight hours after collection. Standard filtration procedures were conducted with glass fiber filters (GF/F, 0.7 μm). Chl_a was determined fluorometrically (Welschmeyer, 1994) while SPM was determined using method 2540D. Total Suspended Solids were dried at 103°C to 105°C as described in Clesceri *et al.* (1998). Total SPM was obtained by pumping a sample directly onto a GF/F filter. The fraction of SPM smaller than 35 μm was obtained by passing the sample through a 35-μm Nitex[®] net prior to pumping onto the GF/F. The fraction greater than 35 μm was not measured directly, but inferred from the difference between the two samples.

3.3.2 Mercury Analysis

Mercury analysis required water sample aliquots to be filtered (0.45 μm) into acid pre-cleaned Teflon bottles, and both filtered and unfiltered fractions were

acidified with ultra-pure HCl at a final concentration of 1 percent (v/v). Samples were then kept refrigerated at 4 °C until analysis. THg concentrations were determined after subjecting water samples to BrCl/SnCl₂, followed by gas-phase purging with Hg-free N₂ and trapping of Hg⁰ onto gold-coated sand. The Hg⁰ was then thermally desorbed from the gold-trap and released into an Hg-free helium stream and quantified by cold vapor atomic fluorescence spectrometry (CV-AFS). MeHg was first separated from its original matrix by extraction in an organic solvent (Bloom, 1989; Horvat et al. 1993) and then ethylated using sodium tetraethylborate (Bloom, 1989), followed by CV-AFS detection after GC-separation and thermal decomposition of alkyl-Hg compounds. Quality assurance/quality control procedures included instrument calibration using standard solutions, certified reference materials, duplicate analyses, and reagent blanks. The detection limit, defined as three times the standard deviation of purged blanks was 0.06 and 0.01 ng/L for Hg and MeHg, respectively. The percent recovery on spiked samples averaged 98±5 percent (*n*=7) for THg and 90±8 percent (*n*=8) for MeHg.

THg in SPM was determined following digestion in a volumetric flask with a 7:3 mixture of concentrated HNO₃/H₂SO₄. Aliquots from the digestate were then analyzed by SnCl₂-reduction technique with detection by CV-AFS. MeHg was determined using a method adapted from Bloom (1989), where it is first released from the sample matrix by solvent extraction, followed by ethylation, Tenax[®] trapping, GC-separation, thermo-decomposition, and detection by CV-AFS. For both THg and MeHg, in addition to reagent blanks and liquid standard solutions, a certified reference material (IAEA-405, estuarine sediments containing an average of

0.81 mg/kg of THg and 5.49 ng/g of MeHg) was run with all digestions/analyses. The percent recovery on the IAEA-405 averaged 95 ± 11 percent ($n=10$), and 93 ± 8 percent ($n=10$) for THg and MeHg, respectively. Details regarding analytical procedures have been described (e.g., Bonzongo et al, 2006; Warner et al., 2003; Donkor et al., 2006).

3.3.3 Data Analysis

SPM, Chl a as well as SPM THg and SPM MeHg concentrations were normalized by the volume of composite reservoir water used in the filtering process ($\mu\text{g/L}$). This established concentrations per unit volume of reservoir water. Samples of total SPM MeHg collected in June, August and September fell below the detection limit (< 0.001 ng/filter). These samples were assigned detection limit concentrations in order to compute the upper limit. THg and MeHg concentrations were normalized by the amount of SPM to produce mass-specific mercury concentrations (C_b , $\mu\text{g/g}$).

THg and MeHg accumulation, K_d (L/Kg), was computed as,

$$K_d = \log\left(\frac{C_b}{C_w}\right) \quad (3.1)$$

where C_w is the dissolved water column concentration (mg/L).

Error in measurements propagates through the various calculations to obtain C_b and K_d . Variability in C_w was defined as the standard deviation in duplicate analysis. Error in SPM and Chl a were determined as the maximum error to rectify mass balance calculations. Mass balance errors were larger than observed variability in duplicate samples and deemed the more conservative approach. Specifically, total SPM was measured less than its subset (SPM $< 35 \mu\text{m}$) on two occasions (error

equal to 7.8%), while total Chl a was measured less than its subset once (error equal to 12.2%).

3.4 RESULTS

3.4.1 Water Column Concentrations and Loads into the Reservoir

Water column DHg and DMeHg concentrations collected at FPO are compared to USGS DHg and DMeHg water quality data collected at Weeks Bridge (Figure 3.2a). Weeks Bridge (USGS site 10312020) is located on the Carson River approximately 8 km upstream from the river's delta and is a surrogate for fluvial concentrations entering the reservoir. DHg was higher at FPO compared to its fluvial counterpart for all sampling dates except March, implying that either DHg originating from the lower section of the Carson River (i.e., below Weeks Bridge) or diffusion from reservoir benthic sediments may be important mechanisms for DHg loading into the reservoir. At FPO, DMeHg concentrations were relatively constant throughout the sampling period with DMeHg measured between 0.5 and 2.1 ng/L. DMeHg concentrations were statistically larger than concentrations at Weeks Bridge only in August, implying that, other than late summer, internal loading of DMeHg from reservoir bottom sediments may not be significant compared to point loads from the Carson River.

DHg and DMeHg fluvial loads (W) were calculated as the product of discharge and concentration. Daily discharge was estimated at the river's delta (entrance to the reservoir's south basin) using a modified version of the US EPA hydrodynamic code RIMOD (Hosseini-pour and Martin, 1990), a tool developed for the CRLR system (Carroll et al., 2004; Carroll et al., 2000, Warwick and Heim,

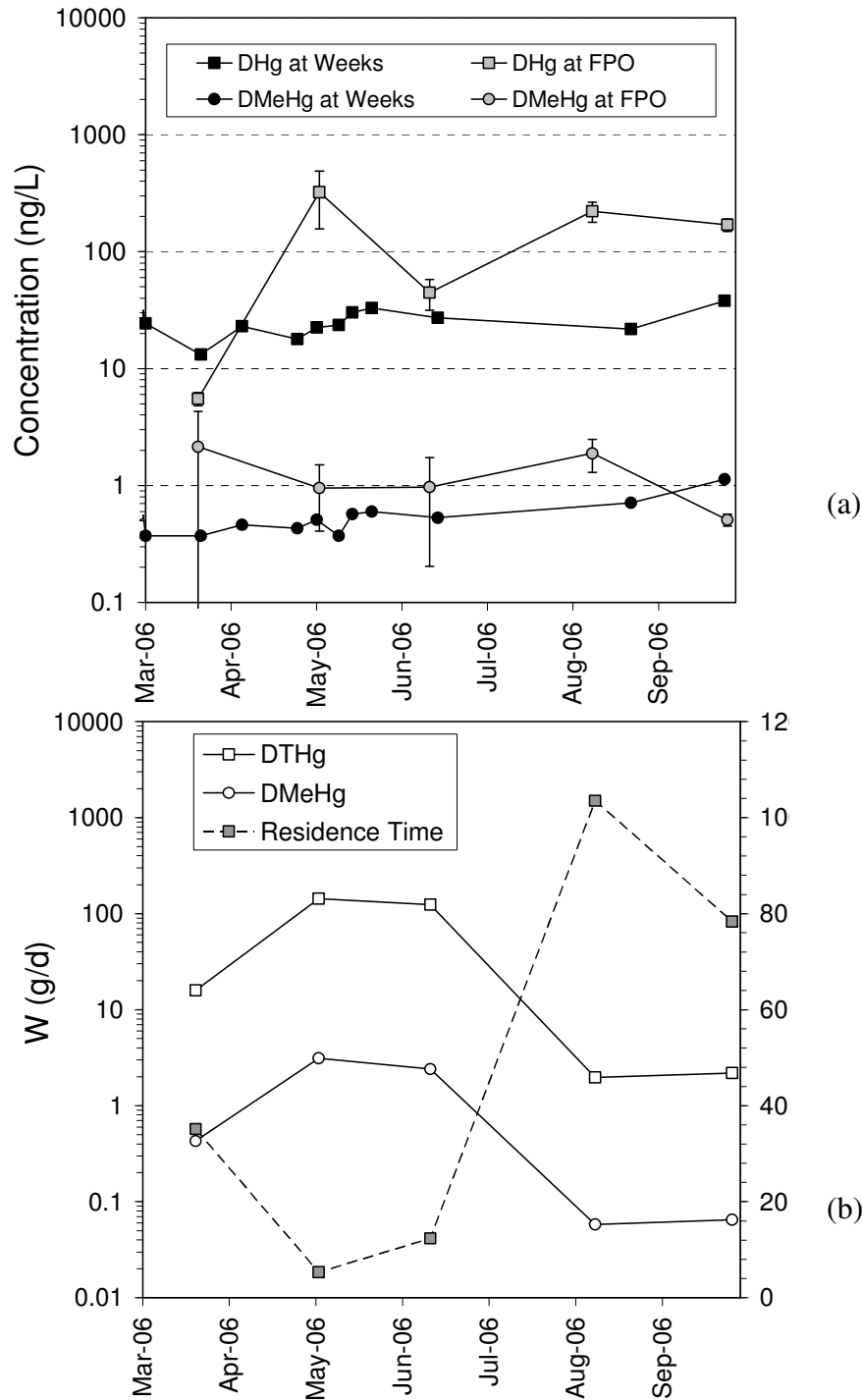


Figure 3.2: (a) water column concentrations collected at Weeks Bridge by the USGS and at FPO. Error bars at FPO represent one standard deviation of the mean. (b) Dissolved mercury loads into the reservoir and computed residence time (τ days) in the reservoir's southern basin.

1995). Loads into the reservoir are provided in Figure 3.2b. Peak loads from the Carson River occurred during spring runoff. Carson River loads entering the reservoir then diminished by two orders of magnitude for both DHg and DMeHg between the spring and the late summer. The residence time (τ) for water moving through the southern basin of the reservoir was also computed using the CRLR model. Residence time was determined as the quotient of water volume divided by the flow rate (done for individual model segments and summed) with calculations accounting for delta migration as a result of fluctuating reservoir level. Estimated resident times for days when samples were collected at FPO ranged from five days in May to 104 days in August (Figure 3.2b).

3.4.2 THg and MeHg Associated with Phytoplankton

Chl a values for phytoplankton <35 μm were relatively consistent throughout the sampling period, but were highest in the spring and late fall with minimum biomass observed in mid-June (Figure 3.3). Chl a values for the entire assemblage were more dynamic, with Chl a >35 μm represented as the difference between the two curves in Figure 3.3. Phytoplankton >35 μm had two growth periods. A small increase in biomass occurred between March and May (0.6 to 2.5 $\mu\text{g/L}$), followed by a decrease in June to nearly 0 $\mu\text{g/L}$. Larger phytoplankton then grew at a substantial rate during the second half of the summer to (24 $\mu\text{g/L}$), with a subsequent decline

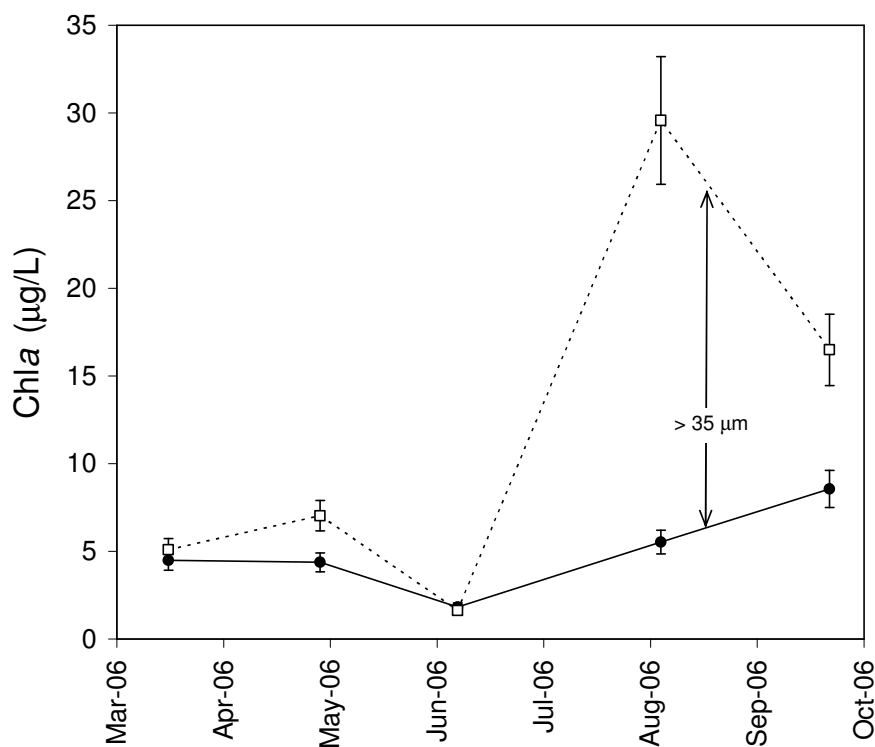


Figure 3.3: Chla concentrations in $\mu\text{g/L}$ for phytoplankton less than $35\ \mu\text{m}$ (●) and total phytoplankton (□). Chla $> 35\ \mu\text{m}$ is the difference between the two curves.

witnessed by the end of September ($8\ \mu\text{g/L}$). The percentage of Chla to SPM (ϕ) mimicked Chla concentrations, and ranged from 0.008% to 0.2% with minimum relative living biomass occurring in June and maximum fractions occurring in August (total phytoplankton) and September (for phytoplankton $<35\ \mu\text{m}$). While the fraction of living biomass is small at FPO, it is comparable to Camp Far West Reservoir located in the western foothills of the Sierra Nevada in California, where mean ϕ ranged from 0.02% to 0.39% (Stewart et al., 2008) and SPM MeHg was used to assess accumulation at the base of the pelagic food web.

THg C_b for total SPM (Fig 3.4a) showed a substantial increase ($6\ \mu\text{g/g}$ to $51\ \mu\text{g/g}$) during May when SPM peaked but ϕ was relatively low. Otherwise THg C_b for

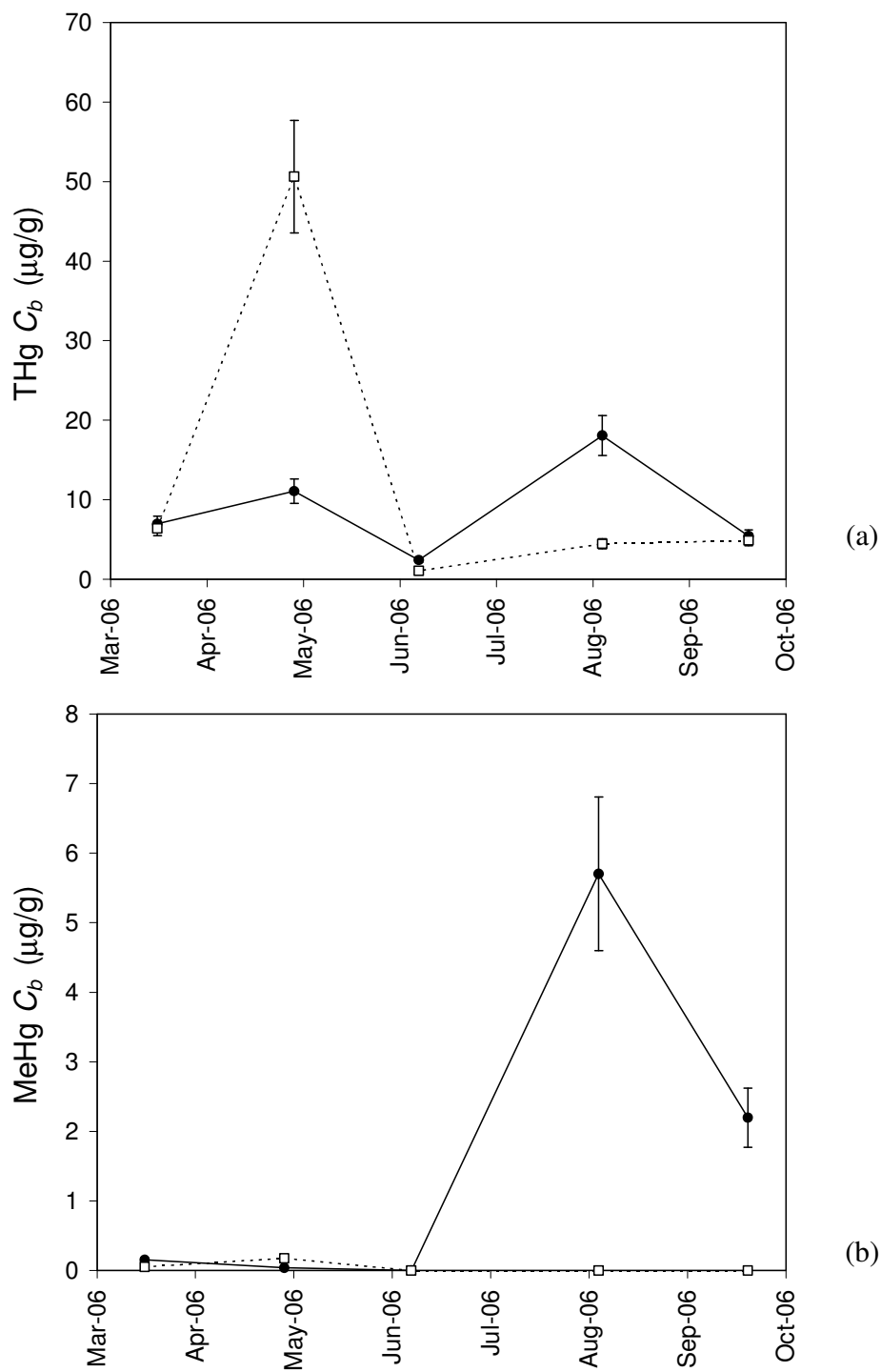


Figure 3.4: Mercury accumulation in SPM < 35 μm (●) and total SPM (□), expressed as mercury concentration per unit mass for (a) THg C_b , (b) MeHg C_b .

total SPM was relatively low ($C_b < 5 \mu\text{g/g}$) despite a period of considerable algal growth in the late summer. THg C_b for the $< 35 \mu\text{m}$ size fraction showed two modest peaks; one in May ($11 \mu\text{g/g}$) and one in August ($18.1 \mu\text{g/g}$). Regression analysis between THg C_b with fluvial contributions of unfiltered THg ($p < 0.001$) and suspended sediment ($p < 0.02$) showed total SPM THg C_b was directly correlated with the particulate fraction originating in the river and was not correlated to fluvial DHg, Chl a or ϕ . THg C_b related to SPM $< 35 \mu\text{m}$, showed no statistically significant correlation with any of the variables examined. Results suggest that THg was primarily associated with sediment derived from the Carson River and was not associated with phytoplankton. This affinity was biased toward larger sediment, since THg C_b for smaller particles peaked when ϕ and Chl a ($< 35 \mu\text{m}$) were increasing but regression analysis was not statistically conclusive.

Seasonal MeHg C_b in the $< 35 \mu\text{m}$ size fraction were relatively low during the spring runoff period ($< 0.2 \mu\text{g/g}$) when DMeHg and sediment loads into the reservoir were high, and increased substantially ($5.7 \mu\text{g/g}$) by August (Figure 3.4b) when loading, and fluvial sediment inputs were relatively low. Spring MeHg C_b for total SMP is comparable to the $0.1 \mu\text{g/g}$ reported from Camp Far West Reservoir by Stewart et al. (2008). Lahontan Reservoir MeHg C_b for total SPM were negligible during the summer and early fall, reflecting concentrations below detection in June, August and September. Trends in SPM size fractions are opposite to those reported by Back et al. (2003) for Lake Superior where the small size fraction ($< 35 \mu\text{m}$) were most important in the spring but the larger size fraction ($> 112 \mu\text{m}$) had concentrations significantly larger than smaller size fractions in August. Difference in systems may

be related to differences in phytoplankton species or trophic status between the systems. Regressions between MeHg C_b for small particles showed a direct relationship with ϕ ($p = 0.17$) and an indirect relationship to DMeHg loads from the river ($p = 0.11$). No correlation was found with Chl a or fluvial sediment contributions. While relationships are weak, they suggest that MeHg concentrations in small sized SPM are more related to living material than THg and are not influenced by fluvial contributions.

Mercury accumulation (K_d) for THg and MeHg are presented in Figure 3.5a and 3.5b, respectively. THg K_d ranged between 4.3 and 6.1 with little difference between total SPM and SPM $<35\mu\text{m}$. THg K_d was largest in the spring when the Carson River inflows contributed large loads of suspended sediment. Spring values of MeHg K_d for total SPM and SPM $< 35 \mu\text{m}$ ranged between 4.4 and 5.0 with little distinction between the total and small size fractions. MeHg K_d then declined for both sizes in June to nearly 2.0. A similar drop in K_d was not witnessed for THg. During June, Chl a was at a minimum for total and small size fractions, but SPM was still high. Large drops in MeHg K_d may reflect a preferential affinity for biomass, compared to THg which may preferentially bind to sediment. During the later portion of the summer, SPM $<35 \mu\text{m}$ experienced a dramatic increase in MeHg K_d (~ 6.6), while MeHg K_d for the total size fraction remained low. Low MeHg K_d in total SPM reflect measured concentrations below detection, and illustrate the diluting nature of large, filamentous phytoplankton on measured MeHg uptake efficiency during the late summer.

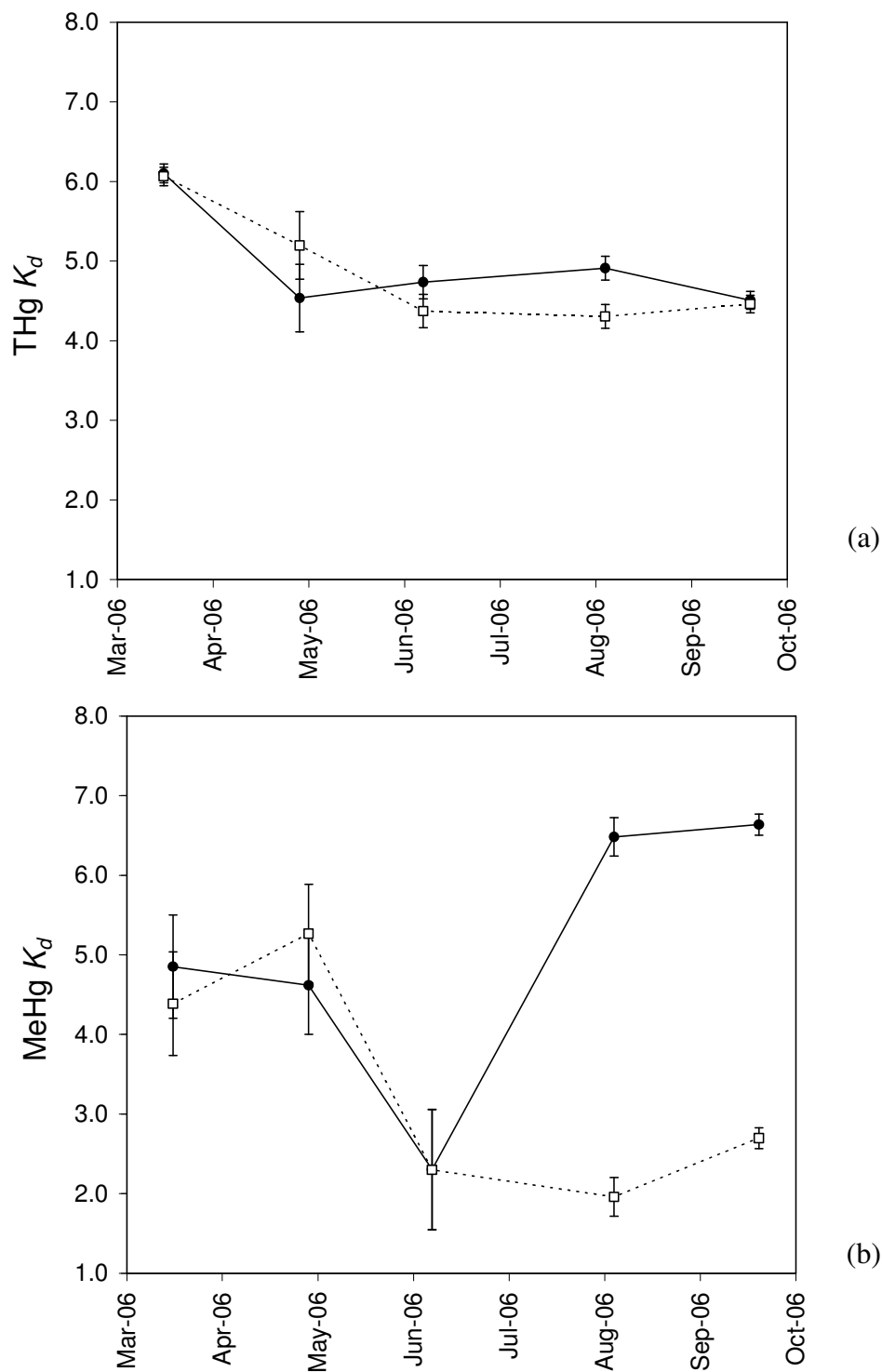


Figure 3.5: Bioaccumulation (K_d) for SPM < 35 μm (●) and total SPM (□), (a) THg K_d and (b) MeHg K_d .

Correlation was done between THg K_d and MeHg K_d with Chl a , SPM, dissolved loads from the river, dissolved water column concentrations at FPO, and residence time in the reservoir. MeHg K_d regressions are provided in Figure 3.6. THg K_d for total SPM showed a tendency to decrease with increased Chl a suggesting dilution by preferential sorption to sediment. However, these trends were not

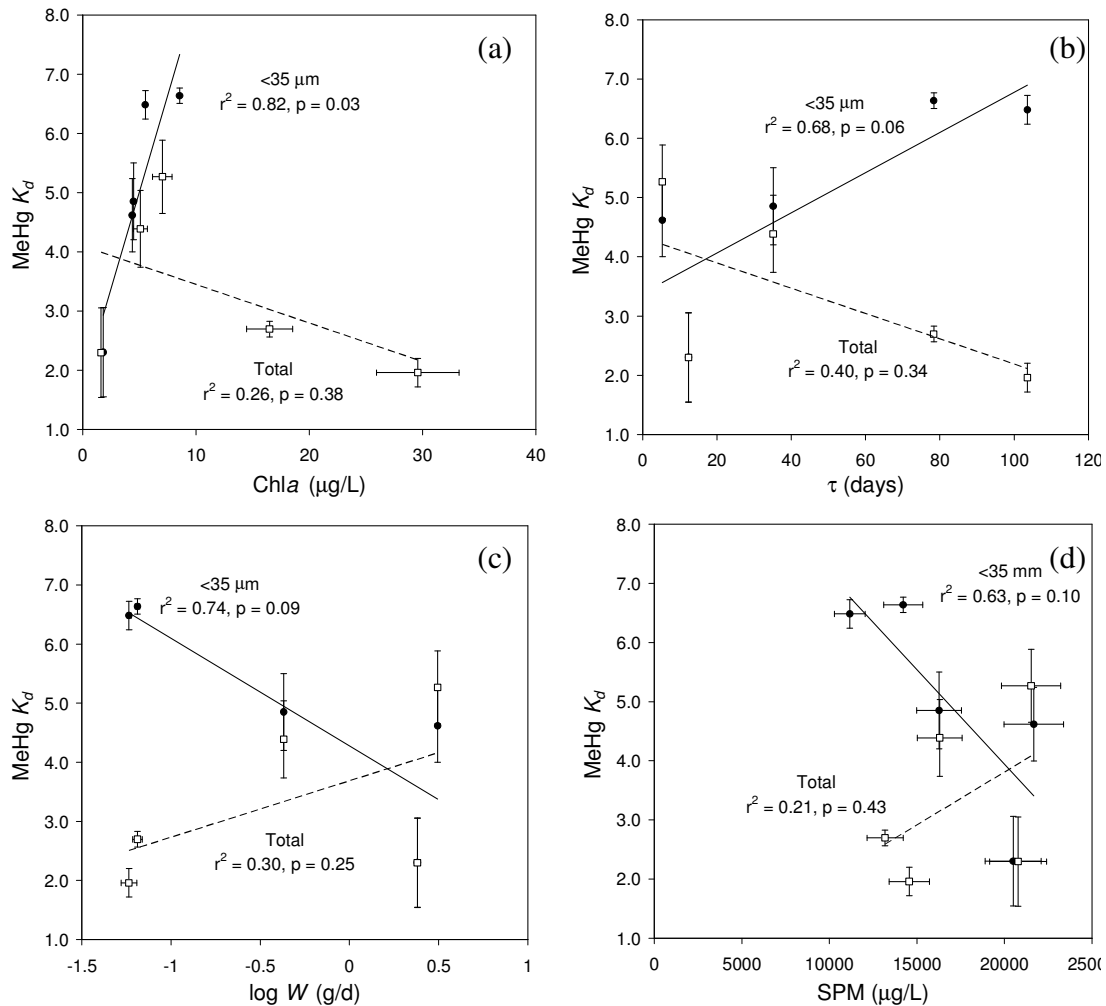


Figure 3.6: MeHg K_d for SPM < 35 μm (●) and total SPM (□) as a function of (a) Chl a , (b) residence time, τ , (c) log-transformed DMeHg loads, W and (d) SPM. Linear regression conducted on mean values with linear regression for SPM < 35 μm shown as a solid line and for total SPM as a dashed line.

significant ($p = 0.38$). All other THg K_d regressions were highly insignificant. MeHg K_d for SPM < 35 μm were directly correlated with Chl a (Figure 3.6a, $p=0.03$) and residence time (Figure 3.6b, $p = 0.06$) and indirectly correlated to log-transformed DMeHg fluvial loads (Figure 3.6c, $p = 0.09$) and SPM (Figure 3.6d, $p = 0.10$). Regressions for total SPM MeHg K_d were less significant ($0.25 < p < 0.43$) in all cases and trended in the opposite direction to the smaller fraction (refer to Figure 3.6). No correlation was found between MeHg K_d and dissolved water column concentrations at FPO.

3.5 DISCUSSION

Results in this study are limited by small data sets and regression techniques and can be only speculative. Yet observations suggest differences exist between THg and MeHg in terms of source, preferential partitioning between living and non-living SPM as well as a size dependence on uptake efficiency. In general, THg in Lahontan Reservoir is preferentially partitioned to sediment originating from the Carson River and is not a function of living biomass in the reservoir. This is evidenced by large THg concentrations (C_b) during the spring when unfiltered THg concentrations were high, while low THg C_b occurred in the late summer when phytoplankton (e.g., *Aphanizomenon flos-aquae*) have large biomass. Results pertain more to particles greater than 35 μm , since particles less than 35 μm produce more ambiguous results. Specifically, THg concentrations in smaller particles showed weak tendencies to accumulate when small phytoplankton had net growth. THg accumulation in SPM, as defined by K_d , is similar between size fractions and remains relatively constant through out the sampling period with no significant trend in K_d with respect to river

loads, reservoir residence time or biologic growth. The lack of trend in K_d hints that THg is a passive, sorption process that is unchanged by metabolic processes of phytoplankton. Insensitivity of THg K_d to biomass reflects preferential sorption to non-living particulates which corroborates work from other studies (Laurier et al., 2003; Schäfer et al., 2006; Pickhardt and Fisher, 2007; Luengen and Flegal, 2009).

MeHg appears to have a greater affinity for living biomass compared to THg as evidenced by trends in C_b and K_d . Our results are supported by Mason et al. (1996) who found MeHg accumulation greater in living diatoms compared to dead diatoms, and by Luengen and Flegal (2009) who found K_d related to factors defining algal bloom as opposed to factors related to sorption or decay. MeHg enrichment for smaller particles increased with increased Chl a . Most studies report Hg dilution with increased biomass (e.g., Pickhardt et al., 2005; Chen and Folt, 2005), but work by Kirkwood et al. (1999) did find a positive correlation between concentration and biomass on a seasonal level. For Lahontan Reservoir, the direct relationship between MeHg accumulation and biomass is isolated to smaller particles. When considering the total fraction of SPM, dilution of MeHg, though statistically weak, does occur. Dilution may be the result of *Aphanizomenon flos-aquae* large size or rapid growth rate during the late summer. Permeability of *Aphanizomenon flos-aquae* cell membrane is not known, nor are *Aphanizomenon flos-aquae* metabolic requirements that would regulate MeHg uptake. However, both could influence the inefficiency of MeHg uptake. None the less, size distinction appears important to MeHg accumulation in phytoplankton. Lumping all sizes into a single SPM sample will skew the analysis toward low MeHg concentrations and low accumulation during the

late summer when *Aphanizomenon flos-aquae* dominated the assemblage. Instead, separating out the smaller size fraction will produce different results. MeHg preference for smaller, more palatable phytoplankton has implications on systematic MeHg accumulation in Lahontan Reservoir.

Cyanobacteria are known to be a low-quality food source for zooplankton. Zooplankton growth and reproduction are inhibited by cyanobacteria's filamentous structure and low digestibility (DeMott, 1999; DeMott et al., 2001; Ghadouani et al., 2003). Early studies have demonstrated that cyanobacteria are not readily ingested or digested by zooplankton (Hayward and Gallup, 1976) and while cladocerans, such as *Daphnia pulex*, can effectively feed on single filaments of *Aphanizomenon flos-aquae*, they do not graze on large colonies (Holm et al., 1983) Therefore, it is assumed that any MeHg accumulation in *Aphanizomenon flos-aquae* acts as a temporary sink for MeHg. Upon *Aphanizomenon flos-aquae* death, sedimentation and decay, MeHg can be reintroduced back into the system via the benthic community. Recent work in a California reservoir found that enrichment of MeHg through a benthic food web was statistically similar to enrichment in a pelagic food web, but for a given trophic position, benthic communities accumulated less MeHg than pelagic communities (Stewart et al., 2008). Low nutritional and MeHg availability from detritus, in comparison to algae and bacteria- rich diets in the pelagic zone, were offered as a reason for the difference. Therefore, if *Aphanizomenon flos-aquae* were found to accumulate more MeHg than more palatable phytoplankton, the benthic transfer of detrital *Aphanizomenon flos-aquae* MeHg would effectively reduce MeHg accumulation in top predator fish. Data from Lahontan Reservoir suggest that

Aphanizomenon flos-aquae MeHg accumulation is minimal and that MeHg accumulation occurs primarily in the smaller size fraction. Smaller-sized phytoplankton are more readily consumed by foraging zooplankton, suggesting that the transfer of MeHg to higher trophic levels are maintained in the pelagic system. A more detailed analysis distinguishing phytoplankton biomass and SPM quality, with the inclusion of zooplankton biomass, species and biochemical composition as well as feeding relationships ($\delta^{13}\text{C}$ and $\delta^{15}\text{N}$) in the pelagic and benthic communities are needed to substantiate this hypothesis.

3.6 CONCLUSIONS

Water column and phytoplankton data collected in Lahontan Reservoir was done to assess the importance of dynamic mercury loading into the reservoir as well as the importance of algal growth on the accumulation of THg and MeHg in two different phytoplankton size fractions (total and those less than 35 μm). The sampling location proved to be turbid with THg associated with SPM explained mostly by unfiltered THg and suspended sediment water column concentrations originating from the Carson River and not by any association with Chl a . The tendency for THg concentrations to decrease with increased Chl a helps to defend this claim. Results for THg in smaller sized SPM are less certain with very weak positive relationships to biomass in the water column. In contrast to THg, MeHg appears to have a stronger affinity to living biomass, with substantial MeHg concentrations and K_d values in smaller particles during the late summer when biomass is larger and reservoir residence times longer. MeHg accumulation, however, is lowest when loading from the river is greatest. Very different results for MeHg accumulation occur if the small

particle fraction is not isolated. Under these circumstances, MeHg accumulation was very low, reflecting the dilution effect of *Aphanizomenon flos-aquae* on the calculation. Inability of *Aphanizomenon flos-aquae* to accumulate MeHg reduces the possible transfer of MeHg from the pelagic system to the benthic system in the form of detrital *Aphanizomenon flos-aquae*. Instead, small, more palatable phytoplankton appear the likely mechanism of MeHg transfer to zooplankton.

Acknowledgements

Funding for this project came from the Nevada Institute of Water Resources Research (NIWRR) contract number 06HQGR0098. The USGS contributed federal money while the Desert Research Institute provided matching support.

References Cited

- Back, R.C., Gorski, P.R., Cleckner, L.B., and Hurley, J.P. 2003. Mercury content and speciation in the plankton and benthos of Lake Superior. *The Science of the Total Environment*. 304: 349-354.
- Bloom, N.S. 1989. Determination of picogram levels of methylmercury by aqueous phase ethylation, followed by cryogenic gas chromatography with Cold vapor atomic fluorescence detection. *Canadian Journal of Fisheries and Aquatic Sciences*. 46: 1131-1140.
- Bonzongo, J.C., Nemer, B.W. and Lyons, W.B. 2006. Hydrologic controls on water chemistry and mercury biotransformation in a closed river system: The Carson River, Nevada. *Applied Geochemistry*, 21: 1999 – 2009.
- Carroll, R., Warwick, J.J., James, A., and Miller, J. 2004. Modeling Erosion and Overbank Deposition During Extreme Flood Conditions on the Carson River, Nevada. *Journal of Hydrology*. 297:1-21.
- Carroll, R.W.H., Warwick, J.J., Heim, K.J., Bonzongo, J.C., Miller, J.R. and Lyons, W.B. 2000. Simulating Mercury Transport and Fate in the Carson River, Nevada. *Ecological Modelling*, 125:255-278.

- Chasar, L.C., Scudder, B.C., Stewart, A.R., Bell, A.H., and Aiken, G.R. 2009. Mercury cycling in stream ecosystems. 3. Trophic dynamics and methylmercury bioaccumulation. *Environmental Science and Technology*. 43(8): 2733-2739.
- Chen, C.Y., and Folt, C.L. 2005. High plankton densities reduce mercury biomagnifications. *Environmental Science and Technology*. 39: 115-121.
- Clesceri, L. S., A. E. Greenberg, and A. D. Eaton [eds.]. 1998. *Standard Methods for the Examination of Water and Wastewater*, 20th ed. American Public Health Association, American Water Works Association, Water Environment Federation.
- Cooper, J.J., S. Vigg, R.W. Bryce and R.L. Jacobson. 1983. *Limnology of Lahontan Reservoir, Nevada: 1980-1981*. Bioresources and Water Resources Centers. Desert Research Institute. DRI Publication 50021.
- DeMott, W. R. 1999. Foraging strategies and growth inhibition in five daphnids feeding on mixtures of a toxic cyanobacterium and a green alga. *Freshwater Biology*. 42: 263–274.
- DeMott, W. R., Gulati, R. D. and Van Donk, E. 2001. Daphnia food limitation in three hypereutrophic Dutch lakes: evidence for exclusion of large-bodied species by interfering filaments of cyanobacteria. *Limnology and Oceanography*. 46: 2054–2060.
- Diamond, M., Ganapathy, M., Peterson, S., and Mach, K. 2000. Mercury dynamics in the Lahontan Reservoir, Nevada: Application of the QWASI fugacity/ equivalence multispecies model. *Water, Air and Soil Pollution*. 117: 133-156.
- Donkor, A.K., Bonzongo, J.C., Nartey, V.K., and Adotey, D.K. 2006. Mercury in different environmental compartments of the Pra River basin, Ghana. *Science of the Total Environment*, 368: 164-176
- Gandhi, N., Bhavsar, S.P., Diamond, M.L., and Kuwabara, J.S. 2007. Development of a mercury speciation, fate and biotic uptake (Biotranspec) model: Application to Lahontan Reservoir (Nevada, USA). *Environmental Science and Technology*. 26 (11): 2260-2273.
- Ghadouani, A., Pinel-Alloul, B. and Prepas, E. E. 2003. Effects of experimentally induced cyanobacterial blooms on crustacean zooplankton communities. *Freshwater Biology*., 48, 363–381.
- Hayward, R.S., and Gallup, D.N. 1976. Feeding, filtering and assimilation in *Daphnia schoedleri* Sars as affected by environmental conditions. *Arch Hydrobiol*. 77: 139-163.

- Holm, N.P., Ganf, G.G. and Shapiro, J. 1983. Feeding and assimilation rates for *Daphnia pulex* fed on *Aphanizomenon flos-aquae*. *Limnology and Oceanography*. 28: 677-687.
- Horvat, M. Liang, L. and Bloom, N.S. 1993. Comparison of distillation with other current isolation methods for the determination of methyl mercury compounds in low level environmental samples. Part II. *Water. Analytica Chemica Acta*. 282: 153-168.
- Hosseini-pour, E.Z. and Martin, J.L., 1990. RIVMOD: a one-dimensional hydrodynamic sediment transport model: model theory and user's guide. U.S. E.P.A, Athens, Georgia.
- Karimi, R., Chen, C.Y., Pickhardt, P.C., Fisher, N.S., and Folt, C.L. 2007. Stoichiometric controls of mercury dilution by growth. *Ecology*. 104(18):7477-7482.
- Kidd, K.A., Helsslein, R.H., Fudge, R.J.P., and Hallard, K.A. 1995. The influence of trophic level as measured by $\delta^{15}\text{N}$ on mercury concentrations in freshwater organisms. *Water, Air and Soil Pollution*. 80: 1011-1015.
- Kirkwood, A.E., Chow-Fraser, P., and Mierle, G. 1999. Seasonal mercury levels in phytoplankton and their relationship with algal biomass in two dystrophic shield lakes. *Environmental Toxicology and Chemistry*. 18(3):523-532.
- Laurier, F.J.G., Gossa, D., Gonzales, L., Breviere, E., and Sarazin, G. 2003. Mercury transformations and exchanges in a high turbidity estuary: The role of organic matter and amorphous oxyhydroxides. *Geochimica Et Cosmochimica Acta* 67:3329-3345.
- Luengen, A.C., and Flegal A.R. 2009. Role of phytoplankton in mercury cycling in the San Francisco Bay estuary. *Limnology and Oceanography*. 54(1): 23-40.
- Mason, R.P., Reinfelder, J.R., and Morel, F.M.M. 1996. Uptake, toxicity, and trophic transfer of mercury in a coastal diatom. *Environmental Science and Technology*. 30:1835-45.
- Monson, B.A., and Brezonik, P.L. 1998. Seasonal patterns of mercury species in water and plankton from softwater lakes in northeastern Minnesota. *Biogeochemistry*. 40:147-162.
- Moye, H.A., Miles, C.J., Philips, E.J., Sargent, B., and Merritt, K.K. 2002. Kinetics and uptake mechanisms for monomethylmercury between freshwater algae and water. *Environmental Science and Technology*. 36(6): 3550-3555.

- Peterson, S.A., van Sickle, J, Herlihy, A.T., and Hughes, R.M. 2007. Mercury concentration in fish from streams and rivers throughout the western United States. *Environmental Science and Technology*. 41: 58-65.
- Pickhardt, P.C., and Fisher, N.S. 2007. Accumulation and methylmercury by freshwater phytoplankton in two contrasting water bodies. *Environmental Science and Technology*. 41: 125-131.
- Pickhardt, P.C., Folt, C.L., Chen, C.Y., Klaue, B., and Blum, J.D. 2005. Impacts of zooplankton composition and algal enrichment on the accumulation of mercury in an experimental freshwater food web. *Science of the Total Environment*. 339: 89-101.
- Schäfer, J., Blanc, G., Audry, S., Cossa, D., and Bossy, C. 2006. Mercury in the Lot-Garonne River system (France): Sources, fluxes and anthropogenic component. *Applied Geochemistry*. 21: 515–527.
- Stewart, A.R., Saiki, M.K., Kuwabara, J.S., Alpers, C.N., Marvin-DiPasquale, M., and Krabbenhoft, D.P. 2008. Influence of plankton mercury dynamics and trophic pathways on mercury concentrations of top predator fish of a mining-impacted reservoir. *Canadian Journal of Fisheries and Aquatic Science*. 65: 2351-2366.
- US EPA. 1996. Method 1996: Sampling ambient water for trace metals at EPA water quality criteria levels. Office of Water Engineering and Analysis Division (4303). Washington, D.C. 20460.
- Watras, C.J., Back, R.C., Halvorsen, S., Hudson, R.J.M. Morrison, K.A., and Wente, S.P. 1998. Bioaccumulation of mercury in freshwater pelagic food webs. *Science of the Total Environment*. 219: 183-208.
- Warner, K. A., Roden, E. E. and Bonzongo, J.C. 2003. Microbial Hg Transformation in Anoxic Freshwater Sediments under Iron-Reducing and Other Electron-Accepting Conditions. *Environmental Science and Technology*., 37(10): 2159-2165
- Warwick, J.J. and Heim, K.J., 1995. Hydrodynamic modeling of the Carson River and Lahontan Reservoir, Nevada. *Water Resources Bulletin*, 31(1): 67-77.
- Welschmeyer, N.A. 1994. Fluorometric analysis of chlorophyll *a* in the presence of chlorophyll *b* and pheopigments. *Limnology and Oceanography*. 39:1985-1992

CHAPTER 4

The Importance of Dynamic Mercury Loads on Body Burdens in a Planktivorous Fish (*Orthodon microlepidotus*): a Bioenergetic and Mercury Mass Balance Perspective

Rosemary W.H. Carroll¹¹, John J. Warwick¹², Sudeep Chandra¹³, Kumud Acharya¹⁴,
Mark Stone¹⁵ and Greg M. Pohl¹⁶

Abstract

A bioenergetic and mercury (Hg) mass balance model (BMMBM) is developed for the Sacramento blackfish (*Orthodon microlepidotus*), a filter feeding cyprinid found in northern California and Nevada. Attention focuses on Lahontan Reservoir in northern Nevada, which receives a large, temporally varying dissolved methylmercury water column (C_w) signal from the Carson River. The system affords the opportunity to look at the sensitivity of predicted body burdens in blackfish to a varying Hg signal in the context of uncertainty in that signal. Predicted Hg body burdens in fish computed with a temporally dynamic C_w are statistically similar to Hg body burdens computed with constant C_w . Lack of distinction in results is based on a large level of input uncertainty in C_w that propagates through the BMMBM.

¹¹ Corresponding Author. Assistant Research Hydrologist, Division of Hydrologic Sciences, Desert Research Institute, 2215 Raggio Parkway, Reno, NV 89512 Rosemary.Carroll@dri.edu.

¹² Vice President of Research, Desert Research Institute, Reno, NV 89512. John.Warwick@dri.edu

¹³ Assistant Professor, Department of Natural Resources and Environmental Science, University of Nevada, Reno, 1000 Valley Road, Reno, NV 89512. sudeep@cabnr.unr.edu

¹⁴ Assistant Research Professor, Division of Hydrologic Sciences, Desert Research Institute, 755 E. Flamingo Road, Las Vegas, NV. Kumud.Acharya@dri.edu

¹⁵ Assistant Professor, Department of Civil Engineering, University of New Mexico, Albuquerque, NM 87131. stone@unm.edu

¹⁶ Program Director, UNR Graduate Program of Hydrologic Sciences; Associated Research Professor, Desert Research Institute, Reno NV USA Greg.Pohl@dri.edu

However, at the reservoir scale, model results driven by a varying C_w boundary condition suggest that coupling of peak C_w loads with periods of maximum plankton growth and maximum fish consumption rates can describe large Hg body burdens observed in the planktivore. Temporal lags in downstream transport from the reservoir's point source (i.e., river delta) decouple modeled processes and Hg body burden estimates decrease. Predicted Hg body burdens are most sensitive to the timing of fluvial inputs in the receiving basin where there is little attenuation in the fluvial C_w signal and less sensitive at locations further from the point source.

KEY WORDS: bioenergetic and mercury mass balance model, Sacramento blackfish

4.1 INTRODUCTION

In 2004, the U.S. Environmental Agency (US EPA) listed 2,436 fish advisories due to mercury (Hg) contamination in our nation's waterways. Many statistical approaches have attempted to predict Hg in fish to elucidate factors impacting the cycling of Hg in aquatic systems as well as to define consumption guidelines (e.g., Peterson et al., 2007). The trophic transfer of mercury accounts for more than 90-99% of the bioaccumulated Hg in fish (Spry and Wiener, 1991), with the majority (95-99%) of total Hg in fish associated with the organic form, or methylmercury (MeHg) (Spry and Wiener, 1991; Bloom, 1992; Watras et al., 1998). In general Hg concentrations in fish tend to increase with age and/or size of the fish. However tremendous variability occurs among fish of the same species and not all fish experience increased Hg levels with age or size. Observed variability has been explained by site specific geochemical, physical and/or biological descriptors of the aquatic system (e.g., McMurtry et al., 1989; Allard and Stokes, 1989; Jackson, 1991;

Lange et al., 1993; Jin et al., 1999; Haines et al., 2003) as well as food web complexity (Cabana and Rasmussen, 1994; Cabana et al., 1994; Kidd et al., 1995; Kidd, 1998), and uptake efficiency at the base of the food web (Stewart et al., 2008). Most of these approaches can give real, quantitative ranking of the variables influencing Hg concentrations in biota but they can not be extrapolated beyond regression ranges or are limited to static or steady state scenarios that fail to capture any time dependencies regarding mercury bioaccumulation.

From a bioenergetic and mercury mass balance perspective, Hg levels in fish will increase if the rate of Hg sequestration is higher than the rate of elimination. This can occur if the growth efficiency of fish decreases for a given quantity of food consumed, or by increased Hg exposure (Borgmann and Whittle, 1992; Rowan et al., 1998). Increased exposure in fish requires a diet shift to more contaminated prey, or a temporal gain in prey bioaccumulation. Planktivorous fish depend on algae and zooplankton for the bulk of their energy needs and these prey are the principal pathway for Hg transfer. Hg accumulation in plankton is, in turn, dependent on contact with contaminated water (Swackhamer and Skoglund, 1993), the appropriate form of Hg (i.e., methylmercury, MeHg), as well as seasonal variability, growth and size (Carroll et al., in review). Therefore, Hg body burdens in planktivorous fish could depend on the timing of Hg loads if the loading signal varies strongly over time. The importance of a temporally varying loading signal may increase if maximum water concentrations are concomitant with high plankton availability and maximum consumption needs/efficiency of the fish.

Bioenergetic algorithms (Petersen and Pauket, 2005; Megrey et al., 2007) are incorporated with Hg mass balance approaches (Trudel and Rasmussen, 2001; 2006) to investigate Hg levels in a planktivorous fish as a function of a highly dynamic water column Hg signal. This study addresses the following questions in an attempt to explain Hg body burdens in the planktivorous Sacramento blackfish (*Orthodon microlepidotus*), a cyprinid found in Lahontan Reservoir, Nevada. (1) can a bioenergetic and mercury mass balance approach adequately represent observed body burdens in Sacramento blackfish? (2) Does accounting for a temporally varying Hg water column concentrations matter in predicting the blackfish Hg burdens? Or does uncertainty in the predicted water column signal, combined with the dampening of the Hg signal up the food chain require only average (or steady state) water column concentrations in the analysis? (3) How sensitive are Sacramento blackfish predicted Hg body burdens to dynamic Hg concentrations in the reservoir?

4.2 SITE DESCRIPTION

Lahontan Reservoir in west-central Nevada (Figure 4.1) is part of the Carson River system listed by the U.S. Environmental Agency (US EPA) as a Superfund site due to its contamination with Hg derived from historic mining, with nearly 6.36×10^6 Kg (7,000 tons) of residual Hg distributed throughout the river bank sediments and floodplain deposits (Miller et al., 1998; Smith and Tingley, 1998). The Carson River is the primary source of total and dissolved Hg loads into Lahontan reservoir, with reservoir benthic fluxes of dissolved species being less significant (Gandhi et al., 2007; Diamond et al., 2000; Carroll et al., in prep). Lahontan Reservoir was

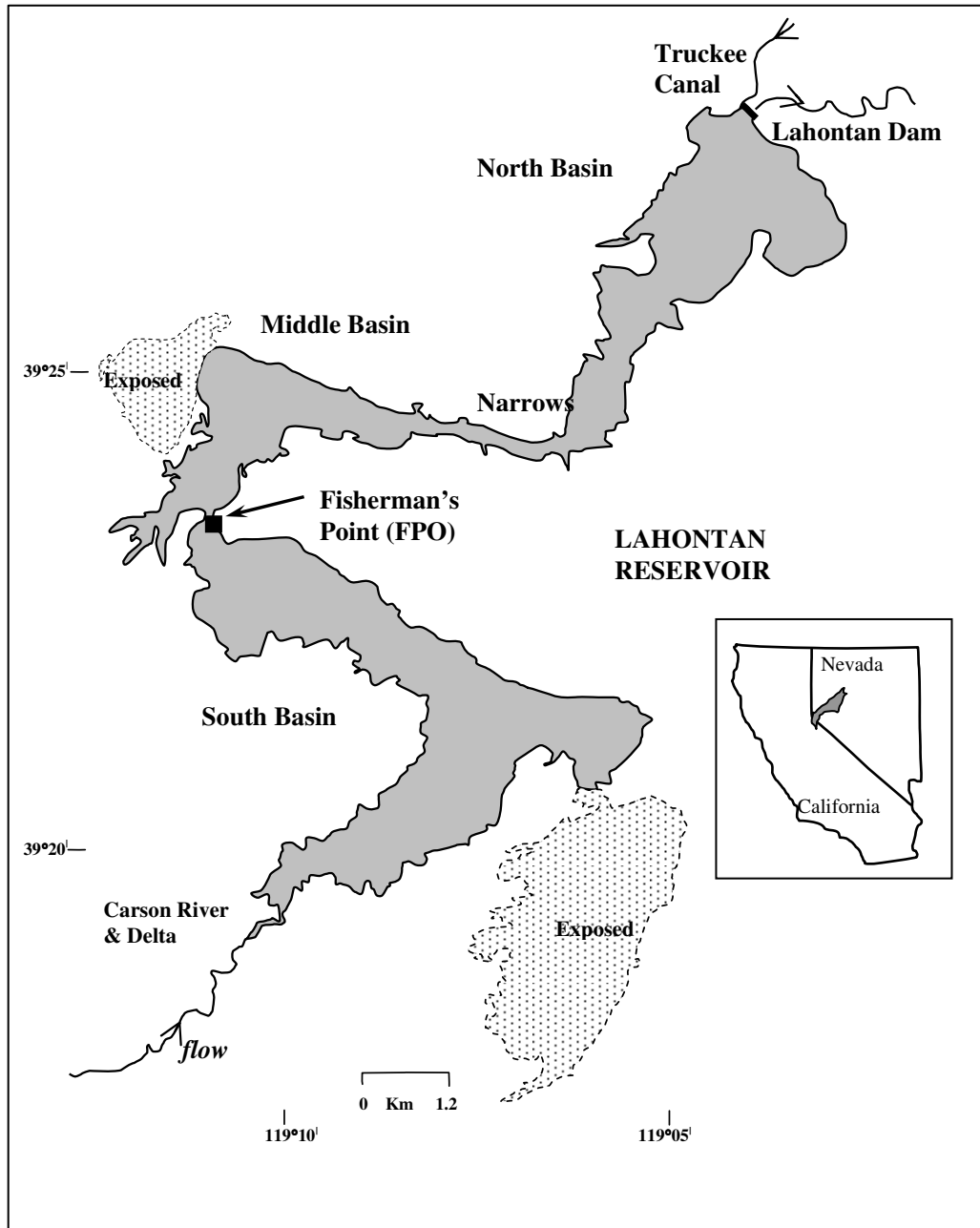


Figure 4.1: Lahontan Reservoir with basins marked. The Carson River enters the southern basin of the reservoir and moves toward the north basin and Lahontan Dam. Fisherman's Point (FPO) and Truckee Canal are marked and the inset shows location of the Carson River – Lahontan Reservoir watershed with respect to the western United States.

constructed in 1915 and its stored waters are used to irrigate fields in Lahontan Valley. The reservoir is also managed as a warm water fishery. It consists of three distinct basins with water from the Carson River entering the south basin and moving northward through the middle basin and into the north basin. The north basin terminates at Lahontan Dam (LDM) with the Truckee Canal contributing flow just upstream of LDM. Narrow channels connect each of the basins and are marked as Fisherman's Point (FPO), which connects the south and middle basins, and the Narrows, which connects the middle and north basins.

Fish populations in Lahontan Reservoir (Figure 4.2) shows large walleye (*Stizostedion Vitreum*) have Hg levels (E&E, 1998) nearly seven times greater than the Federal Action Limit for commercial fish of 1µg/g (FDA, 2000). Likewise, fish such as carp (*Cyprinus carpio*) and Sacramento blackfish (*Orthodon microlepidotus*) have Hg above 1 µg/g (Cooper et al., 1983; E&E, 1998, Craft et al., 2005; Kris Urquhart, NDOW, written communication February 25, 2010) and may represent a public health problem since these fish are harvested commercially for San Francisco markets. The plantivorous blackfish is the species under investigation. Unlike the top predator walleye, and to a lesser degree the benthivorous carp, the blackfish shows no significant trend between contamination and body mass. Instead, data indicate that even small fish (< 30 g) have concentrations nearing 1 µg/g.

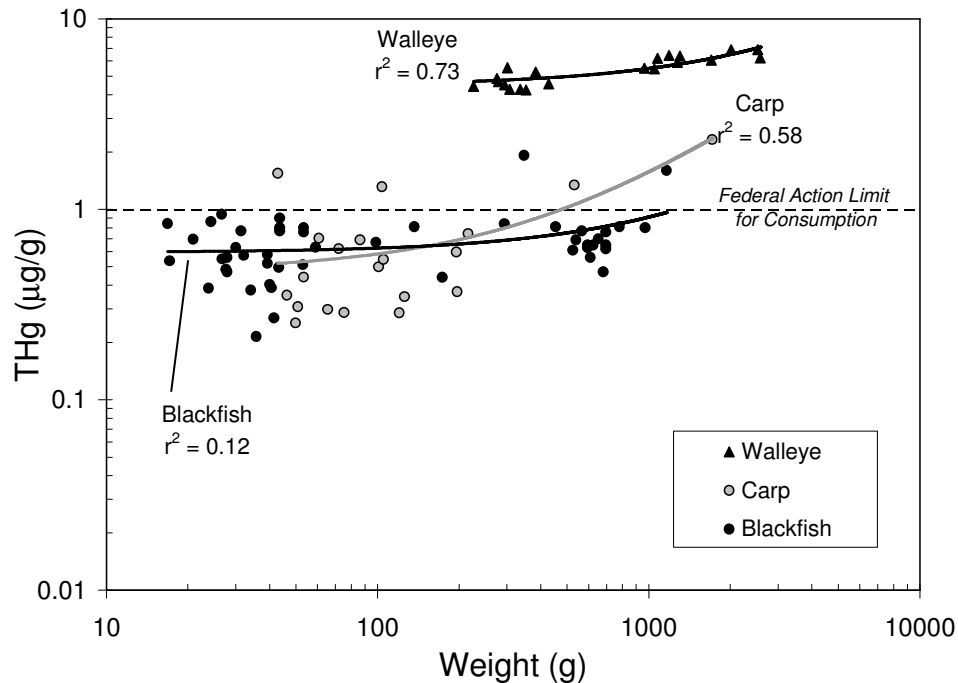


Figure 4.2: Total Hg (THg) contamination as a function of wet weight for three Lahontan Reservoir fish populations: walleye (E&E, 1998), carp (Cooper et al., 1983; E&E, 1998;), and Sacramento blackfish (Cooper et al., 1983; 1985; E&E, 1998; Craft et al., 2005; Kris Urquhart, NDOW, written communication February 25, 2010).

To protect the general population from the bioaccumulative potential of MeHg in aquatic systems, the US EPA (2001; 2009) has adopted its first water quality criterion based on fish tissue. The recommended maximum limit of MeHg concentration in noncommercial fish tissue is 0.3 µg/g. Details of Sacramento blackfish data are provided (Table 4.1). Samples are collected from years 1981 until 2009, with only a few studies designating the location of fish capture. Data show no trend in body burdens based on year of collection. On average, 94.4% of the Hg in Sacramento blackfish is MeHg (E&E, 1998), such that Sacramento blackfish are approximately two to three times over the US EPA recommended MeHg criterion.

Table 4.1: Sacramento blackfish Hg body burdens in Lahontan Reservoir. THg = total Hg; MeHg = methylmercury; (-) = location unknown.

Weight (g)	THg (µg/g)	MeHg ^a (µg/g)	Sample Date	Location	source
136.7	0.81	0.77	1981	-	Cooper et al., 1983 ^b
173.3	0.44	0.42	1981	-	Cooper et al., 1983
293.3	0.84	0.79	1981	-	Cooper et al., 1983
346.7	1.92	1.81	1981	-	Cooper et al., 1983
970.0	0.80	0.76	1981	-	Cooper et al., 1983
98.7	0.67	0.63	8/16/1994	North Basin	E&E, 1998
59.1	0.63	0.60	8/16/1994	North Basin	E&E, 1998
53.0	0.51	0.48	8/16/1994	North Basin	E&E, 1998
34.1	0.38	0.36	8/16/1994	North Basin	E&E, 1998
43.2	0.50	0.47	8/16/1994	North Basin	E&E, 1998
40.6	0.39	0.37	8/16/1994	North Basin	E&E, 1998
40.0	0.40	0.38	8/16/1994	North Basin	E&E, 1998
41.5	0.27	0.25	8/16/1994	North Basin	E&E, 1998
27.6	0.48	0.46	8/16/1994	North Basin	E&E, 1998
30.0	0.63	0.60	8/16/1994	North Basin	E&E, 1998
35.7	0.22	0.20	8/16/1994	North Basin	E&E, 1998
26.7	0.55	0.52	8/16/1994	North Basin	E&E, 1998
32.1	0.57	0.54	8/16/1994	North Basin	E&E, 1998
23.8	0.39	0.36	8/16/1994	North Basin	E&E, 1998
20.9	0.70	0.66	8/16/1994	North Basin	E&E, 1998
26.6	0.94	0.89	8/16/1994	North Basin	E&E, 1998
16.8	0.84	0.80	8/16/1994	North Basin	E&E, 1998
17.1	0.54	0.51	8/16/1994	North Basin	E&E, 1998
24.3	0.86	0.81	8/16/1994	North Basin	E&E, 1998
27.9	0.56	0.53	2/8/1999	-	Craft et al., 2005
27.9	0.47	0.44	2/8/1999	-	Craft et al., 2005
31.3	0.77	0.73	2/8/1999	-	Craft et al., 2005
39.2	0.52	0.49	2/8/1999	-	Craft et al., 2005
39.2	0.58	0.55	2/8/1999	-	Craft et al., 2005
43.6	0.77	0.73	2/8/1999	-	Craft et al., 2005
43.6	0.90	0.85	2/8/1999	-	Craft et al., 2005
43.6	0.80	0.76	2/8/1999	-	Craft et al., 2005
53.4	0.80	0.76	2/8/1999	-	Craft et al., 2005
53.4	0.76	0.72	2/8/1999	-	Craft et al., 2005
524.5	0.61	0.58	3/14/2004	South or Middle	NDOW ^c
538.7	0.69	0.65	3/14/2004	South or Middle	NDOW
609.5	0.56	0.53	3/14/2004	South or Middle	NDOW
694.6	0.62	0.59	3/14/2004	South or Middle	NDOW
595.4	0.63	0.60	3/14/2004	South or Middle	NDOW
595.4	0.65	0.61	3/14/2004	South or Middle	NDOW
680.4	0.47	0.44	3/14/2004	South or Middle	NDOW
694.6	0.76	0.72	3/14/2004	South or Middle	NDOW
694.6	0.65	0.61	3/14/2004	South or Middle	NDOW
779.6	0.81	0.77	3/14/2004	South or Middle	NDOW
1163.0	1.60	1.51	7/7/2009	-	NDOW
624.0	0.65	0.61	7/7/2009	-	NDOW
652.0	0.70	0.66	7/7/2009	-	NDOW
567.0	0.77	0.73	7/7/2009	-	NDOW
454.0	0.81	0.77	7/7/2009	-	NDOW

^aaverage %MeHg = 94.45 from E&E, 1998

^bmuscle weight assumed 30% total weight

^cNDOW = Nevada Division of Wildlife, written communication with Kris Urquhart, 2/25/2010

4.3 METHODS

4.3.1 Model Algorithm

The BMMBM presented is constructed in the object oriented Stella software (HPS, Inc., 2002) and blends published bioenergetic (Petersen and Pauket, 2005; Megrey et al., 2007) and mercury mass balance models (Trudel and Rasmussen, 2001; 2006) into a single approach. The Stella platform removes the need to explicitly compute differential equations, and allows easy changes to both initial and boundary conditions. The governing bioenergetic equation, as presented by Megrey et al. (2007), is given by,

$$\frac{dW}{dt} = [C - (R + SDA + EG + EX)] \frac{ED_{prey}}{ED_{fish}} \cdot W - EGG \cdot W \quad (4.1)$$

where W is the mass of the fish (g), t is time (days), C is the consumption rate (g prey/g fish/day), R is respiration (g prey/g fish/day), SDA is the specific dynamic action or losses due to digestion (g prey/g fish/day), EG is egestion, or losses due to feces (g prey/g fish/day), EX is excretion, or losses due to nitrogenous wastes (g prey/g fish/day), ED_{prey} and ED_{fish} are the energy densities of food (J/g prey) and prey (J/g fish), respectively and EGG is the fraction of body weight lost during spawning (per day). All mass units are in terms of wet weight.

Ideal consumption, or the consumption rate that occurs if food is unlimited, is defined as,

$$C = C_{max} f_c(T) \quad (4.2)$$

where $f_c(T)$ adjusts the maximum consumption rate (C_{\max} , g prey/gfish/d) for a given water temperature T ($^{\circ}\text{C}$). Maximum consumption is an allometric equation based on fish weight (W),

$$C_{\max} = a_c W^{b_c} \quad (4.3)$$

with a_c the intercept and b_c the slope of the exponential function. Slopes are generally negative such that consumption per fish mass decreases with increased fish size.

Consumption's dependence on temperature uses the warm water adjustment (Kitchell et al., 1977; Hanson et al., 1997) and used by Petersen and Pauket (2005) for the Humpback chub (*Gila cypha*), another cyprinid.

$$f_c(T) = V_c^{X_c} \cdot e^{[X_c \cdot (1 - V_c)]} \quad (4.4)$$

$$V_c = \frac{(CTM - T)}{(CTM - CTO)} \quad (4.5)$$

$$X_c = \frac{Z_c^2 (1 + \left(1 + \frac{40}{Y_c}\right)^{0.5})^2}{400} \quad (4.6)$$

$$Z_c = \text{Ln}(CQ) \cdot (CTM - CTO) \quad (4.7)$$

$$Y_c = \text{Ln}(CQ) \cdot (CTM - CTO + 2) \quad (4.8)$$

CTM and CTO are the maximal and optimal temperatures ($^{\circ}\text{C}$) for consumption and CQ is analogous to Q_{10} , or the rate increase given a 10°C increase. Consumption is not modeled as a function of food density, only food mass, therefore food with high caloric content will allow for greater growth. Ideal consumption is modified to actual consumption experienced in the natural system based on prey type and density, filtering efficiency, food preference and selectivity of prey, as well as any possible diet shifts that occur during specific life stages of the blackfish. These

modifications are discussed in the section on bioenergetics in the natural environment (section 4.4.2).

The calculations for respiration loss mirrors consumption gains with allometric coefficients a_r and b_r , with a similar parameter suite containing RTM, RTO and RQ. In addition, respiration is multiplied by an activity multiplier (ACT) (e.g., respiration increase associated with swimming, etc) as well as the ratio of the oxycalorific coefficient (13,500 J/g O₂) to fish energy density. The oxycalorific constant represents the heat lost per gram O₂ consumed for routine metabolism.

EG, EX and SDA losses are assumed simple fractional losses of consumption,

$$EG = E_g \cdot C \quad (4.9)$$

$$EX = E_x \cdot (C - EG) \quad (4.10)$$

$$SDA = S \cdot (C - EG) \quad (4.11)$$

with E_g and E_x equal to 0.1 (Hanson, 1997; Petersen and Pauket, 2005) and S equal to 0.15 (Petersen and Pauket, 2005). Reproductive losses are modeled after Megrey et al. (2007),

$$EGG = a_p \cdot K_{mat} \quad (4.12)$$

assuming losses are a function of the proportion of the population that is reproductive (K_{mat}) for a given age class (dimensionless). The constant a_p represents the daily fraction of weight lost during spawning (per day). Energy losses due to reproduction are assumed to occur only during those months that spawning is known to occur for the blackfish and is not spread out over the entire year.

The Hg mass balance component of the model is fashioned from Trudel and Rasmussen (2001; 2006), such that changes in MeHg body burden (B , μg) over time is given by,

$$\frac{dB}{dt} = (\alpha \cdot C_{\delta} \cdot I \cdot W) - (E + K) \cdot B \quad (4.13)$$

where α is the assimilation efficiency of MeHg from food (dimensionless), C_{δ} is the concentration of MeHg in the food ($\mu\text{g/g}$), I is the ingestion rate of fish (per day), E is the elimination rate of MeHg from the fish (per day) and K is the daily loss of MeHg to the gonads without any exchange back to the fish (per day). The methylation of ingested inorganic Hg may occur in the intestine of the fish but this process is assumed relatively small (0.005-0.4%, Rudd et al., 1980) and ignored. The elimination rate is modeled as a function of body size and temperature (Trudel and Rasmussen, 1997) with empirically derived constants ϕ , β , and γ ,

$$E = \phi \cdot W^{\beta} \cdot e^{\gamma T} \quad (4.14)$$

Loss of mercury to gonads is estimated using,

$$K = \frac{Q_m \cdot GSI}{365} \quad (4.15)$$

where Q_m is the ratio of MeHg concentration in the gonads to MeHg concentration in the fish, GSI is the gastrosomatic index (dimensionless) which is the ratio of gonad weight to total fish weight, and 365 is the number of days in a year. Long exposure to very contaminated prey (55 $\mu\text{g/g}$) can limit fish growth (Houck and Cech, 2004). This feedback mechanism is not modeled in the BMMBM since modeled prey MeHg concentrations never exceed 4 $\mu\text{g/g}$ and are not expected to cause toxic ramifications to growth estimates.

4.3.2 Model Parameterization and Calibration

4.3.2.1 Bioenergetics in the Laboratory - Juvenile Fish

Eleven bioenergetic parameters (a_c , b_c , CTO, CTM, CQ, a_r , b_r , RTO, RTM, RQ and ACT) are adjusted simultaneously to match laboratory observed growth rates (Cech et al., 1982) given warm water temperatures ($T = 28.1$ °C) and a diet of moist Oregon pellets ($ED_{\text{prey}} = 12,142$ J/g wet weight). Reproductive losses are not included in the analysis since fish are not mature enough for spawning. In addition, food availability is in excess of consumption needs and ideal consumption is assumed. Initial mass of the juvenile fish is 3.1 g +/- 0.9 g and final mass after 28 days is 4.6 g +/- 1.0 g. A Monte Carlo approach to calibration is employed similar to Petersen and Pauket (2005). All parameters are sampled from uniform distributions with acceptable ranges assumed equal to other cyprinid species (Petersen and Pauket, 2005). Out of 2000 realizations, only 15 produced growth results within one standard deviation of observed. Acceptable results are weighted based on the inverse of absolute error of the observed mean (plus 0.01 to prevent a division by zero). In this manner, parameter sets that provide the best fits to data are given the largest weights. The resulting weighted means for each of the eleven BMMBM input parameters (Table 4.2) define model input for consumption and respiration.

4.3.2.2 Dynamic Water Column Concentrations (C_w)

The geologic and geochemical controls on total and dissolved inorganic Hg and MeHg transport through the Carson River have been successfully modeled (Carroll et al. 2000; 2004, Warwick and Carroll, 2008, Carroll et al., in prep) using a linked and modified version of RIVMOD (Hosseinipour and Martin, 1990) and

WASP5/MERC4 (Ambrose et al., 1991). It is assumed that dissolved species are a reasonable surrogate for the bioavailable Hg fraction, despite several studies showing that filtered samples still contain a significant portion of Hg bound to colloids (Stordal et al., 1996). In addition, the focus in this study is the transfer of dissolved MeHg (DMeHg) from the water column to plankton and then to fish based on its stronger affinity for living biomass at the plankton level (Moye et al., 2002; Pickhardt and Fisher, 2007; Carroll et al., in review) and a greater potential to bioaccumulate through the food web compared to inorganic species.

Predicted DMeHg water column concentrations (C_w) in the reservoir and uncertainty at the 95% confidence interval are provided by Carroll et al. (in prep) using a fully dynamic Hg transport model of the system. The Hg transport model spans years 1997 through 2008. Temporal variability in predicted reservoir C_w reflects changing river contributions to the reservoir given changing climatic conditions. Spatial variability in predicted reservoir C_w is the result of reservoir velocities based on dam operations and influxes from the Truckee Canal. The average life span of Sacramento blackfish is five years. Data for blackfish span several decades and do not represent any single five year interval. To adjust for the multi-decade record in observed body burden, a typical five year sequence is developed by using a five year running average in C_w (as provided by Carroll et al., in prep) given one year lags. The resultant five year sequence in C_w is provided in Figure 4.3 and serves as a boundary condition in the modeling approach to predict MeHg fish body burdens.

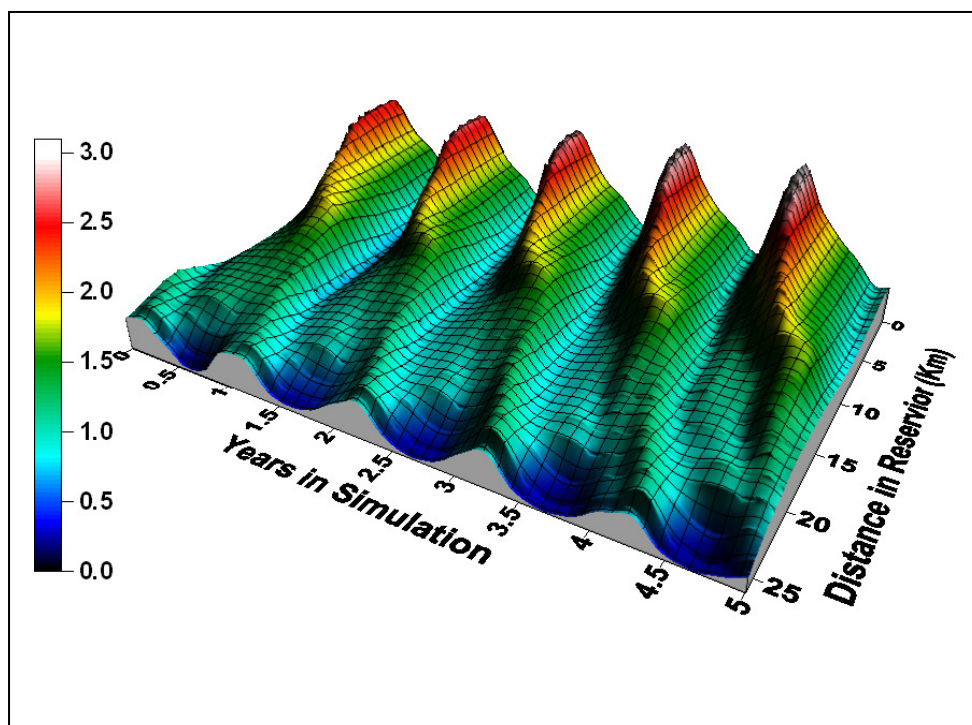


Figure 4.3: Typical five year C_w (ng/L) sequence into/through Lahontan reservoir based on transport model predictions presented by Carroll et al. (in prep) for years 1997 through 2008.

The largest reservoir concentrations ($C_w \sim 3$ ng/L) and the largest prediction uncertainty in C_w (range is 10.7 ng/L) occur in the south basin (distance from delta is 0 to 9 Km) during the warm summer months (July-August). Large C_w occurs when river flows are low and diffusion from river channel bed sediments is important. Uncertainty in reservoir C_w also incorporates uncertainty in MeHg derived from bank erosion during spring runoff which is then repartitioned to the dissolved phase as a function of adsorption coefficients (Carroll et al., in prep). Peak C_w attenuates in the downstream direction based on reservoir velocities, such that the middle basin (distance from delta is 9 to 14 Km) experiences peak C_w in the fall months (September and October).

The reservoir acts like a slow moving river through the south and middle basins, but water velocities slow and retention times increase substantially in the north basin (distance from delta is 17.5 to 26 Km) above LDM. Flows can even move upstream if discharge from the Truckee Canal is large in comparison to outflow from the dam. The north basin experiences an attenuated maximum C_w (1 ng/L) from early winter until the following summer, with uncertainty in predicted C_w at LDM spanning 2.5 ng/L. On average, the transport model suggests a one year lag in C_w from the river delta to the LDM. Predicted water column C_w do experience dilution from the Truckee Canal entering just to the north of the dam and propagating upstream during periods of low drawdown in the reservoir.

4.3.2.3 Bioenergetics in the Natural Environment

The model simulation depicting natural conditions tracks a hypothetical juvenile fish (initial mass = 3.0 g), over the average life span of blackfish, or five years. The initial start day is May 15 to mimic possible hatching and time to grow to the initial fish weight. Spawning is observed to occur for the months of April – May in fish ages one to four years (Staley, 1980). Reproductive losses use a variable K_{mat} (Table 4.1) and an average body mass loss (a_p) for male and female blackfish equal to 0.055 (Staley, 1980). K_{mat} for fish less than one year and greater than 4 years are assumed zero. Energy losses due to spawning are allowed to occur only during the months of spawning.

Table 4.2: Parameters used in the BMMBM with sources defined. Refer to text for parameter definitions.

	Parameter	Value	units	Source
Bioenergetic	CTO	22.85	°C	MC ^a calibration Juvenile Laboratory Conditions ^b
	CTM	28.24	°C	MC calibration Juvenile Laboratory Conditions
	CQ	2.38	--	MC calibration Juvenile Laboratory Conditions
	a _c	0.149	--	MC calibration Juvenile Laboratory Conditions
	b _c	0.253	--	MC calibration Juvenile Laboratory Conditions
	RTO	27.77	°C	MC calibration Juvenile Laboratory Conditions
	RTM	31.33	°C	MC calibration Juvenile Laboratory Conditions
	RQ	2.51	--	MC calibration Juvenile Laboratory Conditions
	a _r	0.00576 0.00295	--	MC calibration Juvenile Laboratory Conditions Calibration Adult Natural Conditions
	b _r	0.078	--	MC calibration Juvenile Laboratory Conditions
	ACT	1.13	--	MC calibration Juvenile Laboratory Conditions
	E _x	0.1	--	Hanson, 1997; Petersen and Pauket, 2005
	E _g	0.1	--	Hanson, 1997; Petersen and Pauket, 2005
	S	0.15	--	Petersen and Pauket, 2005
	a _p	0.055	--	Staley, 1980
	K _{mat} ^c yr 0	0	--	assumed
	K _{mat} yr 1	0.12	--	Staley, 1980
	K _{mat} yr 2	0.51	--	Staley, 1980
	K _{mat} yr 3	0.34	--	Staley, 1980
	K _{mat} yr 4-5	0	--	assumed
ED _{prey} diatoms	1000	J/g	assumed	
ED _{prey} cladocerans	2315	J/g	Hanson et al., 1997	
ED _{prey} copepods	2792	J/g	Hanson et al., 1997	
ED _{fish}	5869	J/g	Hartman and Brandt, 1995; Houck and Cech, 2004	
Hg Mass Balance	α	0.5	--	Houck and Cech, 2004
	C _δ	variable	µg/g	see text
	φ	0.0001	--	calibration adult - see Figure 10
	β	-0.2	--	Hanson et al., 1997; Clarke and Johnson, 1999; Trudel and Rasmussen, 2001; 2006
	γ	0.066	--	Trudel and Rasmussen, 2001
	Q _m	0.59	--	Trudel and Rasmussen, 2001
	GSI	0.03	--	Staley, 1980

^aMC = Monte Carlo approach and parameter ranges taken from Petersen and Paukert, 2005

^bCech et al., 1982 OMP T = 28.1°C

^cK_{mat} values linearly interpolated between year (ends)

Within the BMMBM, water temperature and weight modify consumption, respiration and MeHg elimination. Observed water temperatures in Lahontan Reservoir are described by the cosine function,

$$T = a_T + 0.5b_T \left(1 - \cos\left(2\pi \left(\frac{t_{yr} - c_T}{365} \right) \right) \right) \quad (4.16)$$

where t_{yr} is the number of days in the simulation which is reinitialized back to 1 after every 365-day cycle. Coefficients (a_T , b_T and c_T) are estimated by minimizing the root mean squared error of depth averaged temperature data collected at FPO in 2006 and verified with 2006 data collected at LDM by the USGS. Figure 4.4 shows the resultant curve in comparison to observed reservoir temperatures. Modeled temperatures are highest in late July ($T = 22.6^\circ\text{C}$) and lowest in late January ($T = 2.5^\circ\text{C}$). River temperatures collected 8 Km upstream from the delta help verify the functions lower limit and are included in Figure 4.4.

Ideal consumption in the laboratory does not necessarily exist in the natural environment. Instead, actual consumption is based on feeding strategies, prey selectivity, filtering efficiency and prey availability. Sacramento blackfish use a filter feeding strategy based on pump filtering. A rapid series of suction via the buccal and opercular cavities draw in water and prey for processing (Johnson and Vinyard, 1987). Johnson and Vinyard (1987) measured filter rates (FR, ml/s) of Sacramento blackfish based on fish standard length (SL) and function of three water temperatures ($12^\circ\text{C} < T < 14^\circ\text{C}$, $18.5^\circ\text{C} < T < 22.5^\circ\text{C}$ and $T = 25^\circ\text{C}$). FR is a function of buccal volume (BV, ml), where BV is the volume of water processed by the blackfish with

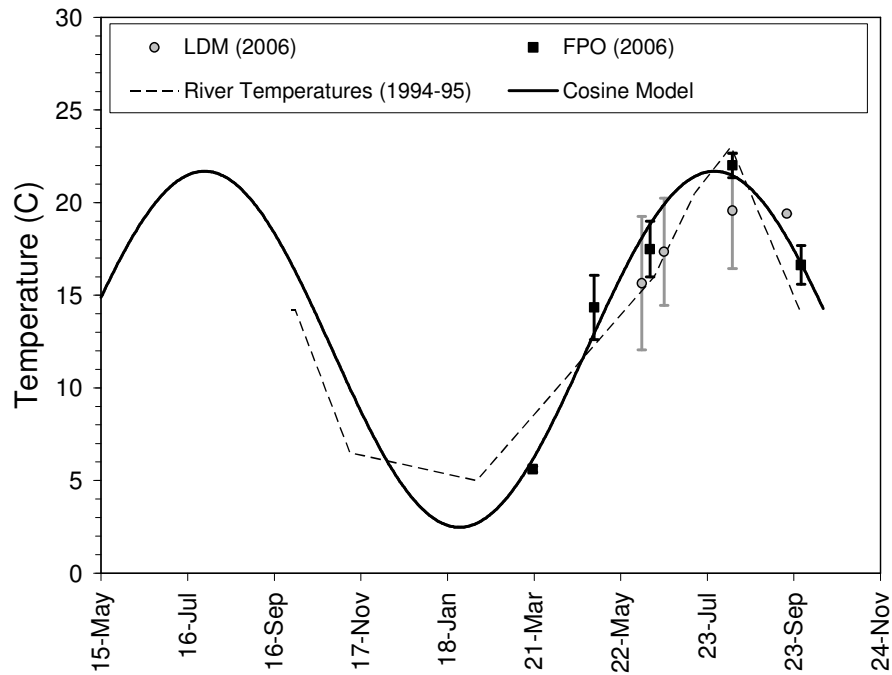


Figure 4.4: Cosine approximation of reservoir water temperatures calibrated to FPO data and verified with LDM data. Carson River data included for comparison.

each suction, and pumping rate (PR, suctions/s). BV increases exponentially with fish size while PR decreases with size. Relationships from Johnson and Vinyard (1987) are used to predict FR,

$$FR = BV \cdot PR \quad (4.17)$$

$$BV = 0.001 \cdot SL^{2.86} \quad (4.18)$$

$$PR = a_{pr} \cdot SL^{b_{pr}} \quad (4.19)$$

$$W = 0.02 \cdot SL^{2.96} \quad (4.20)$$

in which a_{pr} and b_{pr} are provided in Table 4.2 for each temperature range evaluated.

The BMMBM predicts fish W, not SL, therefore the conversion from SL to W is done by taking the inverse of the SL-W correlation given by Johnson and Vinyard (1987).

Juvenile fish forage by site with directed suction on larger prey (e.g., copepods), but switch to more passive filter feeding behavior as they grow (Johnson and Vinyard, 1987). Gut contents (Jacobs, 1977) in adult fish show an exclusion of copepods. Unlike most cladoceran species, copepods are evasive and able to avoid capture. Johnson and Vinyard (1987) observe a shift in feeding strategy when fish are greater than 60 g and less than 350 g. Weight-to-age estimates (Staley, 1980; Johnson and Vinyard, 1987; Kris Urquhart, NDOW, phone conversation, November, 2009) suggest this shift in feeding strategy occurs after approximately one year.

Food selectivity by adult fish is assumed to equal the following proportions of observed gut content by volumes (Jacobs, 1977): cladocerans (*Bosmina* spp. And *Daphnia* spp.) 37%; diatoms (division Chrysophyta) 29%, cyanophyta (e.g., *Aphanizomen flos-aquae*) are 8.7%; copepods 4.6% and finally rotifers 1.6%. While *Aphanizomen flos-aquae* are found in the gut of Sacramento blackfish, analysis of posterior intestine suggest they are not digested (Jacobs, 1977), and likely contribute little or no energy to the fish. Estep and Vigg (1985) help confirm this notion with ^{13}C in Lahontan Reservoir and Pyramid Lake (north of Lahontan Reservoir) found significantly different between *Aphanizomen flos-aquae* and higher trophic levels. Therefore despite the dominance of *Aphanizomen flos-aquae* in Lahontan Reservoir's phytoplankton assemblage (Cooper et al., 1983; Cooper and Vigg, 1985), it is assumed *Aphanizomen flos-aquae* are selected against and/or not digested and are not included in the bioenergetic analysis of Sacramento blackfish. Prey selectivity is re-normalized to exclude *Aphanizomen flos-aquae*: cladoceran (51%), diatoms (41%),

copepods (6%) and rotifers (2%). Juvenile preference for copepods is modeled by simply switching the percentages of diatoms and copepods designated for adults.

Prey availability is not always equal to the preferred food ratios given above. Modeled phytoplankton and zooplankton densities in Lahontan Reservoir use seasonal organism counts from Cooper et al. (1983) and Cooper and Vigg (1985). Diatom counts are averaged over depths of 5 m and 26 m. Surface counts are low and not used in the calculation. Diatom densities are dominated by three species: *Stephanodiscus niagarae*, *Fragilaria crotonensis* and *Melosira distans*. The conversion to wet weight for model use is done in a multi-step process: (1) species specific biovolumes (μm^3) are obtained from Larson and Rathke (1980), (2) biovolume is converted to g carbon/g dry mass using regressions presented by Strathmann (1967), Eppley (1970) and Menden-Deuer and Lessard (2000) as presented by Gosselain et al. (2000) and taking the mean, (3) 19% carbon mass to dry mass assumed for diatoms (Sicko-Goad et al., 1984), and (4) aquatic plant tissues are composed of approximately 90% water (Sladeczek and Sladeczkova, 1963; Hannan and Dorris, 1970; Hanson et al., 1997).

Zooplankton in Lahontan Reservoir is primarily composed of *Daphnia* (*schodleri*, *galeata*), *Diaphanosoma leuchtenbergianum*, *Bosmia coregoni*, *Cyclops vernalis*, *Diaptomus sicilis*, and unidentified rotifers (Cooper et al., 1983). Individual species lengths and associated regression equations to convert to dry mass is done using equations from literature (Burns, 1969; Bottrell et al., 1976; Stenson, 1976; Persson and Ekbohm, 1980; Rosen, 1981; Pace and Orcutt, 1981; Stemberger and Gilbert, 1985). Dry mass is converted to wet mass assuming the fraction of water

ranges from 0.88 to 0.90 (Hanson et al., 1997). Resultant annual prey densities for phytoplankton and zooplankton are given in Figure 4.5.

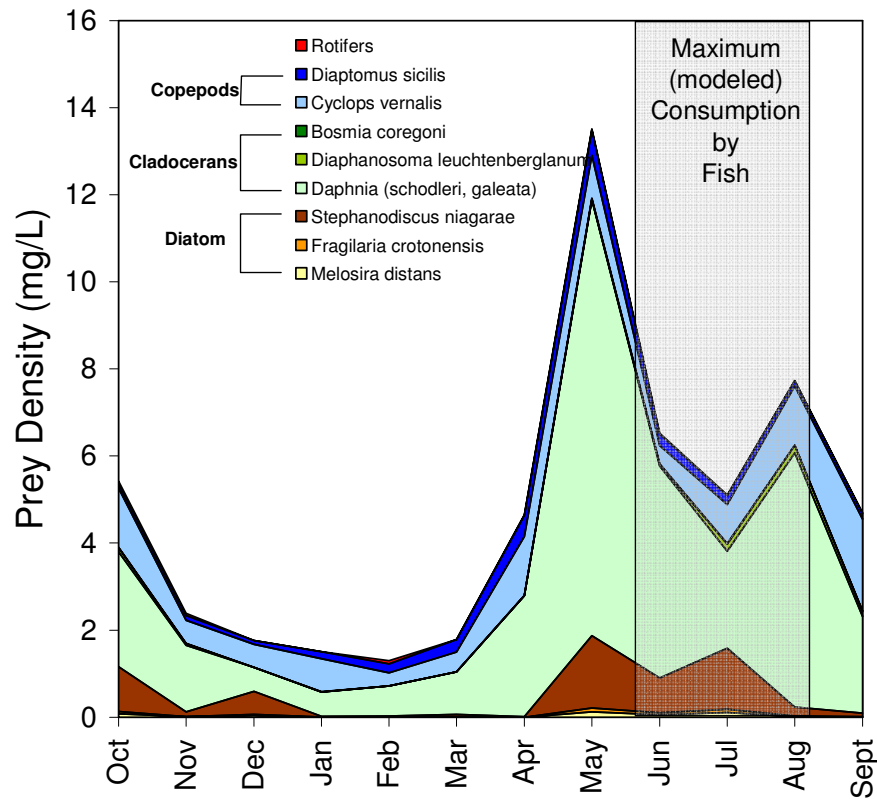


Figure 4.5: Observed annual prey density (mg/L) in Lahontan Reservoir.

The spring peak in zooplankton and diatoms are nearly coincident (at the monthly scale), but the summer peaks are lagged by approximately one month with diatoms rising when the spring zooplankton peak is in decline, and then declines in turn when zooplankton populations rebound later in the summer. Sacramento blackfish modeled consumption rates peak during the summer months of June, July and August and fish feeding is partly responsible for the summer decline in prey. The BMMBM does not simulate a feedback mechanism to adjust prey density due to fish consumption. Instead, plankton is a pre-defined state variable in the model and held

constant for any given day in the simulation. However, prey availability is reduced based on observed data and in this manner, implicitly accounts for predator-prey dynamics.

The prey available for fish consumption (g/d) is the prey density multiplied by the FR. Rotifer densities are very small and are lumped with cladocerans to simplify the modeling process. If diatoms or cladocerans are in short supply compared to the preferred ratio of food consumed, then fish can shift their diet to either diatoms or cladocerans, respectfully, to meet consumption needs. Shortages in food availability, however, can not include diet shifts to more copepods. It is assumed that prey avoidance will limit this tactic. For the defined prey availability in Figure 4.5, the model predicts two periods in the annual cycle with modeled food shortages. One occurs in late summer when consumption rates are high and zooplankton populations suffer a late summer low density. Shortages are on the order of 20% and are short lived, but do occur during maximum energetic needs. Limits on food availability during the late summer result in significantly lower growth rates (all other model parameters equal) compared to modeled growth with no food shortages. Growth reductions in fish are cumulative over time, such that growth is 16% lower in year one, and 26% lower in year five, compared to growth when prey densities are large enough to satisfy ideal consumption. The second food shortage occurs from January to May when all plankton populations are low. The shortage is 40% lower than estimated ideal consumption and sustained over several months, but occurs when consumption needs and associated growth are low. The winter-spring prey limits do not impact modeled fish growth.

Dry weight energy densities in Sacramento blackfish are computed using the cyprinidae regression by Hartman and Brandt (1995). Average moisture content equal to 27% (Houck and Cech, 2004) converts energy into a wet weight basis ($ED_{\text{fish}} = 5870 \text{ J/g}$). Zooplankton energy densities are taken from Hanson et al. (1997), with cladoceran equal to 2315 J/g and copepods at 2792 J/g. Diatoms are assumed less nutritious than zooplankton and given an energy density of 1000 J/g.

Using first-order second moment analysis (FOSMA), the respiratory coefficient a_r is found the most sensitive (and the most uncertain) parameter in the bioenergetic portion of the model (Figure 4.6). To calibrate the five year simulation in a natural environment a_r is decreased by half (0.0058 to 0.00295) to best match observed weights of age five year fish. Lowering a_r effectively reduces respiration losses and modeled weights increase. The reduced a_r still falls within the range of acceptable cyprinid values (0.0004 to 0.01) presented by Petersen and Paukert (2005). Calibration results are provided in Figure 4.7. Observed and predicted values represent the mean weight for a given age class with error bars signifying minimum and maximum values. Tremendous variability in observed and modeled fish mass occurs to allow observed and modeled weights to overlap and the largest observed fish in Lahontan (1,800 g) is well matched with the upper range in prediction. The model under predicts weights for mature, reproducing fish (ages 2-4). While no calibration is done with respect to reproductive parameters, reproductive losses are not large relative to other loss terms, in particular respiration. Allometric equations for consumption gains and respiration losses are kept constant throughout the modeled blackfish lifespan. In reality, there might be a shift in parameter values

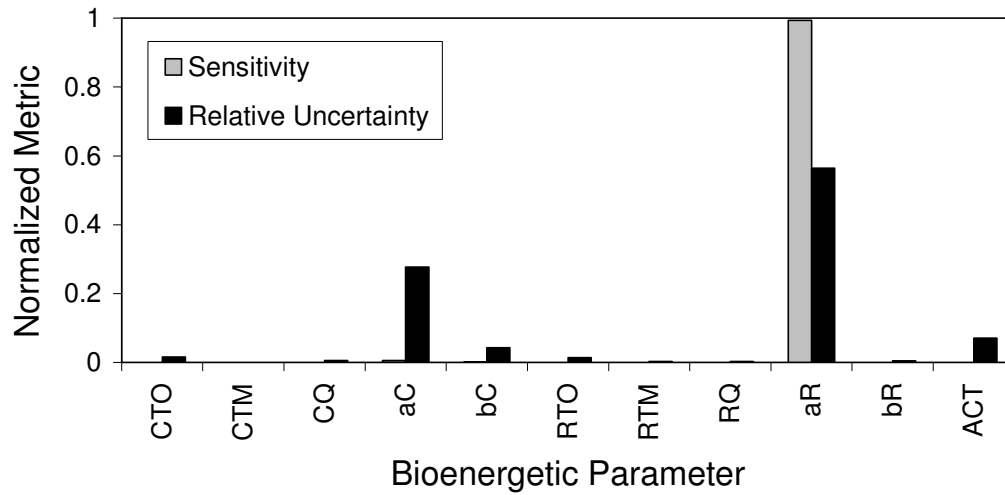


Figure 4.6: First-order second-moment analysis of normalized sensitivity and uncertainty (i.e., sum to 1.0) for bioenergetic parameters based on the 5-year simulation of natural conditions.

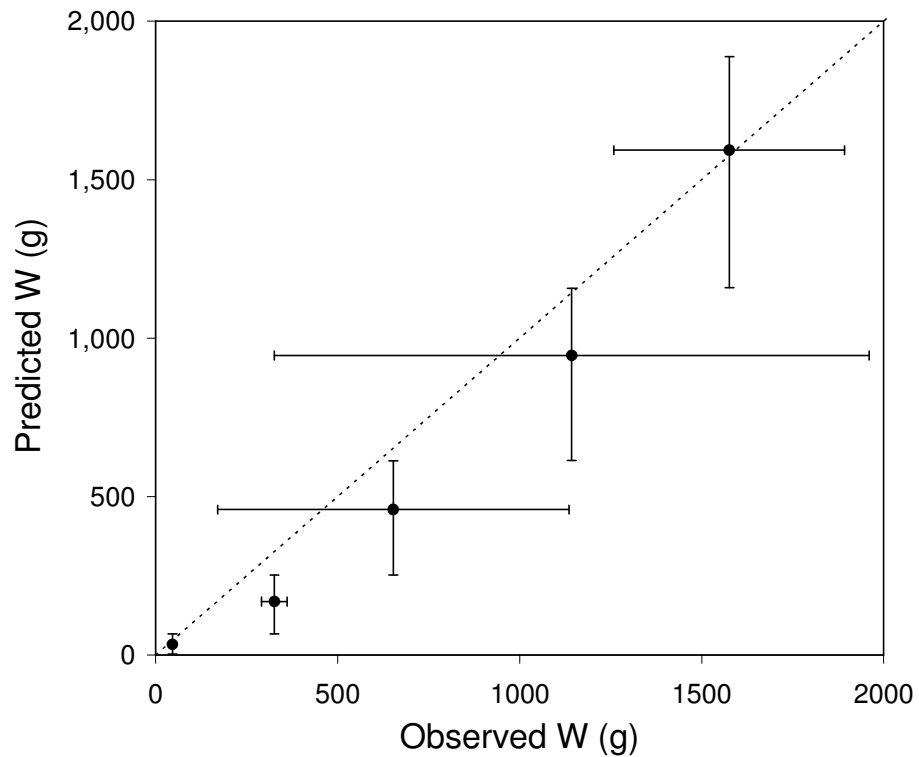


Figure 4.7: Predicted and observed fish weights based on age class. Error bars denote minimum and maximum observed or predicted weights for the given age class.

during reproduction or aging that is not accounted for in the modeling approach.

Despite this limitation, the model captures observed variability in adult fish using one set of parameters and is considered acceptable in terms of relative weight gain over time.

4.3.2.4 Prey Contamination (C_δ)

Zooplankton and water quality data collected in Lahontan Reservoir (E&E, 1998) defines the following linear regression ($n = 3$, $r^2 = 0.997$, moisture content assumed 89%).

$$C_\delta(\text{zoopl}) = 0.2155 \cdot C_w + 0.0062 \quad (4.21)$$

Diatom contamination uses the relationship presented by Carroll et al. (in review) between MeHg bioaccumulation (K_d , L/Kg) and Chlorophyll *a* ($Chla$, $\mu\text{g/L}$) for smaller phytoplankton ($n = 4$, $r^2=0.82$, $p = 0.03$),

$$K_d(\text{diatoms}) = 0.654 \cdot Chla + 1.74 \quad (4.22)$$

And is converted to C_δ by rearranging the EPA definition of bioaccumulation,

$$C_\delta(\text{diatoms}) = \frac{C_w}{10^6} \cdot 10^{K_d} \quad (4.23)$$

The composite C_δ is a mass-weighted average of the prey consumed for a given day. C_δ peaks in August at 3.7 $\mu\text{g/g}$ in the south basin and 1.7 $\mu\text{g/g}$ in the north basin.

4.3.2.5 MeHg Body Burdens

Ingestion (I) in the Hg mass balance component of the model (equation 4.13) is defined with the bioenergetic model (equation 4.1) as $C \cdot ED_{prey} / ED_{fish} \cdot W$. Trudel and Rasmussen (2001) use a modal value of Hg assimilation (α) in piscivorous fish equal to 0.8. Juvenile Sacramento blackfish, however, are observed with lower assimilation values ranging from 0.3 to 0.65 with rates decreasing over a 70 day experiment (Houck and Cech, 2004). For this study a temporally constant α -value of 0.5 is used. MeHg loss to gonads (equation 4.15) is allowed to occur year round. Sacramento blackfish GSI range from 0.01 to 0.10 for males, and 0.005 to 0.03 for females, with low GSI observed immediately after spawning and lasting through the summer for males, and through the New Year for females (Staley, 1980). An average value of 0.03 is assumed and held constant in time. A Q_m value equal to 0.59 is taken from Trudel and Rasmussen (2001).

Using FOSMA techniques with all coefficients in equation 4.14, indicates that ϕ , the coefficient of MeHg elimination, is the most sensitive and uncertain parameter in estimating average MeHg body burdens. Consequently, ϕ is the single calibration parameter in the mass balance component of the study. It is adjusted to a value of 0.0001. This calibrated ϕ is one order of magnitude lower than that used by Trudel and Rasmussen (2001) for piscivorous fish. It is possible to increase ϕ to that of other studies, and maintain acceptable modeled Hg body burdens, but only by simultaneously increasing the assimilation efficiency. The BMMBM assumes a constant α and ϕ over the life span of the fish, despite several studies compiled by Barber (2008) showing assimilation efficiency is not constant in time, but is a

function of total exposure time, body weight, specific growth rate, and specific feeding rates. From these studies, it is acknowledged that a higher than expected α coefficient may be required to offset larger than expected growth rates, lower than expected exposure conditions and/or ignoring contaminant exchange across the gills (Barber, 2008). Non-uniqueness due to the covariant relationship between α and ϕ is also problematic. Using the observed mean for α from Houck and Cech (2004) is done to minimize the potential parameter space from which to choose an acceptable ϕ .

Other parameters defining E are based on literature. Elimination of MeHg is expected to scale with body size (β) and is given the value of -0.2 presented by others (Hanson et al., 1997; Clarke and Johnson, 1999; Trudel and Rasmussen, 2001; 2006). A temperature coefficient (γ) equal to 0.066 is obtained from Trudel and Rasmussen (2001).

4.4 RESULTS AND DISCUSSION

Modeled MeHg body burdens ($\mu\text{g/g}$) in Sacramento blackfish are computed with a dynamic C_w boundary condition (refer to Figure 4.3) and a constant C_w boundary condition (average for the entire reservoir from 1997 through 2008 is 1.33 ng/L). Fish are assumed to have an initial body size of 3.1 g (from juvenile calibration based on Cech et al., 1982) and an initial body burden of 0.05 $\mu\text{g/g}$. Sensitivity of predicted body burdens to initial value is tested by adjusting initial body burdens from 0 to 0.35 $\mu\text{g/g}$. In all cases, body burden results converged by the time fish reached 20 g in size. Model results are compared in Figures 4.8 and 4.9.

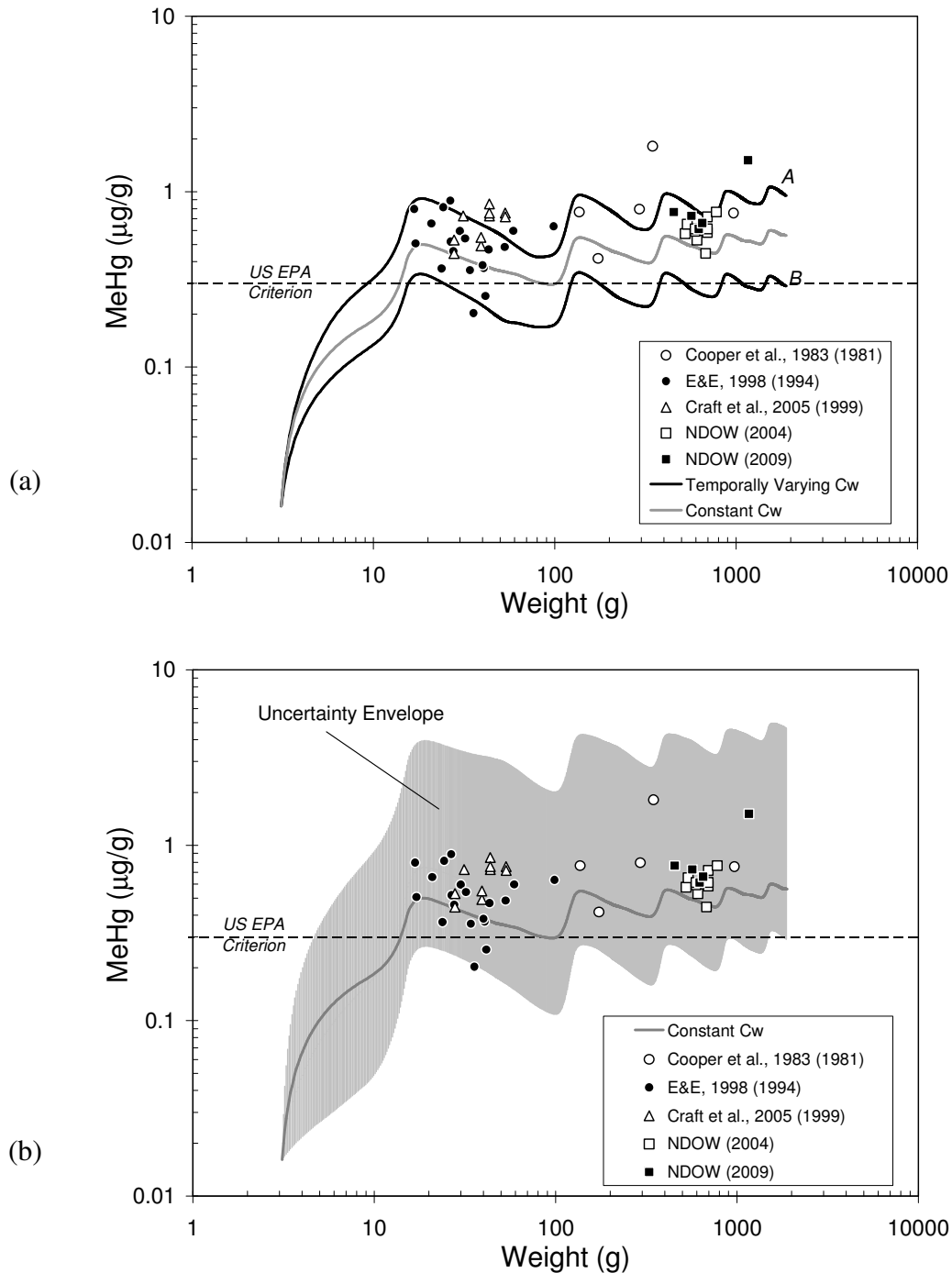


Figure 4.8: Model results compared to observed data with data identified by source and year of sample (refer to Table 4.1). (a) modeled MeHg body burdens in Sacramento blackfish using a constant C_w (1.33 ng/L) and temporally varying C_w boundary conditions (refer to Figure 4.3) at locations A = reservoir south basin and B = just upstream of LDM. (b) Comparison of modeled body burdens using a constant C_w to those body burdens estimated using the upper and lower 95% uncertainty bounds at FPO in the predicted temporally varying C_w .

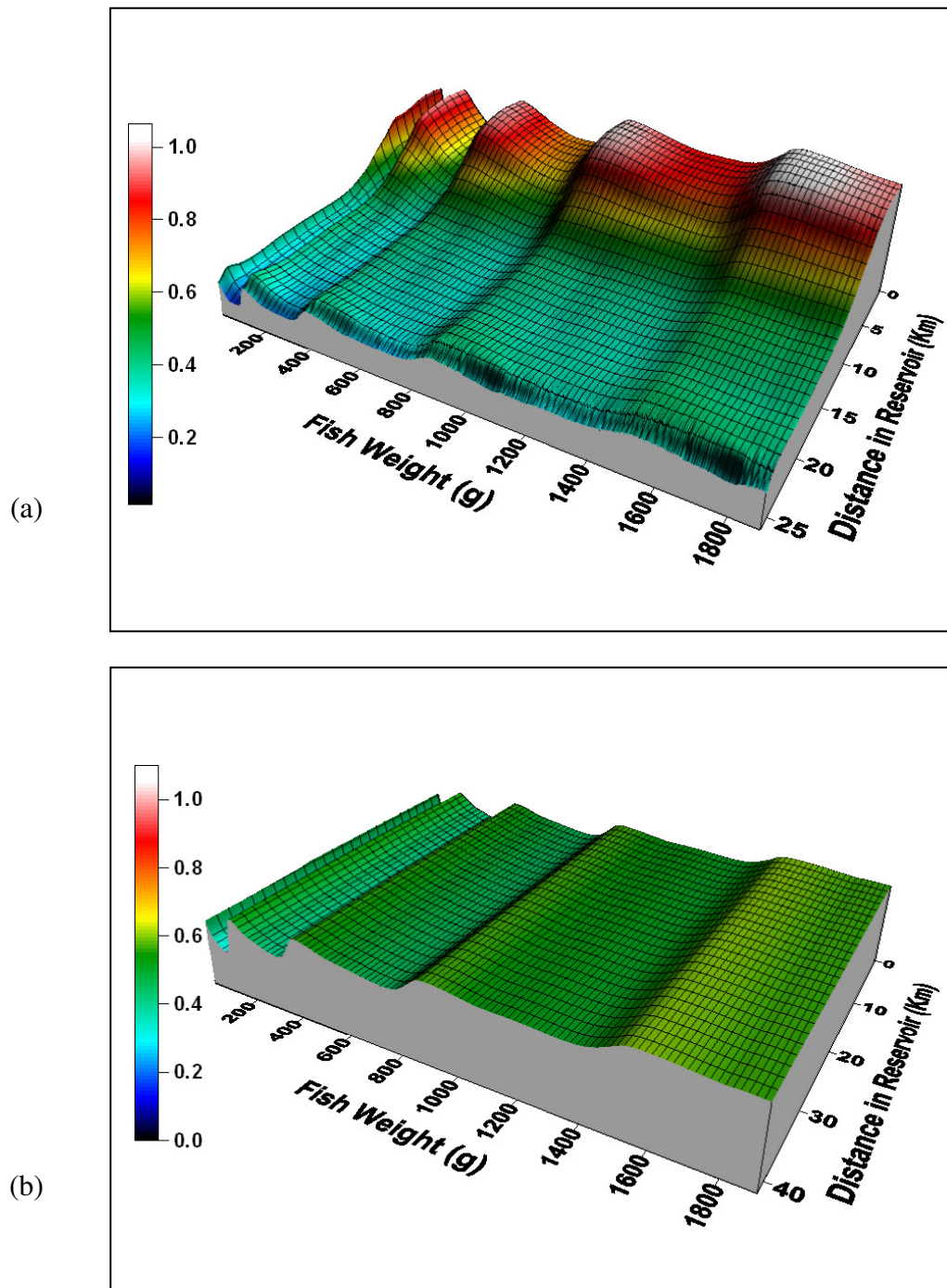


Figure 4.9: Modeled MeHg body burdens ($\mu\text{g/g}$) in Sacramento blackfish along the length of Lahontan Reservoir as a function of fish weight (a) dynamic C_w originating from the Carson River, (b) constant $C_w = 1.33 \text{ ng/L}$.

MeHg body burden is plotted as a function of fish weight. For the BMMBM, fish weight is, somewhat, a surrogate for time as the model tracks a given fish/population from year-of-young through adulthood. There is no accounting for different hatching times and no averaging between different age classes coexisting in the reservoir. In addition, the model does not allow fish to migrate. The model simulates the rise and fall of body burdens with bioenergetic needs of the single fish age class as it moves through time, increases in size and consumes contaminated prey. Model predictions in MeHg body burden “wobble” for both dynamic C_w and for constant C_w scenarios. The modeled oscillation is the result of mercury losses decreasing at a slower rate than mercury inputs via consumption during the colder winter months. Losses during the winter months are mitigated, in part, by a very small ϕ -coefficient in the elimination equation 4.14.

Model predictions in fish body burden using dynamic C_w vary depending on the location in the reservoir. In the south basin of the reservoir body burden estimates are, on average, 67% larger than those produced using a constant C_w . As the modeled pulse in C_w propagates downstream, however, the BMMBM predicts nearly equal body burdens in the middle basin and body burdens nearly half in the north basin compared to body burdens predicted with a constant C_w . The large uncertainty in dynamic C_w predictions (Carroll et al., in prep) propagates through the BMMBM to produce an envelope of MeHg body burden uncertainty equal to 5 $\mu\text{g/g}$ at FPO (Figure 4.8b). Uncertainty in body burden output captures all observed data. With downstream movement, the uncertainty envelope shifts to lower concentrations and simultaneously compresses, such that this envelope is less than 3 $\mu\text{g/g}$ in the north

basin. The uncertainty associated with a temporally (and spatially) varying C_w encapsulates estimated body burdens from the constant boundary condition approach. Therefore, from a modeling perspective, estimated MeHg body burdens using a dynamic C_w signal and a constant C_w are indistinguishable.

While the dynamic and constant loading scenarios produce statistically similar results in body burden, the dynamic approach can provide some insight not gained from output derived from a constant C_w . Modeled transport of DMeHg into the reservoir (Carroll et al., in prep) produces a C_w in the south basin that peaks during the warm summer months when plankton are prolific and can bioaccumulate MeHg more readily (Carroll et al., in review). The resulting large C_δ is coupled with large consumption rates in the blackfish and the potential for fish contamination is very high. Blackfish in the middle basin may experience a significant drop in MeHg contamination despite C_w remaining relatively high (1-2 ng/L). The modeled drop in blackfish MeHg accumulation in the reservoir's middle basin is caused by a temporal lag in peak C_w . Peak C_w in the middle basin occurs in the late fall and early winter when plankton populations and blackfish consumption needs are low. In the north basin of the reservoir, peak C_w occurs approximately one year after entering the south basin with maximum C_w occurring in the late summer when the potential for MeHg to bioaccumulate in the foodweb is large. However, C_w concentrations are significantly attenuated in the north basin and the Truckee Canal further dilutes C_w just above the dam. Blackfish accumulate half the level of MeHg in the north basin compared to the south basin.

Commercial fishing of Sacramento blackfish is not restricted to any specific basin in the reservoir with fisherman following schools of fish where ever schools of fish may reside. While fish may migrate from basin to basin in search of food when the reservoir is full, fish movement (and consequently fishing), into the south basin is limited during substantial reservoir drawdown during drought periods. This was the case in 2007 and 2008 when the only basin with adequate water was in the north (Kris Urquhart, written communication, February, 2010). However, most fishing hauls during the summer of 2009 also occurred in the north basin despite average reservoir conditions. It is not clear if fish are collected in the north basin simply due to the location of several popular boat launch sites (e.g., Churchill beaches 4-10, Virginia Beach and Coyote Island), or if fishing hauls are indicative of a preferred habitat. If fish reside primarily in the north basin, especially during drought years when C_w loading from the river is highest, then the BMMBM suggests that the transfer of MeHg to higher trophic levels (including humans), may on average, be lower than if fish reside in the upper reaches of the reservoir.

Sensitivity of modeled body burdens is investigated by shifting Carson River pulse loads forward four months (south basin C_w peaks in late November), and backward four months (south basin C_w peaks in late March). Figure 4.10 illustrates the effects of a boundary condition lag on predicted MeHg body burdens throughout the reservoir. A backward lag (Figure 4.10a) effectively lowers accumulation in the south basin by 30%. This is caused by a slight decoupling of maximum C_w from maximum consumption for fish. While accumulation is lowered in the south basin, the potential for accumulation rises in the middle basin by 20% because an overlap

now occurs between peak C_w , plankton growth and large fish consumption. Bioaccumulation in blackfish in the north basin remains relatively the same as presented in Figures 4.8a and 4.9a. Forcing a forward lag, with peak C_w in the south basin now occurring in late November (Figure 4.10b), lowers modeled MeHg accumulation in fish residing in the south basin by more than half. Accumulation in the north basin remains unchanged from previous scenarios. However, the model places greater relative importance on MeHg accumulation in the north basin.

4.5 CONCLUSIONS

Uncertainty in C_w predictions is very large and precludes any statistical distinction in predicted fish MeHg body burdens modeled with a dynamic C_w signal and those modeled with a constant C_w . However, at the reservoir scale, model results driven by a variable C_w signal allow speculation on the timing of loads with respect to prey contamination and bioenergetic needs of the blackfish. Future work requires a reduction in modeled C_w uncertainty and a more explicit understanding of blackfish life histories in the reservoir. Data collection also needs to strive toward better understanding bioenergetics of reproducing blackfish, as well as understanding where blackfish spawn, where they prefer to congregate and what, if any, distinction in MeHg body burdens may occur based on location in the reservoir.

Model results and observed data show that the rate of MeHg accumulation is fastest for blackfish less than one year old ($W < 20-60$ g) with MeHg body burdens approaching the species maximum in the first year. Accumulation rates in successive years essentially maintain body burdens reached in that initial year. Questions arise as to the impact of MeHg accumulation in the first year on future accumulation, and if

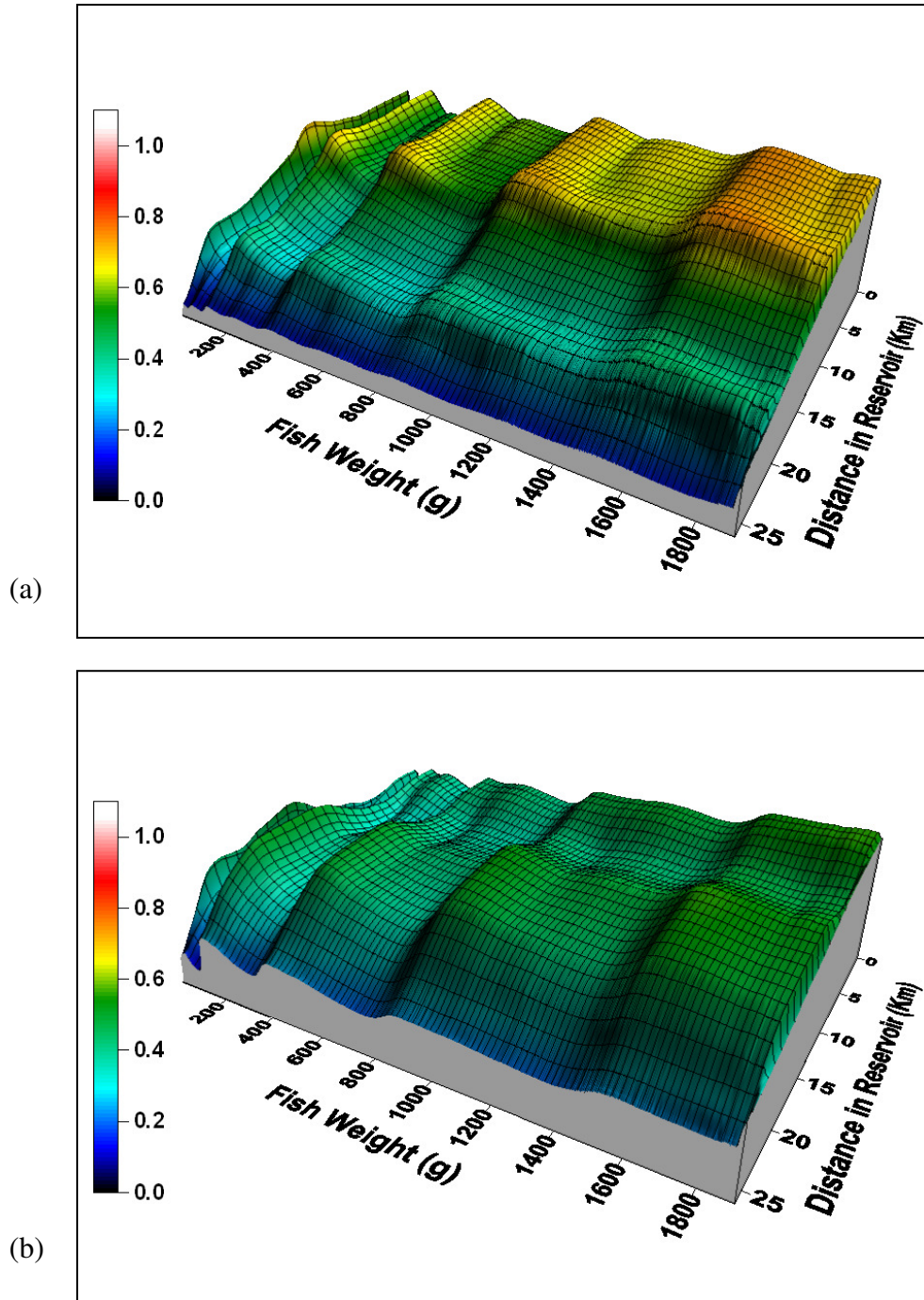


Figure 4.10: Modeled MeHg body burdens ($\mu\text{g/g}$) in Sacramento blackfish along the length of Lahontan Reservoir as a function of fish weight given altered (and hypothetical) loading scenarios. (a) C_w pulse shifted back four months so that peak loads into the south basin occur in late March, (b) C_w pulse shifted forward four months so that peak loads into the south basin occur in late November.

reductions in juvenile fish body burdens will translate to equal, or even larger, reductions in commercially harvested adult fish. Likewise, how will reducing juvenile body burdens impact contamination levels in top predator fish, such as walleye, that feed directly on the young blackfish?

The BMMBM also initiates interesting questions related to pulse loading of C_w . Primarily, can changing the timing of C_w loads based on fish life history and location in the reservoir offer a realistic management alternative for a system like Lahontan Reservoir? Results suggest that decoupling peak C_w loads from periods of maximum plankton growth and maximum fish consumption rates can reduce body burdens substantially. Potential reductions are largest in the reservoir's receiving basin (i.e., south basin) where there is little attenuation of fluvial loads. Sensitivity in modeled MeHg body burdens is decreased at locations further from the point source and in portions of the reservoir with slow velocities.

Acknowledgements

Funding for this project came from the Nevada Institute of Water Resources Research (NIWRR) contract number 06HQGR0098. The USGS contributed federal money while the Desert Research Institute provided matching support. Additional thanks to Dr. Joseph Cech, Jr. at the University of California, Davis, for his willingness to discuss the Sacramento blackfish, share his data and be patient with an onslaught of questions. Similarly, I'd like to thank to Kris Urquhart at the Nevada Division of Fish and Wildlife for his friendly and generous response to many, many questions regarding blackfish within Lahontan Reservoir as well.

References Cited

- Allard, M., and Stokes, P.M. 1989. Mercury in crayfish species from thirteen Ontario lakes in relation to water chemistry and small-mouth bass (*Micropterus dolomieu*) mercury. *Canadian Journal of Fisheries and Aquatic Sciences*, 46: 1040-1046.
- Ambrose, R.B., Wool, T.A., Martin, J.P. and Schanz, R.W. 1991. WASP5.X: A Hydrodynamic and Water Quality Model: Model Theory, User's Manual and Programmer's Guide. US EPA, Athens, Georgia.
- Barber, M.C. 2008. Dietary uptake models used for modeling the bioaccumulation of organic contaminants in fish. *Environmental Toxicology and Chemistry*. 27(4): 755-777
- Bloom, N.S. 1992. On the chemical form of mercury in edible fish and marine invertebrate tissue. *Canadian Journal of Fisheries and Aquatic Science*. 49: 1010-1017.
- Borgmann, U., and Whittle, D.M. 1992. Bioenergetics and PCB, DDE and mercury dynamics in Lake Ontario lake trout (*Salvelinus namaycush*): a model based on surveillance data. *Canadian Journal of Fisheries and Aquatic Science*. 49: 1086-1096.
- Bottrell H.H., Duncan, A., Gliwicz, Z.M., Grygierek, E., Herzig, A., Hillbricht-Ilkowska, A., Kurasawa, H., Larsson, P., and Weglenska, T. 1976. A review of some problems in zooplankton production studies. *Norwegian Journal of Zoology*. 24, 419-456.
- Burns, C. 1969. Relation between filtering rate, temperature and body size in four species of *Daphnia*. *Limnology and Oceanography*. 14(5): 693-700.
- Cabana, G., and Rasmussen, J.B. 1994. Modelling food chain structure and contaminant bioaccumulation using stable nitrogen isotopes. *Nature*. 372: 255-257.
- Cabana, G., Tremblay, A., Kalff, J., and Rasmussen, J.B. 1994. Pelagic food chain structure in Ontario lakes: a determinant of mercury levels in lake trout. *Canadian Journal of Fisheries and Aquatic Science*. 51: 381-389.
- Carroll, R.W.H., Warwick, J.J., James, A., and Miller, J. 2004. Modeling Erosion and Overbank Deposition During Extreme Flood Conditions on the Carson River, Nevada. *Journal of Hydrology*. 297:1-21.

- Carroll, R.W.H., Warwick, J.J., Heim, K.J., Bonzongo, J.C., Miller, J.R. and Lyons, W.B. 2000. Simulating Mercury Transport and Fate in the Carson River, Nevada. *Ecological Modelling*, 125:255-278.
- Carroll, R.W.H., Memmott, J., Warwick, J.J., Fritsen, C.H., Bonzongo, J.C., and Acharya, K. in review. Temporal variation of mercury associated with different phytoplankton size fractions in Lahontan Reservoir, Nevada. *Water, Air and Soil Pollution*.
- Carroll, R.W.H., Warwick, J.J. and Pohll, G.M. in prep. Mercury transport model of the Carson River and Lahontan Reservoir System, Nevada: An investigation of total and dissolved species and associated uncertainty. Intended Journal - *Ecological Modelling*.
- Cech Jr., J.J., Massingill, M.J., and Stern, H. 1982. Growth of juvenile Sacramento blackfish, *Orthodon microlepidotus* (Ayres). *Hydrobiologia*. 97: 75-80.
- Clarke, A., and N.M. Johnson. (1999). Scaling metabolic rate with body mass and temperature in teleost fish. *Journal of Animal Ecology*. 68: 893-905.
- Cooper, J.J., and Vigg, S. 1985. Species composition and seasonal succession of the zooplankton community of eutrophic Lahontan Reservoir, Nevada. *The Southwestern Naturalist*. 30(2): 239-252.
- Cooper, J.J., S. Vigg, R.W. Bryce and Jacobson, R.L. 1983. *Limnology of Lahontan Reservoir, Nevada: 1980-1981*. Bioresources and Water Resources Centers. Desert Research Institute. DRI Publication 50021.
- Craft, D., Fields, J., and Yoder, N. 2005. Appendix 2: Mercury in fish from Lahontan Reservoir – data from the state of Nevada and Reclamation. For Mercury in the Carson River Basin, California and Nevada. Technical Memorandum TSC-2005-8290-001.
- Diamond, M., Ganapathy, M., Peterson, S., and Mach, K. 2000. Mercury dynamics in the Lahontan Reservoir, Nevada: Application of the QWASI fugacity/ equivalence multispecies model. *Water, Air and Soil Pollution*. 117: 133-156.
- E & E., Ecology and Environment, Inc. 1998. *Ecological Risk Assessment Carson River Mercury Site*. Prepared for the U.S. Environmental Protection Agency. ARCS Region 9 and 10. Contract No. 68-W9-0020, Work Assignment No. 20-11-9LR6, Document Control No. ZS3490.

- Eppley, R.W., Reid, F.M., and Strickland, J.D.H. 1970. The ecology of the plankton off of La Jolla, California, in the period April through September 1967 – pt. III. Estimates of phytoplankton, crop size, growth rate and primary production. *Bulletin Scripps Institute Oceanography*. 17: 33-42.
- Estep, M.L., and Vigg, S. 1985. Stable carbon and nitrogen isotope tracers of trophic dynamics in natural populations and fisheries of the Lahontan Lake system, Nevada. *Canadian Journal of Fisheries and Aquatic Sciences*. 42: 1712-1719.
- FDA. US Food and Drug Administration. 2000. Guidance for industry: action levels for poisonous or deleterious substances in human food and animal feed. <http://www.fda.gov/Food/GuidanceComplianceRegulatoryInformation/GuidanceDocuments/ChemicalContaminantsandPesticides/ucm077969.htm#merc>. Download 2/26/2010/
- Gandhi, N., Bhavsar, S.P., Diamond, M.L., and Kuwabara, J.S. 2007. Development of a mercury speciation, fate and biotic uptake (Biotranspec) model: Application to Lahontan Reservoir (Nevada, USA). *Environmental Science and Technology*. 26 (11): 2260-2273.
- Gosselain, V., Hamilton, P.B., and Descy, J-P. 2000. Estimating phytoplankton carbon from microscopic counts: an application for riverine system. *Hydrobiologia*. 438: 75-90.
- Haines, T. A., May, T. W., Finlayson, R. T. and Mierzykowski, S.E. 2003. Factors affecting food chain transfer of mercury in the vicinity of the nyanza site, Sudbury River, Massachusetts. *Environmental Monitoring Assessment*. 86: 211-232.
- Hannan, H.H., and Dorris, T.C. 1970. Succession of a macrophyte community in a constant temperature river. *Limnology and Oceanography*. 15: 442-453.
- Hanson, P.C., Johnson, T.B., Schindler, D.E., and Kitchell, J.F. 1997. Bioenergetics model 3.0 for Windows. University of Wisconsin, Sea Grant Institute Technical Report. WISCU-T-97-001, Madison.
- Hartman, K., and Brandt, S.B. 1995. Estimating energy density in fish. *Transactions of the American Fisheries Society*. 124: 347-355.
- HPS, Inc. 2002. <http://www.hps-inc.com>
- Hosseini-pour, E.Z. and J.L. Martin, J.L. 1990. RIVMOD: a one-dimensional hydrodynamic sediment transport model: model theory and user's guide. U.S. E.P.A, Athens, Georgia.

- Houck, A., and Cech, J.J., Jr. 2004. Effects of dietary methylmercury on juvenile Sacramento blackfish bioenergetics. *Aquatic Toxicology*. 69: 107-123.
- Jackson, T.A. 1991. Biological and environmental control of mercury accumulation by fish in lakes and reservoirs of northern Manitoba, Canada. *Canadian Journal of Fisheries and Aquatic Sciences*, 48: 2449-2470.
- Jacobs, S.E. 1977. On the feeding ecology of the Sacramento blackfish (*Orthodon microlepidotus*) of Clear Lake, Lake County, California. University of California, Davis. 28 p.
- Jin, L., Hui, Y. and Xu, X. 1999. Predictive model for mercury accumulation in carp (*Cyprinus carpio*) of reservoirs in China. *Water, Air, and Soil Pollution*. 115: 363-370.
- Johnson, P.C., and Vinyard, G.L. 1987. Filter-feeding behavior and particle retention efficiency of Sacramento blackfish. *Transactions of the American Fisheries Society*. 116: 634-640.
- Kidd, K.A. 1998. Use of stable isotope ratios in freshwater and marine biomagnification studies. In. *Environmental Toxicology*. Ed. J. Rose. Pp. 357-376.
- Kidd, K.A., Helsslein, R.H., Fudge, R.J.P. and Hallard, K.A. 1995. The influence of trophic level as measured by $\delta^{15}\text{N}$ on mercury concentrations in freshwater organisms. *Water, Air and Soil Pollution*. 80: 1011-1015.
- Kitchell, J.F., Stewart, D.J., and Weininger, D. 1977. Applications of bioenergetics model to yellow perch (*Perca flavescens*) and walleye (*Stizostedion vitreum*). *Journal of Fisheries Research Board of Canada*. 34: 1922-1935.
- Lange, T.R., H.E. Royals, and Connor, L.L. 1993. Influence of water chemistry on mercury concentrations in largemouth bass from Florida lakes. *Transactions of the American Fisheries Society*, 122: 74-84.
- Larson, D., and Rathke, D.E. 1980. Zooplankton distributions in the central and western basins of Lake Erie. Pages 272-293 in C. E. Herdendorf, editor. *Lake Erie nutrient control program: an assessment of its effectiveness in controlling lake eutrophication*. U.S. Environmental Protection Agency, Technical Report 600/3-80-062, Washington, D.C.
- Menden-Deuer, S., and Lessard, E.J. 2000. Carbon to volume relationships for dinoflagellates, diatoms and other protist plankton. *Limnology and Oceanography*. 45: 569-579.

- McMurtry, M.J., D.L. Wales, W.A. Scheider, G.L. Beggs, and P.E. Dimond, P.E. 1989. Relationship of mercury concentrations in lake trout (*Salvelinus namaycush*) and smallmouth bass (*Micropterus dolomieu*) to the physical and chemical characteristics of Ontario lakes. *Canadian Journal of Fisheries and Aquatic Sciences*, 46: 426-434.
- Megrey, B.A., Rose, K.A., Klumb, R.A., Hay, D.E., Werner, F.E., Eslinger, D.L., and Ian Smith, S. 2007. A bioenergetics-based population dynamics model of pacific herring (*Clupea harengus pallasii*) coupled to a lower trophic level nutrient-phytoplankton-zooplankton model: description, calibration and sensitivity analysis. *Ecological Modelling*. 202: 144-164.
- Miller, J.R., Lechler, P.J., and Desilets, M. 1998. The role of geomorphic processes in the transport and fate of mercury in the Carson River basin, west-central Nevada. *Environmental Geology*, 33(4): 249-262.
- Moye, H.A., Miles, C.J., Philips, E.J., Sargent, B., and Merritt, K.K. 2002. Kinetics and uptake mechanisms for monomethylmercury between freshwater algae and water. *Environmental Science and Technology*. 36(6): 3550-3555.
- Pace, M.L., and Orcutt, J.D., Jr. 1981. The relative importance of protozoans, rotifers and crustaceans in a freshwater zooplankton community. *Limnology and Oceanography*. 26, 822-830.
- Persson G. and Ekbohm, G. 1980. Estimation of dry weight in zooplankton populations: Methods applied to crustacean populations from lakes in the Kuokkel Area, Northern Sweden. *Arch. Hydrobiologia.*, 89, 225-246.
- Petersen, J.H., and Paukert, C.P. 2005. Development of a bioenergetics model for Humpback chub and evaluation of water temperature changes in the Grand Canyon, Colorado River. *Transactions of the American Fisheries Society*. 134: 960-974.
- Peterson, S.A., van Sickle, J., Herlihy, T.A., and Hughes, R.M. 2007. Mercury concentration in fish from streams and rivers throughout the western United States. *Environmental Science and Technology*. 41: 58-65.
- Pickhardt, P.C., and Fisher, N.S. 2007. Accumulation and methylmercury by freshwater phytoplankton in two contrasting water bodies. *Environmental Science and Technology*. 41: 125-131.
- Rosen R.A. 1981. Length-dry weight relationships of some freshwater zooplankton. *Journal of Freshwater Ecology.*, 1, 225-229.

- Rowan, D.J. Chant, L.A., and Rasmussen, J.B. 1998. The fate of radiocesium in freshwater communities – Why is biomagnification variable both within and between species? *Journal of Environmental Radioactivity*. 40: 15-36.
- Rudd, J.W., Furutani, A., and M.A. Turner. (1980). Mercury methylation by fish intestinal contents. *Applied Environmental Microbiology*. 40(4): 777-782.
- Sicko-Goad, L.M., Schelske, C.L., and Stoermer, E.F. 1984. Estimation of intracellular carbon and silica content of diatoms from natural assemblages using morphometric techniques. *Limnology and Oceanography*. 29: 1170-1178.
- Sladeczek V., and Sladeczkova, A. 1963. Relationship between wet weight and dry weight of the periphyton. *Limnology and Oceanography*, 8, 309–311.
- Smith, G.H. and Tingley, J.V. 1998. The history of the Comstock Load, 1850-1997. Nevada Bureau of Mines and Geology in association with the University of Nevada Press.
- Spry, D.J., and Wiener, J.G. 1991. Metal bioavailability and toxicity to fish in low alkalinity lakes: a critical review. *Environmental Pollution*. 71: 243-304.
- Staley, C.S. 1980. Life history aspects of the Sacramento blackfish, *Orthodon microlepidotus* (Ayres) in the Beach/Stone Lakes Basin, California. M.S. Thesis, Biologic Sciences. California State University, Sacramento. Pp. 1-55.
- Stemberger, R.S., and Gilbert, J.J. 1985. Body size, food concentration, and population growth in planktonic rotifers. *Ecology*. 66(4): 1151-1159.
- Stenson, J.A.E. 1976. Significance of predator influence on composition of *Bosmina* spp. Populations. *Limnology and Oceanography*. 21(6): 814-822.
- Stewart, A.R., Saiki, M.K., Kuwabara, J.S., Alpers, C.N., Marvin-DiPasquale, M., and Krabbenhoft, D.P. 2008. Influence of plankton mercury dynamics and trophic pathways on mercury concentrations of top predator fish of a mining-impacted reservoir. *Canadian Journal of Fisheries and Aquatic Science*. 65: 2351-2366.
- Stordal, M.C., Gill, G.A., Wen, L.-S., and Santschi, P.H. 1996. Mercury phase speciation in the surface waters of selected Texas estuaries: Importance of colloidal forms. *Limnology and Oceanography*. 41(1): 52-61.

- Strathmann, R.R. 1967. Estimating the organic content of phytoplankton from cell volume or plasma volume. *Limnology and Oceanography*. 12: 411-418.
- Swackhamer, D.L. and Skoglund, R.S. 1993. Bioaccumulation of PCBs by phytoplankton: kinetics vs. equilibrium. *Environmental Toxicology and Chemistry*. 12: 831-838.
- Trudel, M., and Rasmussen, J.B. 2006. Bioenergetics and mercury dynamics in fish: a modelling perspective. *Canadian Journal of Fisheries and Aquatic Science*. 63: 1890-1902.
- Trudel, M., and Rasmussen, J.B. 2001. Predicting mercury concentrations in fish using mass balance models. *Ecological Applications*. 11(2): 517-529.
- Trudel, M., and Rasmussen, J.B. 1997. Modeling the elimination of mercury by fish. *Environmental Science and Technology*. 31: 1716-1722.
- US EPA. (2001) Human health criteria: methylmercury fish tissue criterion. Fact Sheet.
<http://www.epa.gov/waterscience/criteria/methylmercury/factsheet.html>
l. downloaded 2/26/2010.
- US EPA (2009). Guidance for implementing the January 2001 Methylmercury water quality criterion. EPA 823-R-09-002. U.S. Environmental Protection Agency, Office of Water, Washington, DC. 211 p.
- Watras, C.J., Back, R.C., Halvorsen, S., Hudson, R.J.M. Morrison, K.A., and Wente, S.P. 1998. Bioaccumulation of mercury in freshwater pelagic food webs. *Science of the Total Environment*. 219: 183-208.
- Warwick, J.J. and Carroll, R.W.H. 2008. Evaluating the impacts of uncertainty in geomorphic channel changes on predicting mercury transport and fate in the Carson River system, Nevada. *International Journal of Soil, Sediment and Water*. 1: 1-15. Full text at:
<http://scholarworks.umass.edu/intljssw/vol1/iss1/4>

CONCLUDING REMARKS

The significance of a varying water column signal in predicting mercury (Hg) body burdens in a planktivore is done by linking a fully dynamic Hg transport model with observed bioaccumulation in the lower food web and a bioenergetic-mercury mass balance model of Sacramento blackfish. Accurate prediction of Hg bioaccumulation depends upon understanding mercury loading mechanisms, and associated uncertainty, into the river-reservoir system. The first phase of research (Chapters 1 and 2) identifies the geologic and biogeochemical controls on Hg transport through the Carson River and Lahontan Reservoir. These are successfully modeled using a linked and modified version of the US EPA hydrodynamic code RIVMOD and water quality routines WASP5/MERC4. Building on previous studies, model improvements to Hg transport include the addition of a bank package that accounts for flow history which imparts a vertically variable calculation of methylmercury (MeHg) in the channel banks, as well as detailed cross sections and stage modeling in the reservoir to ensure a correctly moving delta region.

Transport modeling and Monte Carlo simulation (Chapter 1) finds that geomorphic process of bank erosion and overbank deposition can describe observed variability in THg prior to and during the 1997 flood, with greater uncertainty in modeled behavior placed on earlier overbank discharge events than later events. This is most evident in river reaches with shallower channel slopes that experience large channel widening during earlier events. Geomorphic processes alone, however, can not account for observed variability in THg following the flood, and one speculates if this failure is due to a fundamental change in THg transport as a result of the flood.

Chapter 2 builds a more detailed conceptual model by quantifying loading mechanisms of total and dissolved Hg species during four flow regimes (extremely low, low, medium-high and overbank). First-order second-moment and a multi-criteria GLUE approaches evaluate uncertainty of 16 model input parameters based on Hg species, flow regime and location in the basin. In general, results suggest that concentrations and trends in modeled species are well represented. THg loading and transport is highly constrained in the calibration process, but reproduces a wide range of concentrations over diverse climatic conditions with acceptable accuracy. Sediment transport processes dominate THg transport and input parameter posterior means from the GLUE analysis indicate that a sizable increase in exposed THg concentrations in the river banks occurred as a result of a massive flood in 1997. The size and statistical significance of this change is not obscured by including a large number of parameters in the uncertainty analysis, further implying that it is a physical phenomenon and not solely a relic of numeric technique. Uncertainty in model input translates to uncertainty in predicted water column concentrations on the order of one-order of magnitude, with total species having the greatest uncertainty during higher flows.

In contrast to the transport of THg, DHg loading and transport is found to be complex and difficult to model unless several additional input parameters are introduced. While these additional parameters allow relatively good predictions of DHg at low and medium flows, and THg during overbank flows, the model still fails to capture reasonable DHg concentrations during overbank flows. Improvement of the DHg conceptual model may be warranted. Despite the potential problems

encountered with DHg transport, un-calibrated DMeHg water column concentrations are modeled exceptionally well using observed M/D rates, bank moisture history and reported adsorption coefficients. Reservoir dissolved concentrations are not sensitive to diffusion loads originating from the reservoir benthic sediments and the transport model assigns greater importance to external loading of dissolved species from the Carson River compared to internal sources of benthic sediments.

Sampling different phytoplankton size fractions to assess THg and MeHg bioaccumulation (Chapter 3) finds THg primarily associated with non-living particulate matter. However, MeHg accumulation for the small size fraction is strongly associated with living biomass in the later portion of the summer when algal growth occurs and reservoir residence times are long. Very different results for MeHg accumulation occur if the small particle fraction is not isolated. Under these circumstances, MeHg accumulation is very low, reflecting the dilution effect of *Aphanizomenon flos-aquae* on the calculation. Inability of *Aphanizomenon flos-aquae* to accumulate MeHg reduces the possible transfer of MeHg from the pelagic system to the benthic system in the form of detrital *Aphanizomenon flos-aquae*. Instead, small, more palatable phytoplankton appear the likely mechanism of MeHg transfer to higher trophic levels.

Regressions relating a dynamic water column DMeHg signal to plankton concentrations serve as a boundary condition in a bioenergetic and mercury mass balance model of the Sacramento blackfish. Modeled fish MeHg body burdens using a dynamic signal are compared to predicted body burdens using a constant DMeHg signal. The two approaches are found statistically similar. Lack of distinction in

results is based on a large level of input uncertainty in the water column concentration as determined by the Hg transport model presented in Chapter 2. However, results driven by a varying boundary condition allow speculation on the timing of loads with respect to prey contamination and bioenergetic needs of the blackfish. The model suggest that coupling of peak water column concentrations with periods of maximum plankton growth and maximum fish consumption rates can describe large MeHg body burdens observed in the planktivore. Temporal lags in downstream transport from the reservoir's point source (i.e., river delta) decouple modeled processes and MeHg body burden estimates decrease. Sensitivity of modeled fish body burden to pulse inputs from the river decrease with distance from the delta